AD-A130 292 LABORATORY INVESTIGATION OF CONTAINMENT IN UNDERGROUND NUCLEAR TESTS(U) SRI INTERNATIONAL MENLO PARK CA J C CIZEK ET AL. 15 FEB 82 DNA-6121F DNA001-80-C-0040 1/2

UNCLASSIFIED F/G 18/3 NL

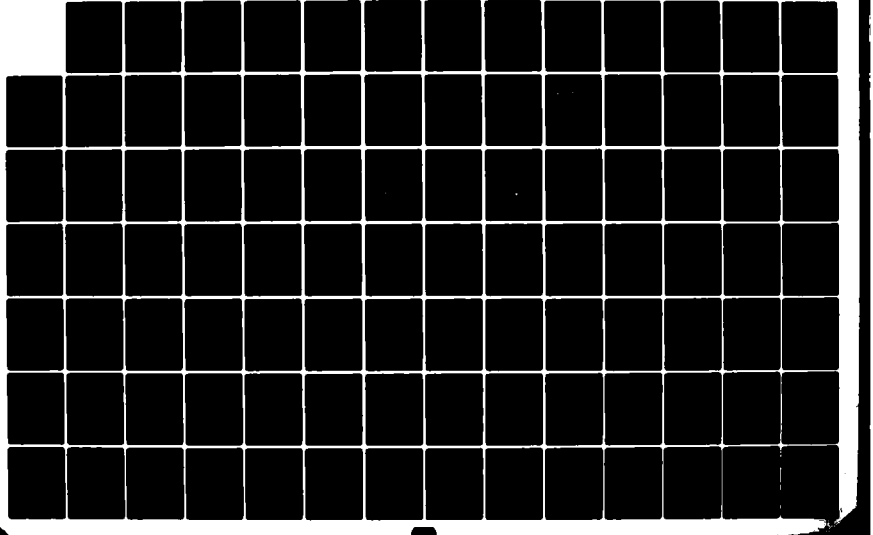

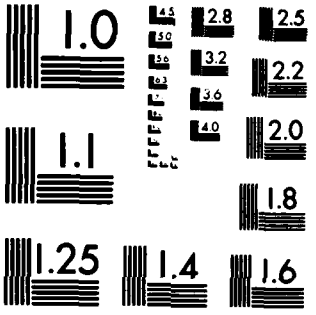

(12)

DNA 6121F

LABORATORY INVESTIGATION OF CONTAINMENT IN UNDERGROUND NUCLEAR TESTS

J. C. Cizek
A. L. Florence

SRI International
333 Ravenswood Avenue
Menlo Park, California 94025

15 February 1982

Final Report for Period 15 February 1981—15 February 1982

CONTRACT No. DNA 001-80-C-0040

APPROVED FOR PUBLIC RELEASE;
DISTRIBUTION UNLIMITED.

THIS WORK WAS SPONSORED BY THE DEFENSE NUCLEAR AGENCY
UNDER RDT&E RMSS CODE B345081466 J24AAXYX00017 H2590D.

Prepared for
Director
DEFENSE NUCLEAR AGENCY
Washington, DC 20305

Destroy this report when it is no longer needed. Do not return to sender.

PLEASE NOTIFY THE DEFENSE NUCLEAR AGENCY, ATTN: STTI, WASHINGTON, D.C. 20305, IF YOUR ADDRESS IS INCORRECT, IF YOU WISH TO BE DELETED FROM THE DISTRIBUTION LIST, OR IF THE ADDRESSEE IS NO LONGER EMPLOYED BY YOUR ORGANIZATION.

UNCLASSIFIED

SECURITY CLASSIFICATION OF THIS PAGE (When Data Entered)

REPORT DOCUMENTATION PAGE		READ INSTRUCTIONS BEFORE COMPLETING FORM
1. REPORT NUMBER DNA 6121F	2. GOVT ACCESSION NO. AD-A130 292	3. RECIPIENT'S CATALOG NUMBER
4. TITLE (and Subtitle) LABORATORY INVESTIGATION OF CONTAINMENT IN UNDERGROUND NUCLEAR TESTS		5. TYPE OF REPORT & PERIOD COVERED Final Report for Period 15 Feb 81—15 Feb 82
		6. PERFORMING ORG. REPORT NUMBER SRI PYU-1289
7. AUTHOR(s) J. C. Cizek and A. L. Florence		8. CONTRACT OR GRANT NUMBER(s) DNA 001-80-C-0040
9. PERFORMING ORGANIZATION NAME AND ADDRESS SRI International 333 Ravenswood Avenue Menlo Park, CA 94025		10. PROGRAM ELEMENT, PROJECT, TASK AREA & WORK UNIT NUMBERS Subtask J24AAXYX000-17
11. CONTROLLING OFFICE NAME AND ADDRESS Director Defense Nuclear Agency Washington, D.C. 20305		12. REPORT DATE 15 February 1982
		13. NUMBER OF PAGES 102
14. MONITORING AGENCY NAME & ADDRESS(if different from Controlling Office)		15. SECURITY CLASS (of this report) UNCLASSIFIED
		15a. DECLASSIFICATION/DOWNGRADING SCHEDULE N/A

16. DISTRIBUTION STATEMENT (of this Report)

Approved for public release; distribution unlimited.

17. DISTRIBUTION STATEMENT (of the abstract entered in Block 20, if different from Report)

18. SUPPLEMENTARY NOTES

This work sponsored by the Defense Nuclear Agency under RDT&E RMSS Code B345081466 J24AAXYX00017 H2590D.

19. KEY WORDS (Continue on reverse side if necessary and identify by block number)

Nuclear	Cavity	Overburden
Underground	Hydrofracture	Uncoupled cavity
Explosion	Fracture initiation	Residual stress
Containment	Crack growth	Stress relaxation

20. ABSTRACT (Continue on reverse side if necessary and identify by block number)

In support of the DNA program for stemming and containment of underground nuclear tests, existing laboratory techniques were further developed and applied to investigate the mechanics of containing gases in cavities formed by underground nuclear explosions.

The experimental procedure includes constant flow rate hydrofracture from a central exploded cavity in an externally pressurized grout sphere simulating a geologic material subjected to overburden. The experiments provide hydro-

DD FORM 1 JAN 73 1473 EDITION OF 1 NOV 65 IS OBSOLETE

UNCLASSIFIED

SECURITY CLASSIFICATION OF THIS PAGE (When Data Entered)

20. ABSTRACT (Continued)
fracture records consisting of the time history of cavity pressure as fluid is pumped into the cavity. Hydrofracture records for exploded cavities, which have a surrounding residual stress field, are compared with those for unexploded cavities, which have no residual stress field, to assess the potential benefit to containment of the residual stress field.

The hydrofracture records are reproducible and for each of the cases, unexploded and exploded cavity, have a characteristic shape. Fracture pressures for exploded cavities in saturated grout representing Nevada Test Site tuff are over three times as high as the fracture initiation pressures for unexploded cavities for the highest pumping rate used, which gives a measure of the benefit to containment of the residual stress field. When the same grout is provided with 13% closed voids of air to represent a material property trend toward alluvium, the residual stress field is negligible.

Slower pumping rate and delayed hydrofracture experiments indicate that residual stress relaxation occurs. At the slowest rate, the fracture pressures for an exploded cavity in saturated grout were 75% higher than the fracture initiation pressures for unexploded cavities.

Experiments with uncoupled cavities (air around explosive) with an initial cavity-to-charge radius ratio of three showed that the residual stress field strength was negligible.

Because of the importance of continuum mechanics computer codes to containment, additional correlative data, mainly particle velocities, were generated to aid calculators working for the DNA containment program.

PREFACE

This research was conducted under Contract DNA 001-80-C-0040 in support of the DNA stemming and containment program for underground nuclear tests.

The authors are indebted to the technical monitor, Carl Keller (FCDNA), for technical ideas, suggestions, and overall guidance, to Terra Tek, Inc., for material property evaluations, and to the containment participants at Systems, Science and Software, and Pacifica Technology for the insights provided by their theoretical work and critical commentaries.

The authors are also indebted to the personnel at SRI International who contributed directly to the research program. In particular, appreciation is extended to L. J. Dary for preparing the models, assisting in the experiments, and suggesting improvements, and to G. R. Abrahamson for overall supervision.

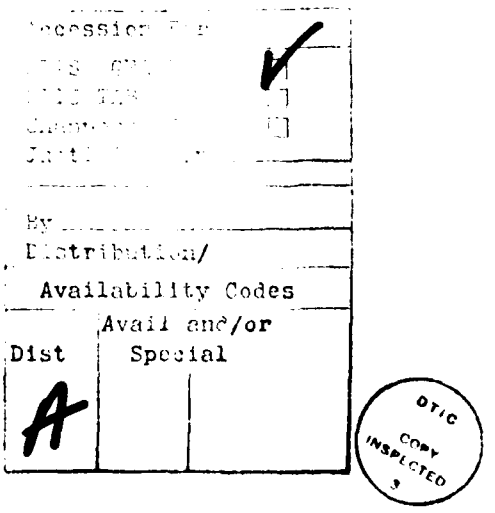

CONVERSION FACTORS

To Convert From	To	Multiply By
atmosphere (normal)	kilo pascal (kPa)	1.013 25 X E +2
bar	kilo pascal (kPa)	1.000 000 X E +2
foot	meter (m)	3.048 000 X E -1
inch	meter (m)	2.540 000 X E -2
mil	meter (m)	2.540 000 X E -5
ounce	kilogram (kg)	2.834 952 X E -2
poise	kilogram/meter-second (kg/m·sec)	1.000 000 X E -1
pound-force (lbf avoirdupois)	newton (N)	4.448 222
pound-force/inch^2 (psi)	kilo pascal (kPa)	6.894 757
pound-mass (lbm avoirdupois)	kilogram (kg)	4.535 924 X E -1

TABLE OF CONTENTS

TABLE OF CONTENTS (continued)

LIST OF ILLUSTRATIONS

LIST OF ILLUSTRATIONS (continued)

LIST OF ILLUSTRATIONS (continued)

LIST OF TABLES

SECTION 1
INTRODUCTION AND SUMMARY

1.1 INTRODUCTION

In underground nuclear tests, it is required that radioactive gases not be released into the atmosphere. Consequently, tunnels from the nuclear device cavity must be stemmed and residual cavity gases must be contained by the adjacent surrounding medium. Containment of the gases by the surrounding medium may be aided by the residual stress field created by the explosion. The extent of this aid is governed by residual stress field strength relative to cavity gas pressure, relaxation, and potential weaknesses in the field strength caused by nearby geological and man-made features typical of those found at the Nevada Test Site (NTS). Although containment has been achieved for many years and stemming has generally been successful in recent nuclear tests, the complexities associated with underground testing require that planned events still receive extensive containment evaluation.

Over the years, the DNA stemming and containment (SAC) program has consisted of five main parts: code development for ground motion, tunnel closure, and grout flow calculations; material properties determination; laboratory investigations; scaled high explosive tests; and field diagnostics. Over the past several years SRI has been conducting laboratory investigations.[1-8]

Our laboratory investigations during the last year have focused on containment. One purpose of the experimental program has been to aid understanding of the mechanisms of underground nuclear explosions and containment of the cavity gases. An essential part of this understanding is the generation of data under controlled reproducible conditions for validation of continuum mechanics computer codes of calculators working for the DNA program.[9-11]

Although the experiments are not strictly scalable to underground nuclear events, they are designed so that much of the physical behavior is represented. Consequently, the effects on containment of various physical conditions in past or planned nuclear events can receive a preliminary assessment.

In our basic containment experiments, a small sphere of PETN* explosive in a thin-walled Lucite container is cast at the center of a sphere of rock-matching grout (RMG 2C4). After aging, the grout has properties similar to those of Nevada Test Site tuff. Also cast in the grout sphere is a stainless steel access tube located on a radius and ending just short of the Lucite container. External pressure is applied hydraulically to the sphere to represent overburden pressure. The explosive is detonated to create the exploded cavity. The end of the steel tube is located so that it just protrudes into the exploded cavity. Fluid is pumped into the cavity at a constant rate until fracture is initiated and propagated to the outside of the RMG sphere. During the pumping, fluid pressure and flow are monitored so that a hydrofracture record can be constructed.

The effect of the explosively generated residual stress field on containment is assessed by conducting a separate hydrofracture test on a sphere with an unexploded cavity comparable in size to the exploded cavity. Relaxation of the stress field is assessed by performing hydrofracture experiments on exploded cavities at different flow rates or by holding the cavity gas pressure at a constant value for the duration of interest before hydrofracturing.

Series of exploded and unexploded cavity hydrofracture tests were performed on RMG spheres of 12-inch (30.48-cm) diameter to establish the effects of parameter variations on the basic containment experiment. In the standard exploded cavity test, a 3/8-gram charge generated a 0.808-inch-diameter (2.05-cm) cavity. In unexploded cavity tests, a smooth and unlined cavity having a 3/4-inch-diameter (1.90-cm) cavity was cast.

---

*Pentaerythritol tetranitrate ($C_5H_8O_{12}N_4$).

The reference parameters were overburden pressure [1000 psi (6.895 MPa)], viscosity of the hydrofracture fluid (1 centipoise), and rate of fluid flow into the cavity (122.4 cm^3/min.). Surface gages monitored fracture arrival in selected tests.

An independent series of tests was performed on 11-inch-diameter (27.94-cm) RMG spheres to establish particle velocity profiles in the region surrounding exploded cavities.

The specific areas of investigation were as follows:

- Flow rate. A constant flow rate of 122.4 cm^3/min was chosen so that hydrofractures could be performed within a scaled time of relevance. Comparisons were made with previous results obtained at flow rates of 4.26 and 40.8 cm^3/min.
- Material property. Rock-matching grout (RMG 2C4), which simulates relevant properties of tuff, low density rock-matching grout (LD 2C4), which represents a shift in material properties toward alluvium, and tuff, which was cored from the Nevada Test Site, were hydrofractured.
- Stress relaxation. Hydrofracture experiments, in which pumping was delayed for 10 seconds following charge detonation, were performed. This enabled us to measure cavity gas pressure decay and to study the effects of residual stress relaxation on containment.
- Uncoupled cavity. Exploded cavity spheres having an initial cavity diameter 1.5 or 3 times the charge diameter were hydrofractured to assess residual stress intensity in the region surrounding an uncoupled cavity.
- Reduced overburden. Coupled and uncoupled exploded cavity spheres subjected to 500 psi (3.447 MPa) external pressure were hydrofractured to determine the effects of a reduced depth of burial on containment.
- Nearby explosive charge. Two explosive charges were cast in a RMG 2C4 sphere to assess the effects on containment of the cavity gas pressure and asymmetric stress field associated with simultaneous detonation of nearby charges.
- Particle velocity measurements. Particle velocity profiles were measured at various distances from the explosive charge in coupled and uncoupled exploded cavity RMG 2C4 spheres.

In addition, a steel pressure vessel with a spherical cavity was designed and assembled to measure cavity gas pressure decay and to simulate the

initial phases of hydrofracture in a rigid uncoupled cavity. The pressure pulse generated in the overburden fluid during exploded cavity tests was monitored to provide additional data for verifying calculations. Finally, a theoretical analysis was performed to determine particle velocity attenuation in the elastic region surrounding an exploded cavity.

The tests performed during the current phase of the laboratory program are tabulated according to category in Section 3.1. Section 2 describes existing experimental techniques and recent developments. Section 3 presents and discusses the hydrofracture and particle velocity results. Appendix A contains the results of rigid uncoupled exploded cavity tests. Appendix B presents circumferential strain records obtained from the particle velocity measurements. Appendix C contains the pressure pulses measured in the overburden fluid during exploded cavity tests. Appendix D describes the theoretical elastic analysis for determining particle velocity attenuation. Finally, Appendix E describes relevant material properties for rock-matching grout RMG 2C4, low density rock-matching grout LD 2C4, and Nevada Test Site tuff.

1.2 SUMMARY

The principal findings of the above investigations were as follows:

- Reproducibility of the unexploded cavity hydrofracture records is good for all flow rates (Figures 3.1, 3.2, and 3.3).
- Large flow rate increases produced small fracture initiation pressure increases in RMG 2C4 and LD 2C4 unexploded cavity spheres (Figures 3.1 and 3.2).
- A comparison of results for RMG 2C4 and LD 2C4 unexploded cavity spheres shows that a small increase in material strength produces a small increase in fracture initiation pressure (Figure 3.3).
- Reproducibility of the coupled exploded cavity hydrofracture records is good for all flow rates (Figures 3.4, 3.6, and 3.7).
- Large flow rate increases produced significant hydrofracture pressure increases in exploded cavity RMG 2C4 spheres by reducing cavity gas pressure decay and stress relaxation. Maximum hydrofracture pressures were nearly four times those generated in unexploded cavity spheres (Figures 3.4 and 3.5).

- For LD 2C4, exploded cavity hydrofracture pressures were comparable to unexploded cavity pressures for all flow rates, implying that a negligible residual stress field was developed (Figures 3.5, 3.6, and 3.7).
- Uncoupled 3R exploded cavities in RMG 2C4 yield fracture initiation pressures comparable to those for unexploded cavities, implying that a negligible residual stress field is formed. Drainlines represent a perturbation that reduces hydrofracture pressures. Water in the 3R cavity increases hydrofracture pressures by increasing the effective coupling. Results for 1.5R uncoupled cavities indicate water in the cavity; maximum hydrofracture pressures were one-half those generated in a fully coupled test (Figures 3.8, 3.9, 3.10, and 3.11).
- A reduction in overburden had no effect on a fully coupled exploded cavity test in RMG 2C4, indicating that residual stress dominates the overburden stress (Figure 3.12).
- A nearby explosive charge in a RMG 2C4 sphere resulted in asymmetric cavity growth and lower hydrofracture pressures (Figure 3.14).
- Cavity expansion in an exploded cavity tuff cylinder was less than that in a RMG 2C4 sphere, and resulted in dynamic cracking of the tuff. This effect is attributed to differences in material properties at high stresses and strain rates (Figure 3.15).
- Particle velocity profiles for a coupled exploded cavity in RMG 2C4 reveal significant residual strains near the cavity. The corresponding strains for a 3R uncoupled cavity are reduced by a factor of five (Figures 3.16, 3.17, 3.18, and 3.19).

In conclusion, based on the experimental results for RMG 2C4 and LD 2C4, the implications for containment are

- A beneficial residual stress is probably established in saturated tuff for coupled explosions.
- The residual stress field in tuff probably decreases in intensity by means of the material property of relaxation.
- Uncoupled explosions in tuff may establish a residual stress field that is too weak to benefit containment.
- Coupled explosions in alluvium may establish a residual stress field that is too weak to benefit containment.
- If a residual stress field is sufficiently strong, as expected when a coupled explosion occurs in tuff, the depth of burial may be reduced until surface interactions become important.

Laboratory research during the next phase of the program should include investigations of the effects on containment of

- Geological and man-made features of the type found at the Nevada Test Site; for these experiments, the flow rate used in the current study should be used to provide a relevant time scale.
- Tuff and alluvium simulant in order to relate results to more realistic materials.
- Asymmetric tectonic stress fields.

SECTION 2
EXPERIMENTAL TECHNIQUES

2.1 CONCEPT

The experiment shown schematically in Figure 2.1 was devised[4] to simulate in the laboratory several relevant conditions associated with an underground nuclear test. A small amount of PETN explosive sealed in a thin-walled Lucite sphere represents the device. The charge is then cast at the center of a rock-matching grout sphere. After aging, the grout has properties similar to those of Nevada Test Site tuff. Also cast in the grout sphere is a stainless steel access tube located on a radius and ending near the charge [Figure 2.1(a)]. External pressure is then applied hydraulically to the sphere to represent overburden pressure [Figure 2.1(b)]. The explosive is detonated to form the exploded cavity. The end of the steel tube is located so that it just protrudes into the explosively formed cavity [Figure 2.1(c)]. Fluid is pumped into the cavity at a constant rate until a fracture is initiated and propagated to the outside of the grout sphere [Figure 2.1(d)]. During the pumping fluid pressure and flow are monitored so that a hydrofracture record can be constructed. An alternative source configuration was also developed to provide decoupling of the explosive charge from the surrounding material by means of an annular region of air.

The hydrofracture portion of the experiment is included to determine the effect of the residual stress field on containment by comparing the cavity pressures required to crack a grout sphere with and without residual stresses. In the experiments without a residual stress field, spherical cavities are cast in the grout sphere; these unexploded cavities are comparable in size to the fully coupled exploded cavities.

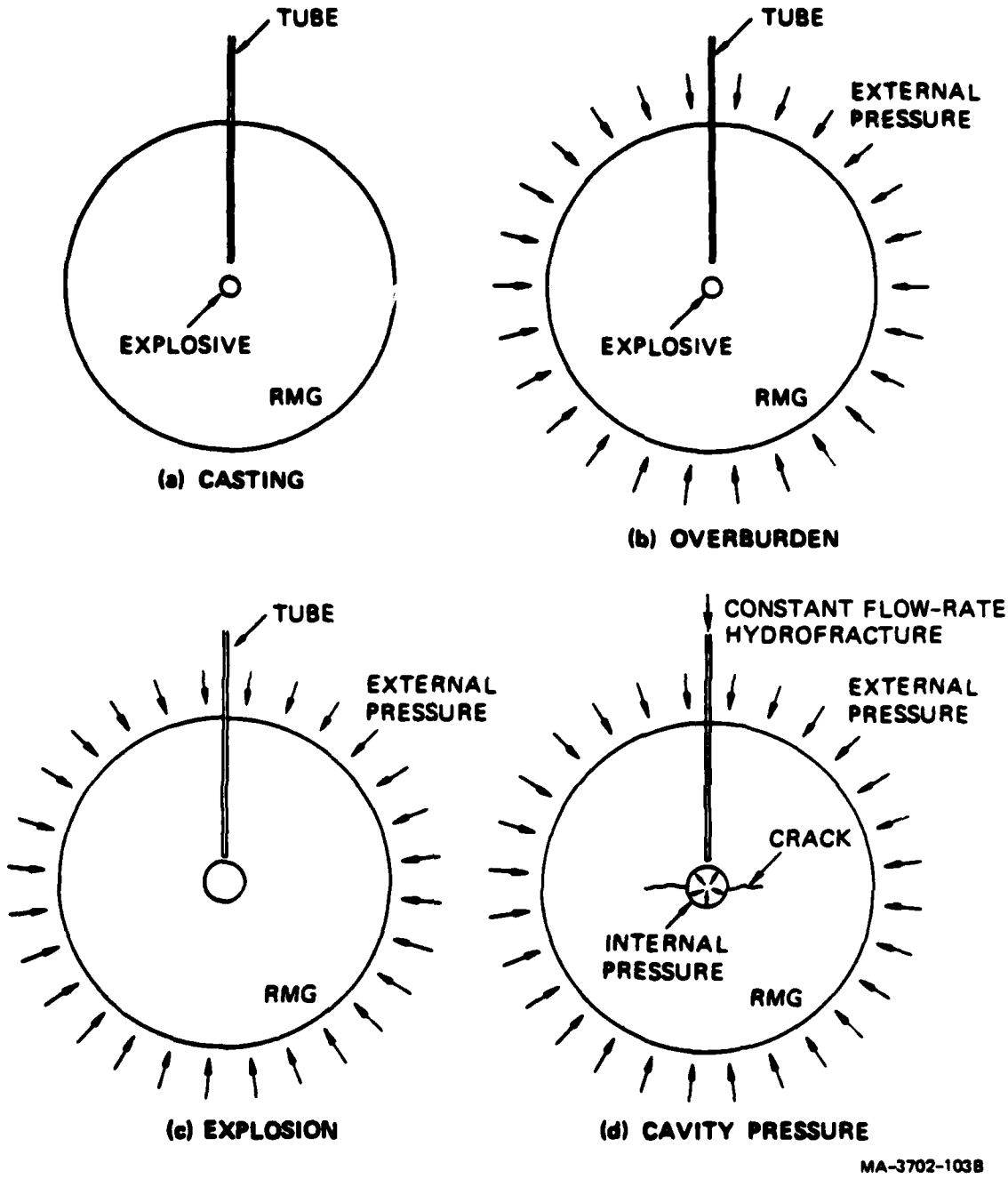

FIGURE 2.1 SEQUENCE OF OPERATIONS IN CONTAINMENT EXPERIMENTS

2.2 EXISTING EXPERIMENTAL TECHNIQUES

Figure 2.2 shows the experimental apparatus. A 12-inch-diameter (30.48-cm) RMG sphere is shown inside a steel vessel containing oil or water that can be pressurized to the desired overburden. The sphere is suspended from the lid by the stainless steel tube cast in the grout. The fluid in the vessel is maintained at a constant pressure throughout the test by incorporating a high-pressure nitrogen reservoir and valve in the water supply line. A quartz gage mounted in the bottom of the vessel monitors the pressure pulse generated by charge detonation.

The constant flow-rate system shown schematically in Figure 2.3 conforms with standard hydrofracture practice. The specifications of this system have been described in a previous report.[8]

Compliance of the hydrofracture system is measured by performing a pressure test in which the cavity is replaced by a rigid vessel of equivalent volume. The pressure-volume curve for this test is then used to compensate for the effects of system compliance on the hydrofracture records.

Brief descriptions of the experimental techniques for unvented exploded cavity tests, unexploded cavity tests, particle velocity measurements, and surface fracture detection are given below.

Unvented Exploded Cavity Tests

The basic configuration for unvented exploded cavity hydrofracture tests is shown in Figure 2.4. Figure 2.5 shows the charge design, which consists of 3/8-gram of PETN in a 10-mm-OD Lucite case with a wall thickness of 20 mil (0.508 mm). A constant explosive density of 1 g/cm^3 was used for reproducibility; PETN weight varied slightly from charge to charge as a result of variations in machining accuracy. Hence, 3/8 gram was the nominal weight of the explosive. Charge assembly has been described in a previous report.[12]

Cavity gas pressure was measured and hydrofracture was performed by following the sequence of steps shown in Figure 2.6. Before charge detonation, the entire system was filled with hydrofracture fluid.

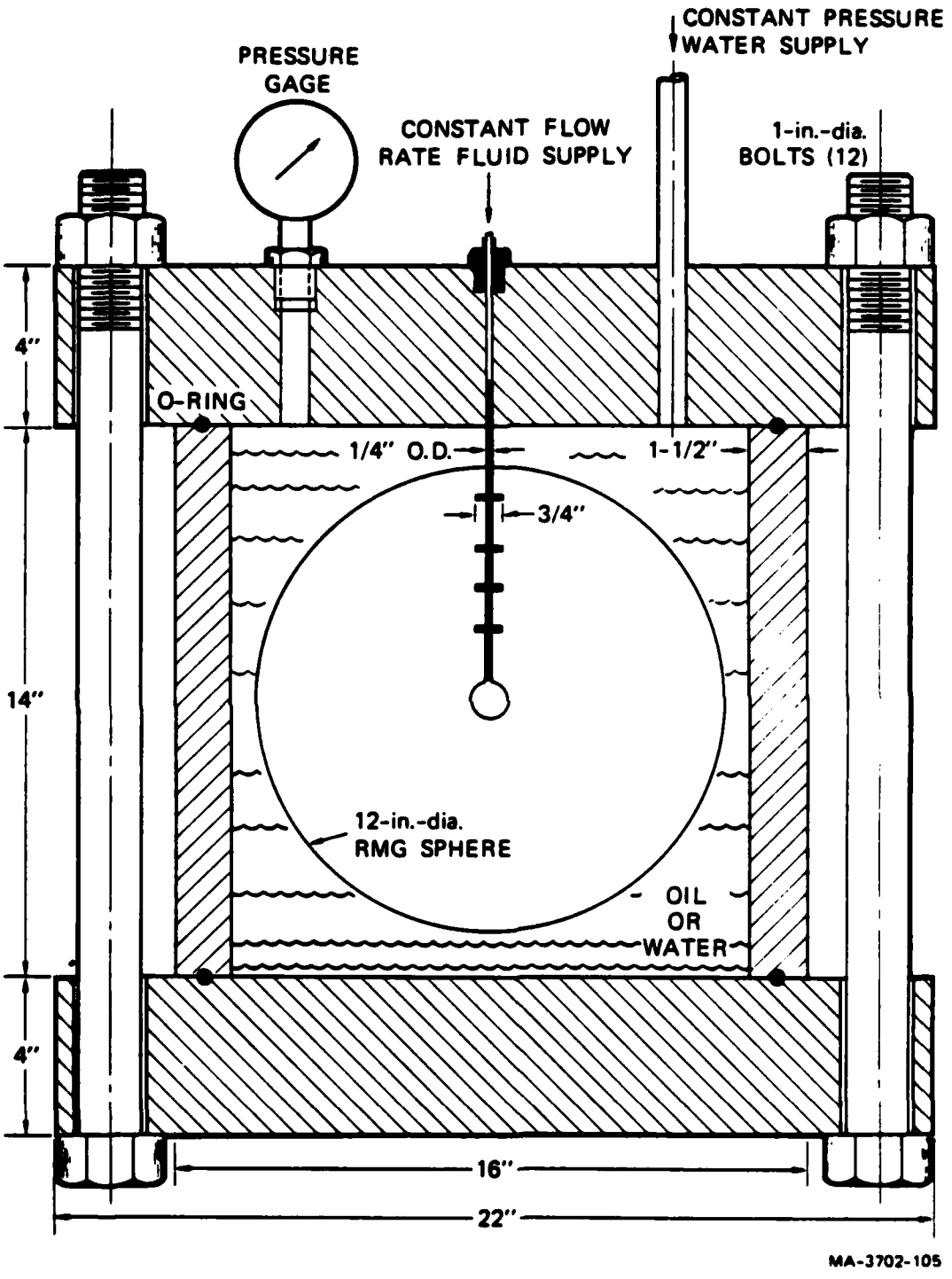

FIGURE 2.2 CONTAINMENT EXPERIMENT APPARATUS

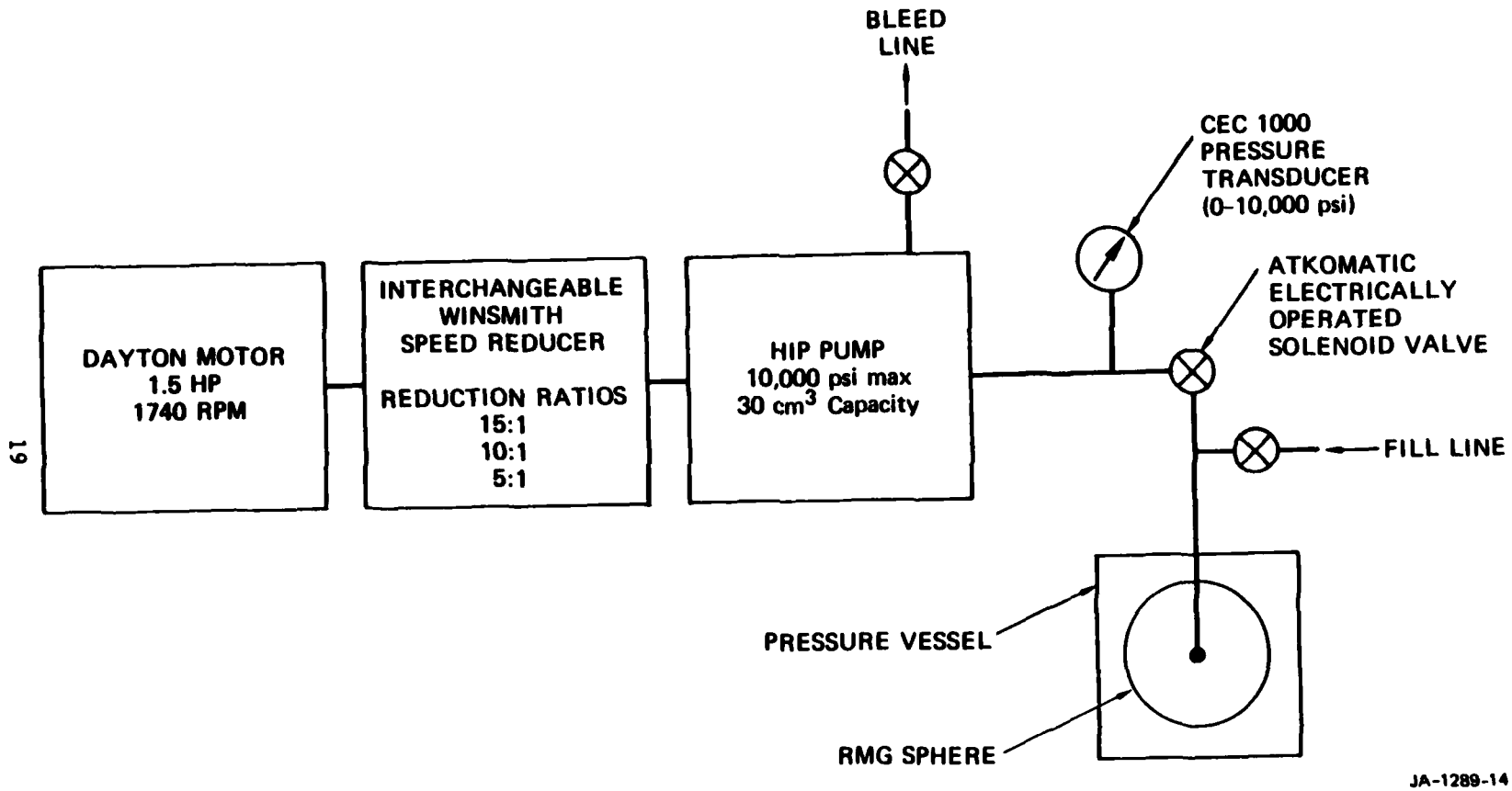

FIGURE 2.3 CONSTANT FLOW-RATE HYDROFRACTURE SYSTEM

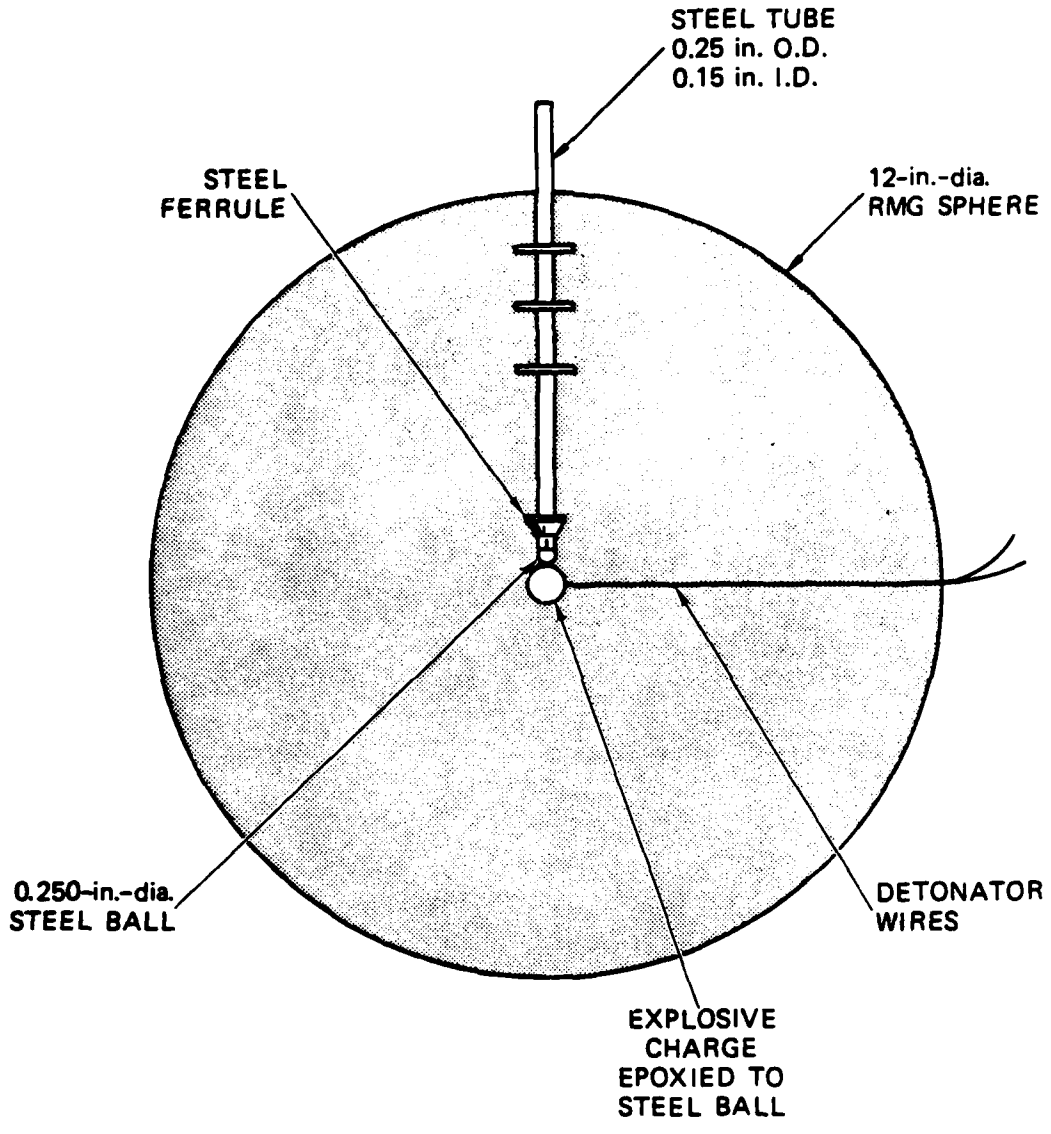

FIGURE 2.4 OVERALL CONFIGURATION FOR UNVENTED EXPLODED CAVITY TESTS

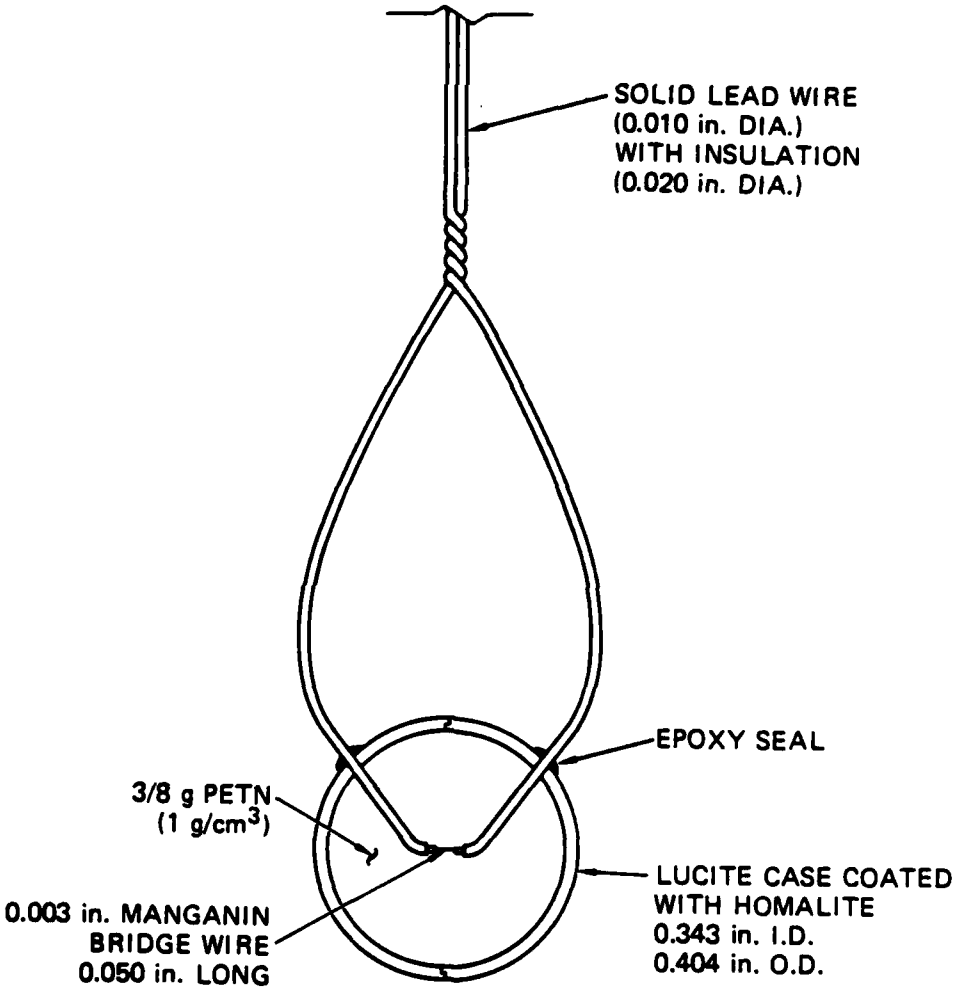

FIGURE 2.5 EXPLOSIVE CHARGE

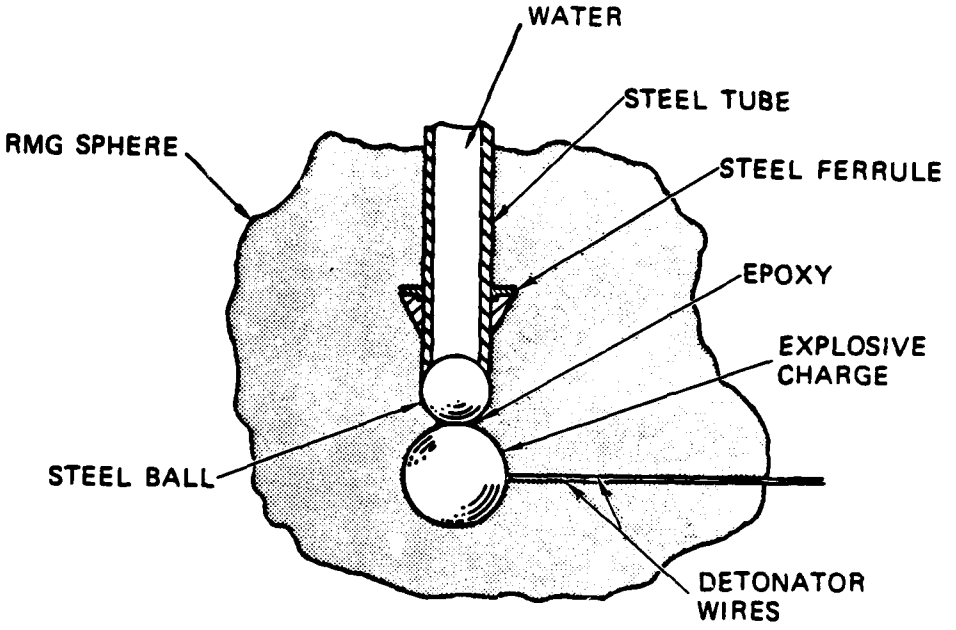

(a) INITIAL CONFIGURATION

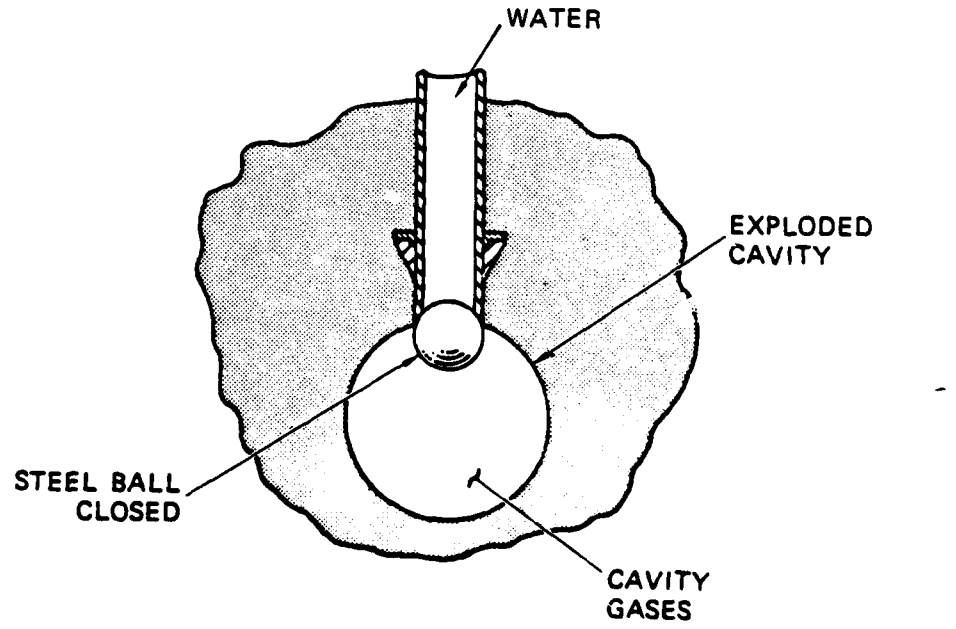

(b) CHARGE EXPLODED

MA-5958-96A

FIGURE 2.6 SEQUENCE OF OPERATIONS FOR UNVENTED EXPLODED CAVITY TESTS

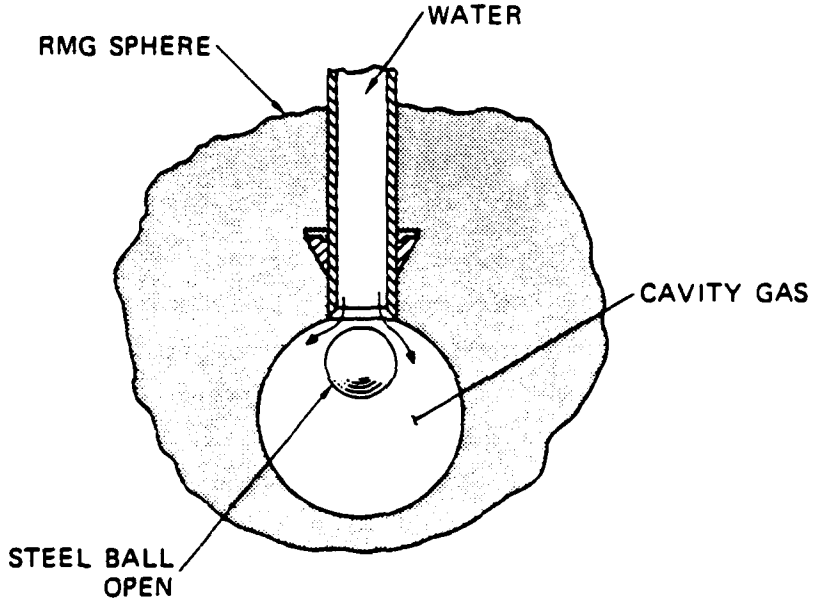

(c) START OF HYDROFRACTURE PROCESS

MA-5958-97A

FIGURE 2.6 SEQUENCE OF OPERATIONS FOR UNVENTED EXPLODED CAVITY TESTS (Concluded)

The steel ball sealed the end of the access tube [Figure 2.6(a)]. Charge detonation expanded the cavity past the end of the tube [Figure 2.6(b)], and the ball valve opened the access tube [Figure 2.6(c)] when the cavity gas and hydrofracture fluid pressures reached equilibrium. These equilibrium pressures were measured by a pressure transducer located in the fluid supply line. Pumping began immediately with charge detonation. Hence the time required to open the access tube depended on the rates at which cavity gas pressure decayed and hydrofracture fluid was pressurized. In an alternative configuration, the steel ball was replaced by a steel piston which was machined to slide freely inside the access tube. This technique allows for cavity gas pressure measurements to begin at the time of charge detonation.

Unexploded Cavity Tests

The basic configuration for unexploded cavity hydrofracture tests is shown in Figure 2.7. The cavity was formed by first inserting a rubber membrane (balloon) through the access tube and expanding the tip with water to the desired diameter. A spherical shape was maintained by means of a wire cage, temporarily fastened to the end of the tube. After 48 hours, the membrane assumed a permanent shape and the cage was removed. The membrane and tube were then positioned in a Lucite mold and the grout was cast around them. After the grout cured, the membrane was removed, leaving a smooth unlined cavity.

Particle Velocity Measurements

Particle velocity profiles were obtained in 11-inch-diameter (27.94-cm) exploded cavity spheres by means of concentric circular loops of wire cast symmetrically about the charge.[12] A magnetic field was generated normal to the plane of the loops by passing current through a coil that surrounds the sphere. Charge detonation produces radial motion of the loops that cuts the magnetic flux lines. In accordance with Faraday's law, the voltage induced in each conducting loop is proportional to the particle velocity. A history of particle velocity at several radii was thus obtained for mechanics code validation.

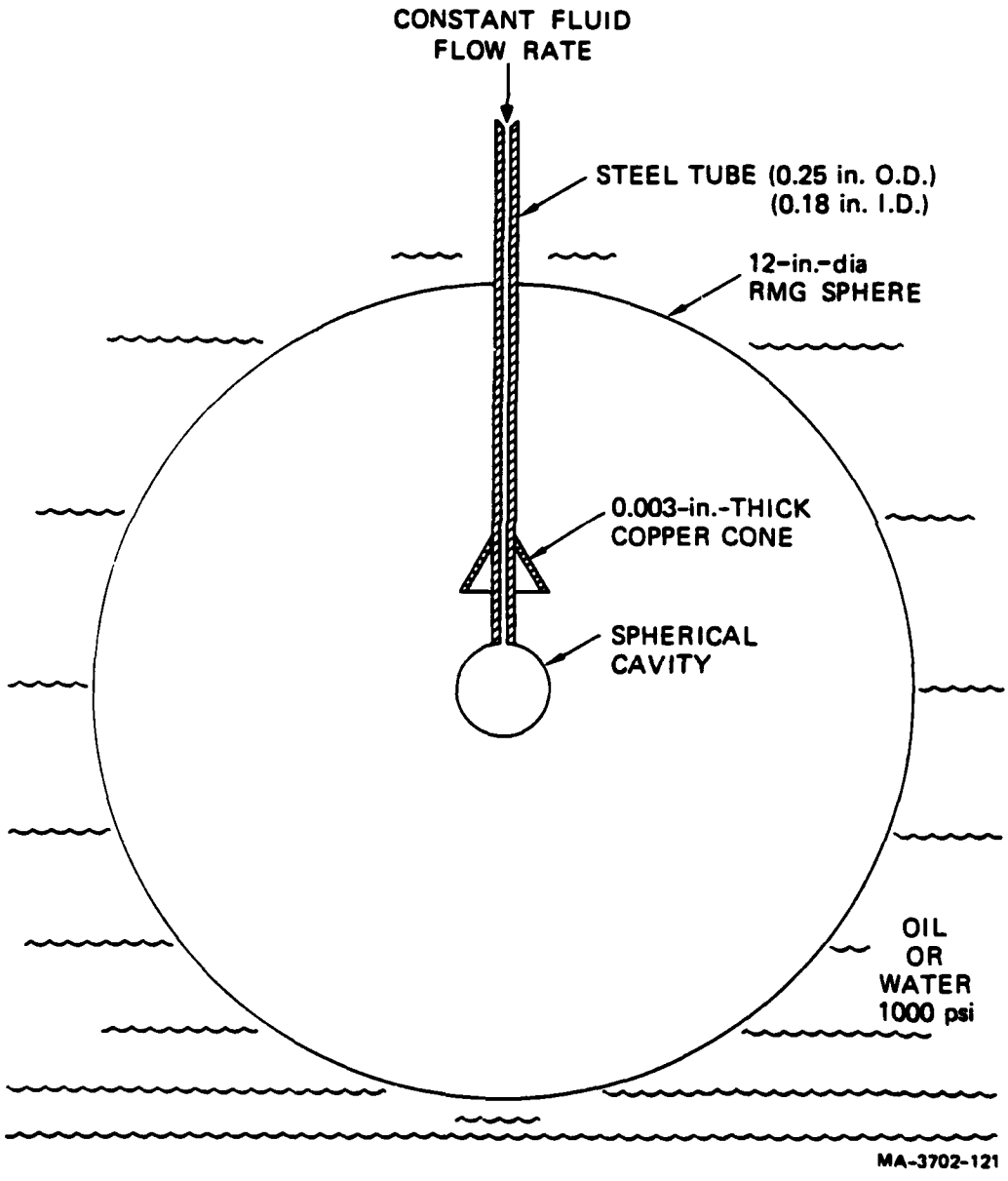

FIGURE 2.7 BASIC CONFIGURATION FOR UNEXPLODED CAVITY TESTS

Surface Fracture Detection

Surface fracture of selected grout spheres was detected by means of a 1/16-inch-wide (1.59-mm) stripe of electrically conductive silver-based paint. Typical surface regions covered by the gage are shown in Figure 2.8.

2.3 EXPERIMENTAL TECHNIQUE DEVELOPMENTS

Uncoupled Exploded Cavity Tests

The basic configuration for uncoupled exploded cavity hydrofracture tests is shown in Figure 2.9. A thin-walled glass hemisphere with a 0.25-inch-diameter (0.635-cm) hole was Homolited to a washer on the access tube. A standard explosive charge was centered in the equatorial plane of the hemisphere and held in place by a plastic rod and Homalite. The rod was threaded into a steel ball that was Homalited to the end of the access tube. The lead wires from the charge were brought out through a notch in the glass, and a second glass hemisphere was Homalited in place to provide an annular region of air surrounding the charge. Rock-matching grout was poured around the glass sphere. The degree of uncoupling between the explosive source and surrounding grout was determined by the ratio of glass sphere diameter to charge diameter. In an alternative configuration, the steel ball was replaced by a Mylar diaphragm which was epoxied to the end of the access tube. This technique permits cavity gas pressure measurements to begin at the time of charge detonation.

In several tests, a moisture sensitive probe was installed at the bottom of the cavity to detect the presence of water. In other tests, a radial steel drainline extending from the cavity was cast in the equitorial plane of the grout sphere to allow for removal of water before testing.

Cavity Gas Pressure Measurements

Figure 2.10 shows the experimental apparatus for measuring gas pressure produced by charge detonation in a rigid uncoupled cavity. The steel pressure vessel contains a machined spherical cavity and axial holes for the charge wires and for access to the quartz pressure transducers. The coupling parameter was varied by installing a spherical insert having the desired diameter. The initial portion of a hydrofracture record was simulated by attaching the vessel to the hydrofracture system.

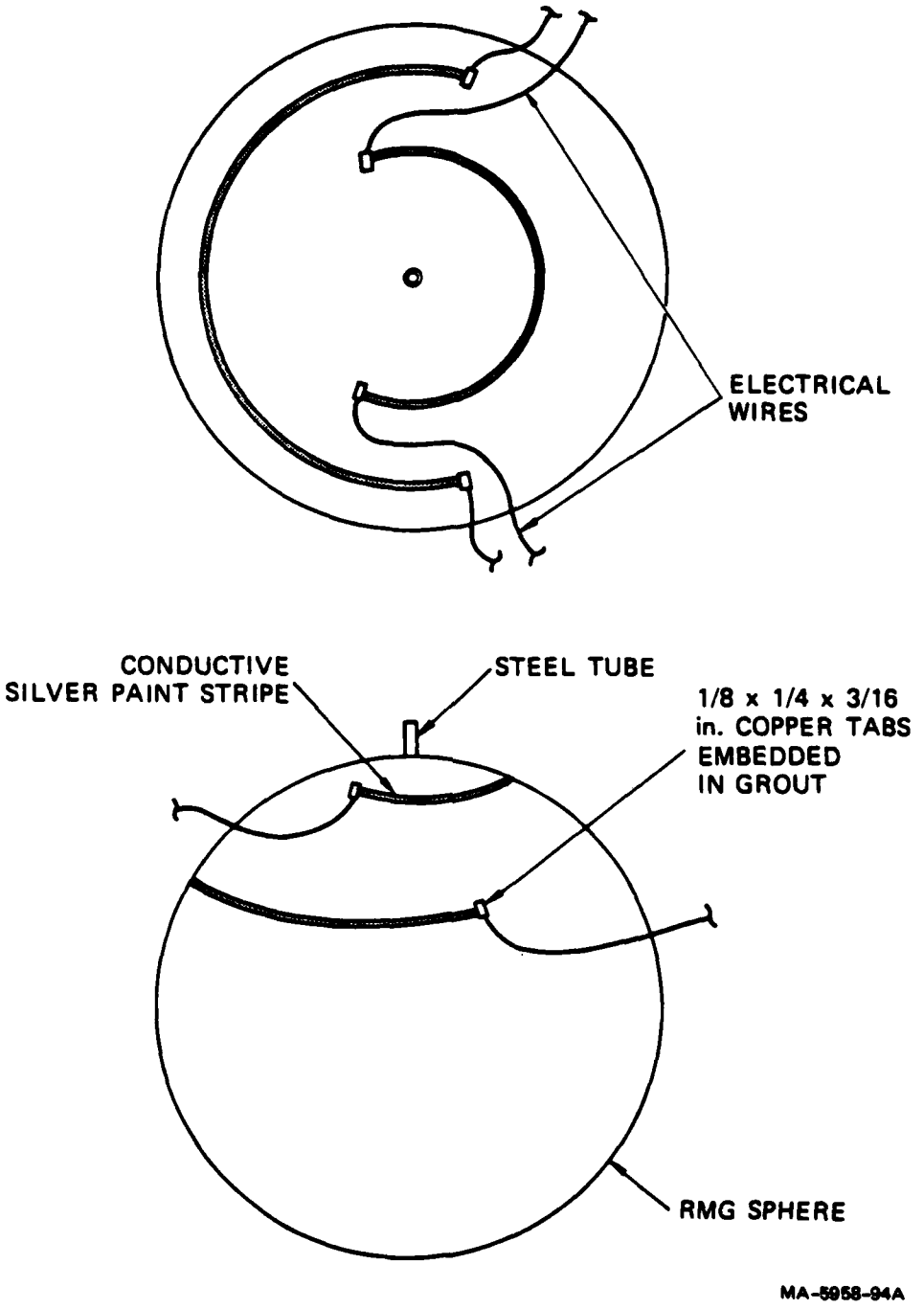

FIGURE 2.8 SURFACE FRACTURE GAGES

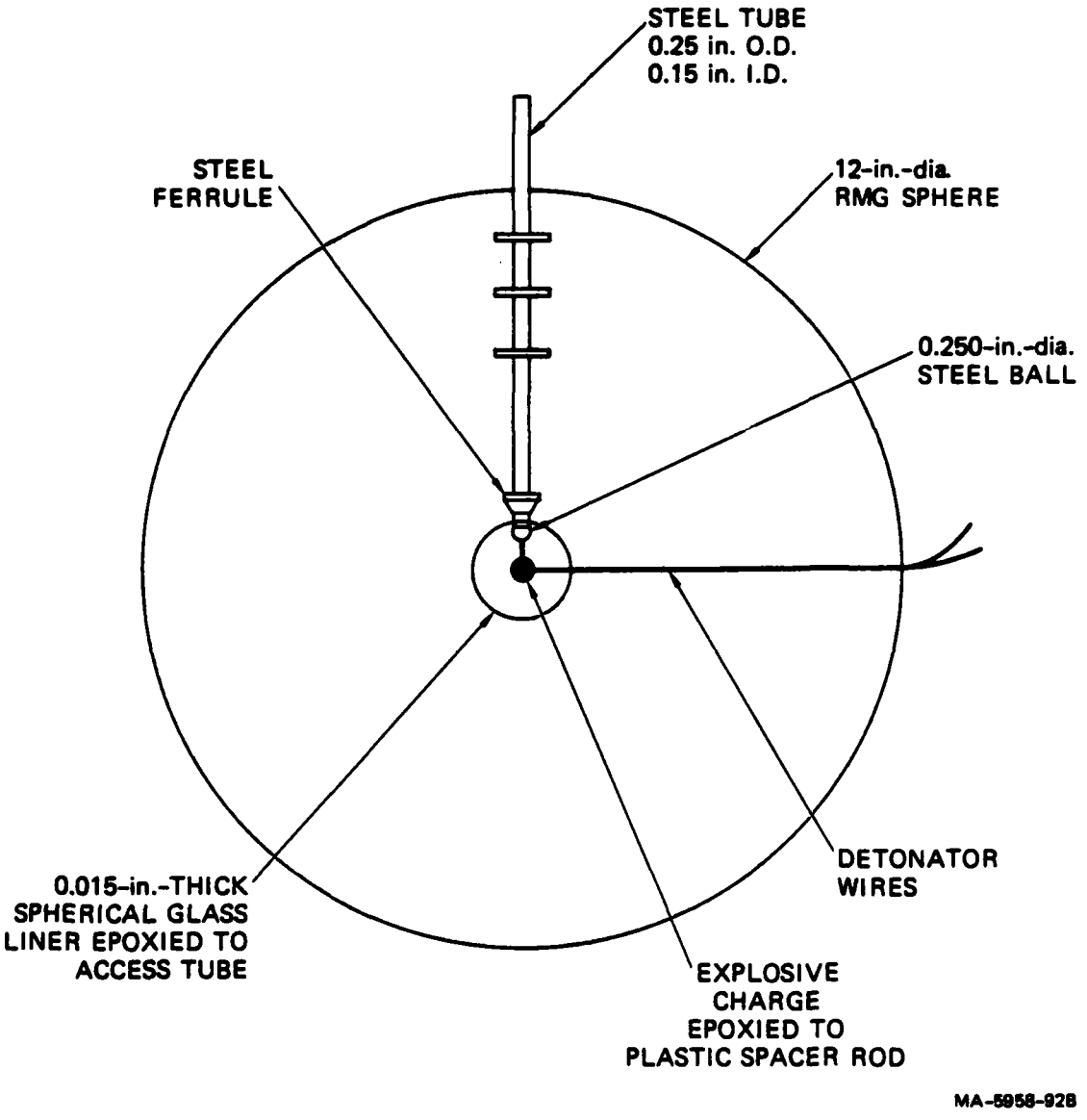

FIGURE 2.9 OVERALL CONFIGURATION FOR UNCOUPLED EXPLODED CAVITY TESTS

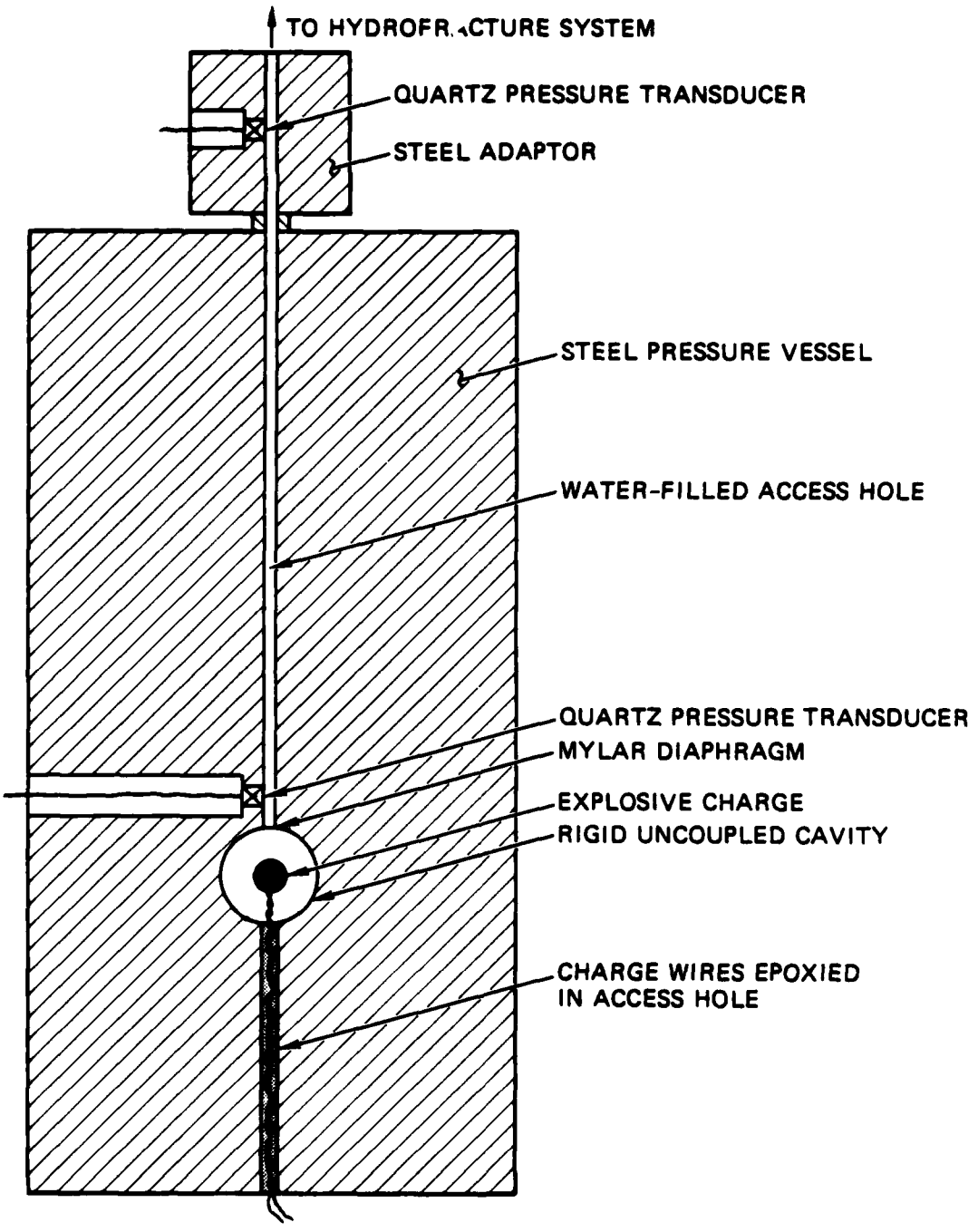

FIGURE 2.10 OVERALL CONFIGURATION FOR RIGID UNCOUPLED CAVITY TESTS

Exploded Cavity Test in Tuff Cylinder

Figure 2.11 shows a trial configuration for an exploded cavity hydrofracture test in tuff. Coring and drilling operations produced stepped axial holes extending to the center of the tuff cylinder. The access tube with attached monel ball and explosive charge was then grouted into the hole. An epoxy plug provided the final seal.

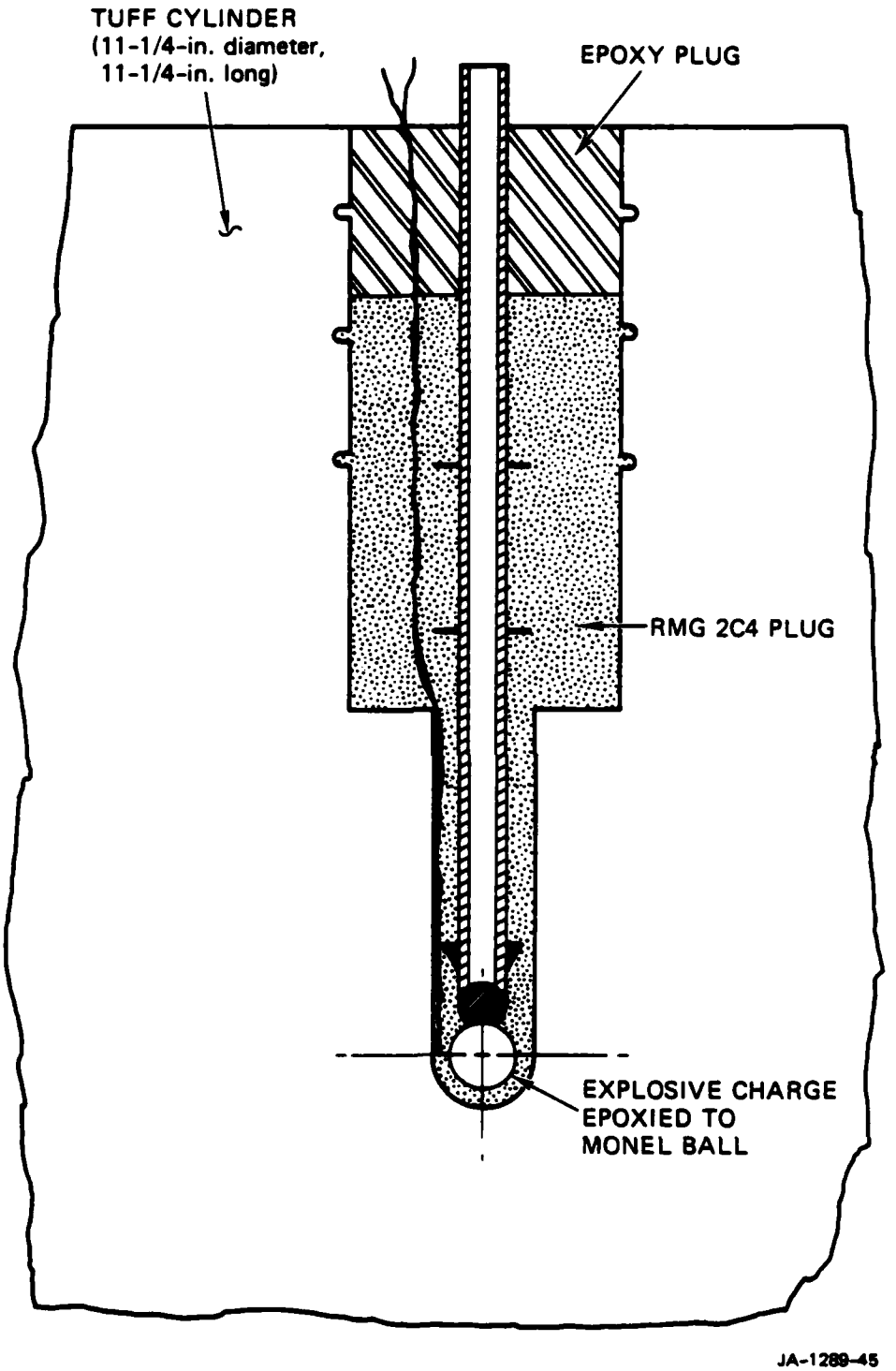

FIGURE 2.11 CONFIGURATION FOR EXPLODED CAVITY TESTS IN TUFF CYLINDER

SECTION 3
EXPERIMENTAL RESULTS

3.1 TEST SERIES

Hydrofracture tests were performed on unexploded and exploded cavity spheres so that by comparing pressure records we could assess the contribution of residual stress to containment. The experiments were specifically designed to provide the influence on containment of relevant parameters such as flow rate, material property, stress relaxation, cavity uncoupling, reduced overburden, and a nearby charge. In addition, sensors were embedded in separate spheres to provide particle velocity profiles in the region surrounding coupled and uncoupled exploded cavities. This section provides a complete description of the results. Conclusions based on these findings are in the summary of Section 1.2.

The types of experiments and the principal observations are summarized in Table 3.1. Unexploded cavity hydrofracture tests are grouped in Series 1 through 3; exploded cavity hydrofracture tests are grouped in Series 4 through 10; particle velocity tests are grouped in Series 11 and 12. In general, at least two tests were performed in each series to establish a measure of reproducibility. The specific areas of investigation were as follows:

- Flow rate (series 1, 2, and 5). The constant rate of fluid flow into a cavity is a parameter that controls the time to hydrofracture. In unexploded cavity tests, this parameter allows us to correlate fracture initiation with the time-dependent process of flow into microscopic imperfections. In exploded cavity tests, this parameter allows us to correlate fracture initiation with cavity gas pressure decay and residual stress relaxation. A flow rate of 122.4 cm^3/min was chosen so that hydrofractures could be performed within a scaled time of relevance (2 seconds) for underground nuclear tests (a scale factor of 1200 gives 40 minutes).

Table 3.1

SUMMARY OF CONTAINMENT INVESTIGATIONS

Series	General Description	Test Results (Figure)	Initial Cavity Diameter (in.)	Flow Rate (cm^3/min)	Test Numbers	Observations
Unexploded Cavity Hydrofracture Tests						
1	Flow Rate (RMG 2C4)	3.1	0.750	4.26 40.8 122.4	160 225 257,258 265	Fracture initiation pressure increased 14% with overall flow rate increase for RMG 2C4.
2	Flow Rate (LD 2C4)	3.2	0.750	4.26 122.4	193,194 275,276	Fracture initiation pressure increased 19% with flow rate increase for LD 2C4.
3	Material Property (LD 2C4 vs RMG 2C4)	3.3	0.750	122.4	275,276 257,258 265	Fracture initiation pressure 14% higher for RMG 2C4 than for LD 2C4 implying a greater fracture toughness.
Exploded Cavity Hydrofracture Tests						
4	Stress Relaxation (RMG 2C4)	3.4	0.404	122.4	244,245 248,254 281,284	Significant stress relaxation is indicated by 49% reduction in fracture initiation pressure as hydrofracture time is increased from 2s to 70s.
		3.5		4.26 40.8 122.4	158,159 169,170 227,229 232,249 244,245 248,254	
5	Flow Rate/ Stress Relaxation (LD 2C4)	3.6	0.404	4.26 122.4	215,216 262,266	Negligible stress relaxation is indicated by 11% reduction in fracture initiation pressure as hydrofracture time is increased from 3s to 127s.
		3.5	0.404	4.26 122.4	215,216 262,266	
6	Material Property (LD 2C4 vs RMG 2C4)	3.7	0.404	122.4	262,266 244,245 248,254	Fracture initiation pressure 35% lower for LD 2C4 than for RMG 2C4 implying a weaker residual stress field.
7	Uncoupled Cavity (3R and 1.5R)	3.8	0.404 1.212	122.4	244,245 248,254 261	Negligible residual stress formed around 3R cavity. Drainline reduced hydrofracture pressures. Water in cavity increased fracture initiation pressure. Water content of 1.5R cavities is uncertain.
		3.9	1.212	122.4	261,267 268	
		3.10	1.212	122.4	261,263 282	
		3.11	0.404 0.606	122.4	244,245 248,254 259,260	
8	Reduced Overburden (Coupled and 3R Uncoupled Cavity)	3.12	0.404	122.4	244,245 248,254 270	Reducing overburden had no effect on a coupled cavity, but reduced fracture initiation pressure of a 3R uncoupled cavity.
		3.13	1.212	122.4	261,285	

Table 3.1 (Concluded)

Series	General Description	Test Results (Figure)	Initial Cavity Diameter (in.)	Flow Rate (cm^3/min)	Test Numbers	Observations
9	Nearby Explosive Charge	3.14	0.404	122.4	244,245 248,254 280,283	Nearby explosive resulted in asymmetric cavity growth and lower hydrofracture pressures.
10	Material Property and Geometry (Tuff Cylinder vs RMG 2C4 Sphere)	3.15	0.404	122.4	244,245 248,254 278	Cavity expansion was less in tuff than in RMG 2C4 and resulted in dynamic cracking of the cavity.
Particle Velocity Tests						
11	Coupled Cavity	3.16 3.17	0.404	None	273 272,273	Particle velocity profiles for a coupled cavity reveal large residual strains to a radius of 4 cm.
12	Uncoupled Cavity (3R)	3.18 3.19	1.212	None	274 277	Residual strains surrounding a 3R uncoupled cavity are 20% those of a coupled cavity.

- Material property (series 3, 6, and 10). Rock-matching grout RMG 2C4, which approximates the documented properties of Nevada Test Site tuff, was chosen as the standard material. Effects of material property variations on hydrofracture were studied by testing a slightly weaker low-density grout containing air voids (LD 2C4). Unexploded and exploded cavity spheres were tested. In addition, exploded cavity testing of a tuff cylinder cored from the Nevada Test Site was performed.

- Stress relaxation (series 4 and 5). The explosively formed residual stress field surrounding an exploded cavity in RMG 2C4 is degraded with time because of material relaxation. Hydrofracture experiments, in which pumping was delayed for 10 seconds following charge detonation while cavity gas pressure decayed, were performed to measure the gas pressure and to study stress relaxation.

- Uncoupled cavity (series 7 and 8). In a fully coupled exploded cavity test, an explosive charge is in direct contact with the surrounding medium, and maximum residual stresses and cavity gas pressures are generated. In an uncoupled exploded cavity test, the explosive charge is separated from the surrounding by an annular region of air and the resulting residual stresses and cavity gas pressure are reduced. The coupling parameter (ratio of initial cavity diameter to charge diameter) defines the degree of uncoupling. Hydrofracture tests were performed on uncoupled exploded cavity spheres with coupling parameters of 1.5 and 3 to assess relevant combinations of residual stress and cavity pressure.

- Reduced overburden (series 8). External pressure applied to a grout sphere simulates the in situ overburden stress associated with depth-of-burial of an underground nuclear test. A pressure of 1000 psi (6.895 MPa) simulates the stress for a typical test. Coupled and uncoupled exploded cavity tests were performed with 500 psi (3.447 MPa) external pressure to assess the effects on containment of a reduced depth-of-burial.

- Nearby charge (series 9). Simultaneous detonation of nearby nuclear devices represents an economical means of increasing the rate of underground testing. Hydrofracture experiments, in which two explosive charges were cast in a RMG 2C4 sphere, were performed to assess the cavity pressure and asymmetric stress field associated with simultaneous detonation of nearby charges.

- Particle velocity measurements (series 11 and 12). The particle velocity profile associated with charge detonation in RMG 2C4 provides a measure of the residual stress field intensity and represents a valuable source of data for verification of mechanics codes. Particle velocity pulses were measured at various distances from the explosive charge in coupled and uncoupled exploded cavity spheres.

3.2 UNEXPLODED CAVITY HYDROFRACTURE TESTS

The configuration shown in Figure 2.7 was used for all unexploded cavity tests. A cavity diameter of 3/4 inch (1.90 cm) was chosen because it corresponds to the exploded cavity diameter generated by a 3/8-gram charge in previous tests. The external pressure applied to each sphere was fixed at 1000 psi (6.895 MPa) to simulate the hydrostatic overburden pressure in nuclear tests typically conducted at a depth of 1100 feet (335 m) in tuff with a density of 2.1 g/cm^3. Water dyed with Rhodamine B was the hydrofracture fluid.

Series 1 - Flow Rate (RMG 2C4)

The pressure records for unexploded cavity RMG 2C4 spheres hydrofractured at three different flow rates (4.26, 40.8, and 122.4 cm^3/min) are shown in Figure 3.1. The low flow rate test (160) and the intermediate flow rate test (225) were performed previously[7,8] and are typical results included for comparison purposes. The high flow rate tests (257, 258, 265) were performed primarily to provide a comparison for exploded cavities hydrofractured within scaled times of relevance, but they also provide data for fracture initiation studies in unexploded cavities. The records in Figure 3.1 are representative of unexploded cavity tests in that a smooth increase in pressure is followed by a sharp drop to form a well-defined peak. Previous fracture initiation studies[5] have shown that the pronounced spike represents initiation of a microscopic crack in the cavity wall. Average fracture initiation pressures for the low, intermediate, and high flow rate tests were 1870 psi (12.89 MPa), 1850 psi (12.75 MPa), and 2140 psi (14.75 MPa), respectively. Hence a 14% increase in fracture initiation pressure is attributed to the highest flow rate, indicating that fracture initiation is slightly influenced by the flow rate creating pressure gradients in microscopic imperfections in the cavity wall.

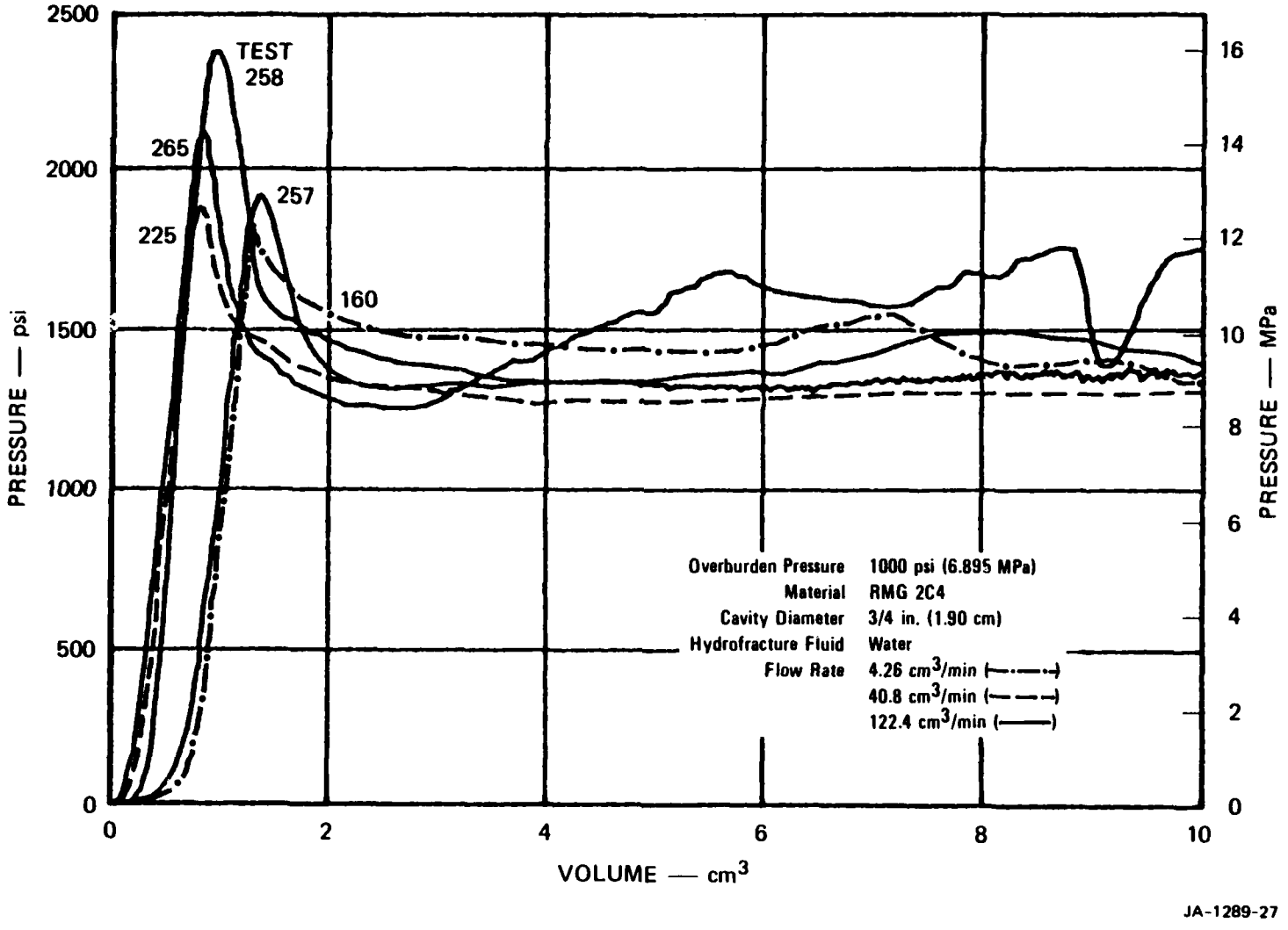

FIGURE 3.1 HYDROFRACTURE PRESSURES FOR UNEXPLODED CAVITY TESTS–FLOW RATE EFFECT IN RMG 2C4

Following fracture initiation of an unexploded cavity, a crack continues to grow as cavity pressure decays to a plateau. This steady-state pressure provides a measure of flow resistance along the fracture plane. In test 265, cavity pressure increased slowly and erratically from the plateau, indicating an increasing and unsteady pressure gradient along the fracture plane. High late-time pressures are typically associated with a fracture intersecting the surface of the sphere over a small arc, which occurred in test 265.

Series 2 - Flow Rate (LD 2C4)

The pressure records for unexploded cavity LD 2C4 spheres hydrofractured at two different flow rates (4.26 and 122.4 cm^3/min) are shown in Figure 3.2. Records from low flow rate tests (193, 194) performed previously[7] are included for comparison. The high flow rate tests (275, 276) were performed to provide data for flow rate effects on unexploded cavity spheres, comparison data for exploded cavity spheres hydrofractured within scaled times of relevance, and data for RMG 2C4 spheres to show the effects on containment of changes in material properties.

The records of Figure 3.2 are representative of unexploded cavity tests in that a smooth increase in pressure is followed by a decrease to form a well-defined fracture initiation peak. Average fracture initiation pressures for the low and high flow rate tests were 1570 psi (10.82 MPa) and 1870 psi (12.89 MPa), respectively, so the higher rate caused an increase in pressure of 19%.

Series 3 - Material Property (LD 2C4 versus RMG 2C4)

The results of high flow rate tests in RMG 2C4 (Series 1) and LD 2C4 (Series 2) are compared in Figure 3.3 to show the effects on containment of changes in material properties. The average fracture initiation pressure decreased from 2140 psi (14.75 MPa) for RMG 2C4 to 1870 psi (12.89 MPa) for LD 2C4. The 13% decrease reflects the 13% lower tensile strength of the low-density material, and implies a lower fracture toughness.

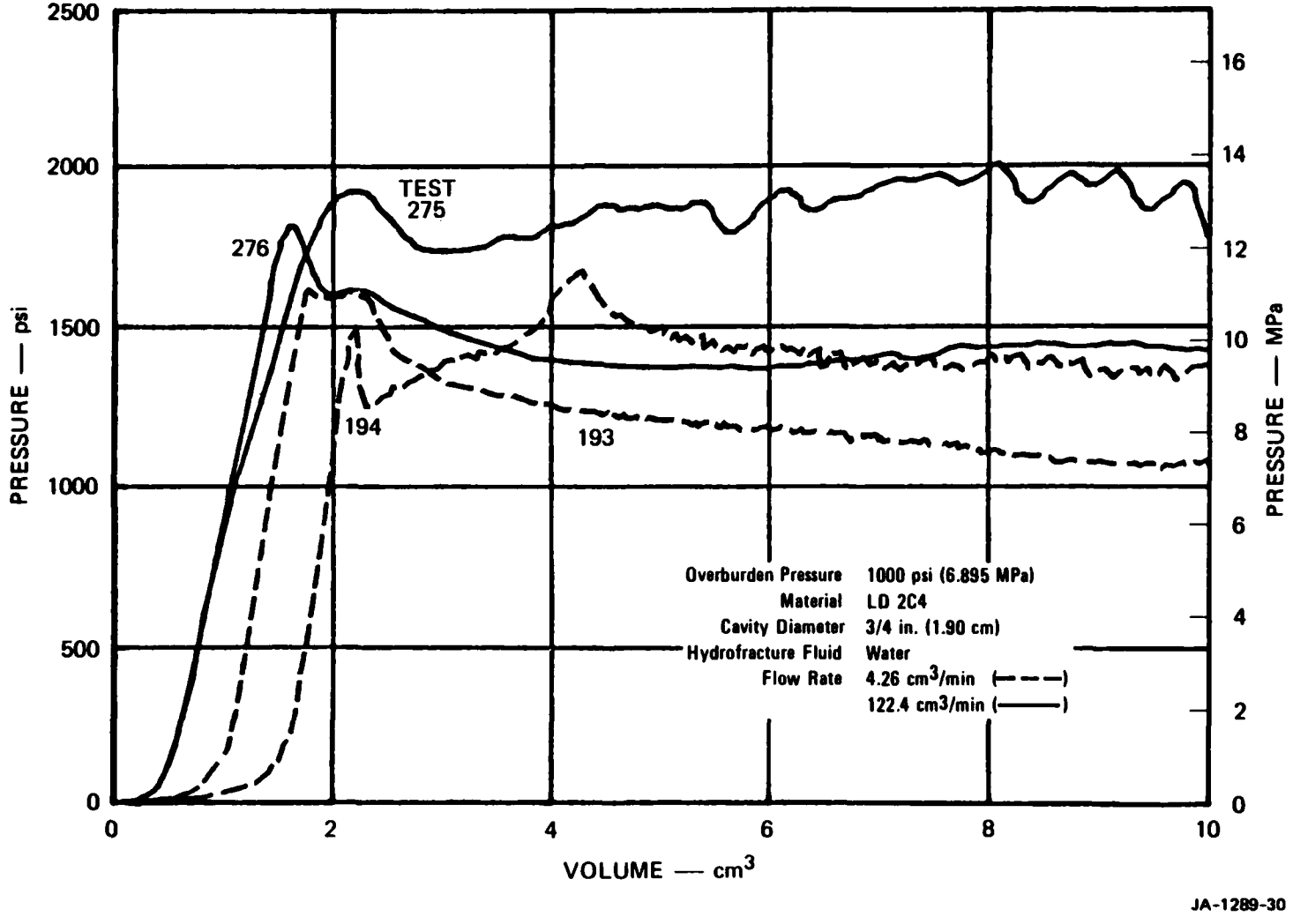

FIGURE 3.2 HYDROFRACTURE PRESSURES FOR UNEXPLODED CAVITY TESTS–FLOW RATE EFFECT IN LD 2C4

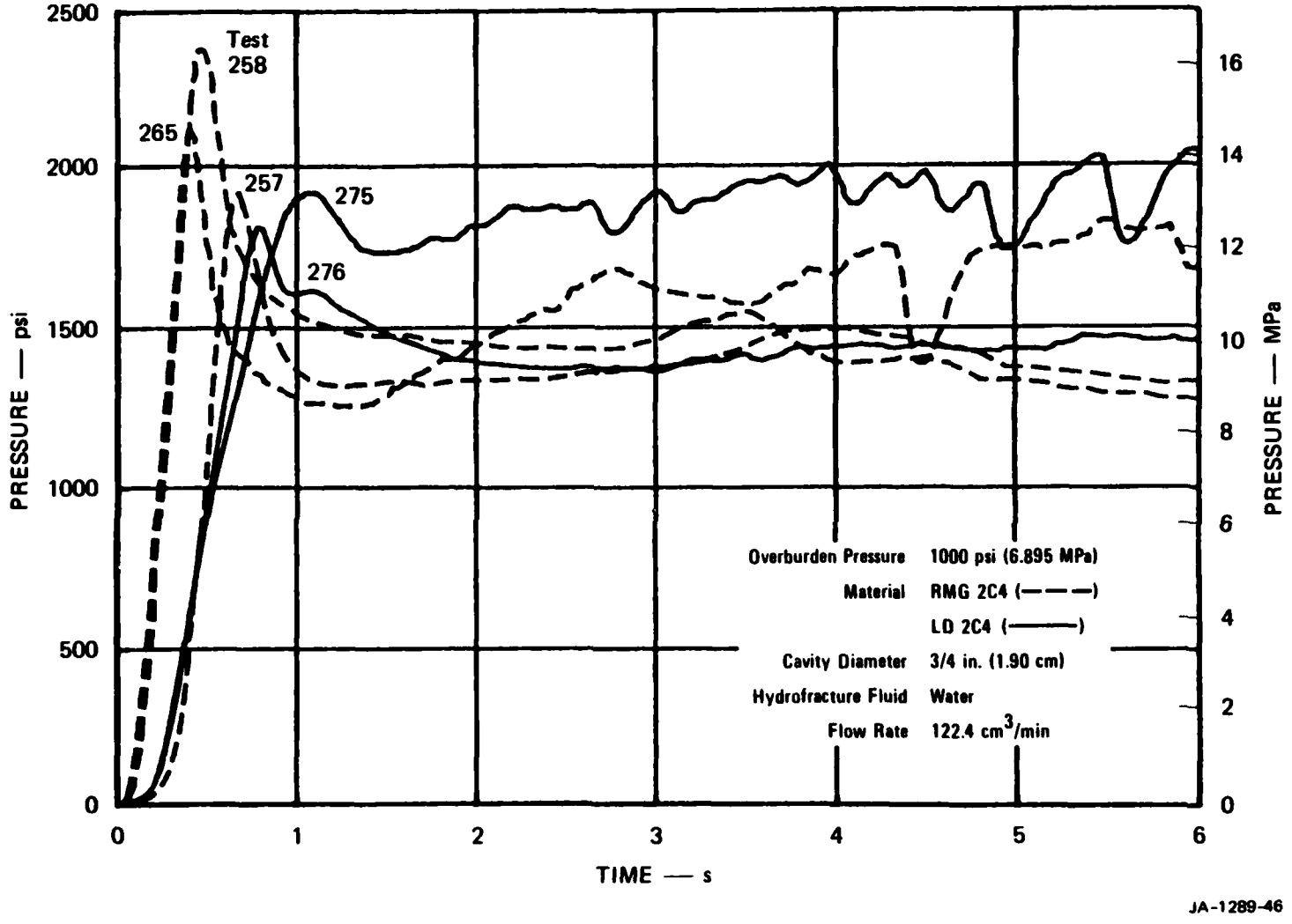

FIGURE 3.3 HYDROFRACTURE PRESSURES FOR UNEXPLODED CAVITY TESTS–MATERIAL PROPERTY EFFECT (LD 2C4 versus RMG 2C4)

3.3 EXPLODED CAVITY HYDROFRACTURE TESTS

The basic configuration shown in Figure 2.4 was used for fully coupled exploded cavity tests. The configuration shown in Figure 2.9 was used for uncoupled tests. The standard external pressure applied to a sphere was 1000 psi (6.895 MPa). Water dyed with Rhodamine B was the hydrofracture fluid in all tests.

Series 4 - Stress Relaxation (RMG 2C4)

Figure 3.4 shows the pressure records for coupled exploded cavity tests (281 and 284) in which pumping was delayed for 10 seconds following charge detonation while the decaying cavity gas pressure was measured. The subsequent hydrofracture records were thus influenced by unloading at the cavity wall as well as the extended period of stress relaxation. For comparison, the dashed curves in the figure show typical pressure records for standard experiments, performed at the same flow rate, but in which pumping started at the time of charge detonation. The effect of the cavity unloading and stress relaxation was to reduce the average fracture initiation pressure from 5610 psi (38.68 MPa) to 4780 psi (32.96 MPa).

An overall indication of the effects of stress relaxation on containment is shown in Figure 3.5, where average fracture initiation pressures are plotted against time from detonation. Results from all relevant flow rate tests and delayed hydrofracture tests are included. For RMG 2C4, significant stress relaxation occurs during the first 10 seconds following charge detonation. However, because the 3000 psi (20.68 MPa) average fracture initiation pressure obtained after 80 seconds is 60% higher than the corresponding value of 1870 psi (12.89 MPa) for an unexploded cavity sphere, a beneficial residual stress remains for an extended period of time.

The cavity gas pressure shown in Figure 3.4 for tests 281 and 284 decays more rapidly than the corresponding pressure shown in Figure A.1 for a rigid 2R cavity. The pore water available in RMG 2C4 probably contributes to the pressure decay by cooling the detonation products.

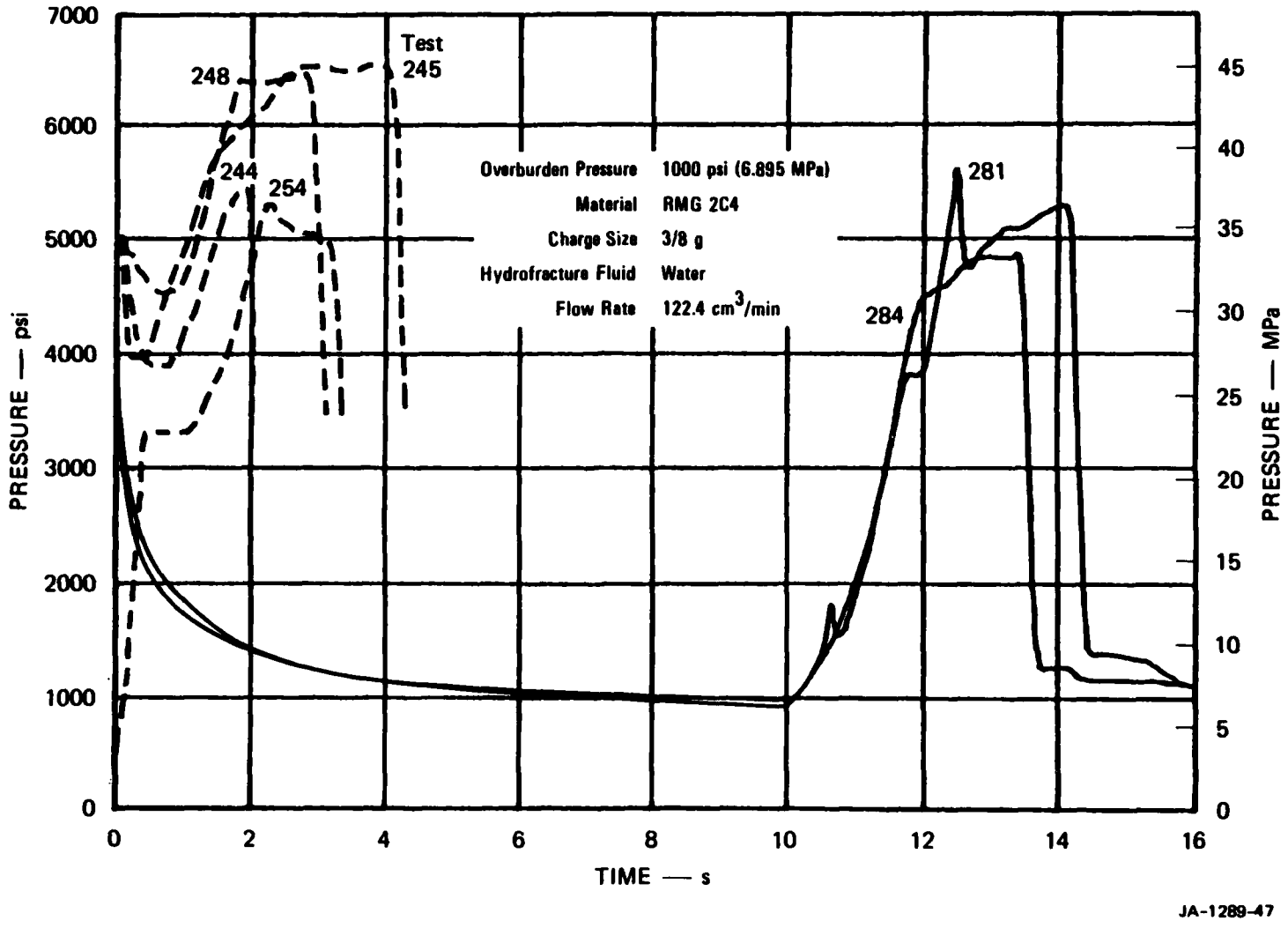

FIGURE 3.4 HYDROFRACTURE PRESSURES FOR UNVENTED EXPLODED CAVITY TESTS–STRESS RELAXATION EFFECT IN RMG 2C4

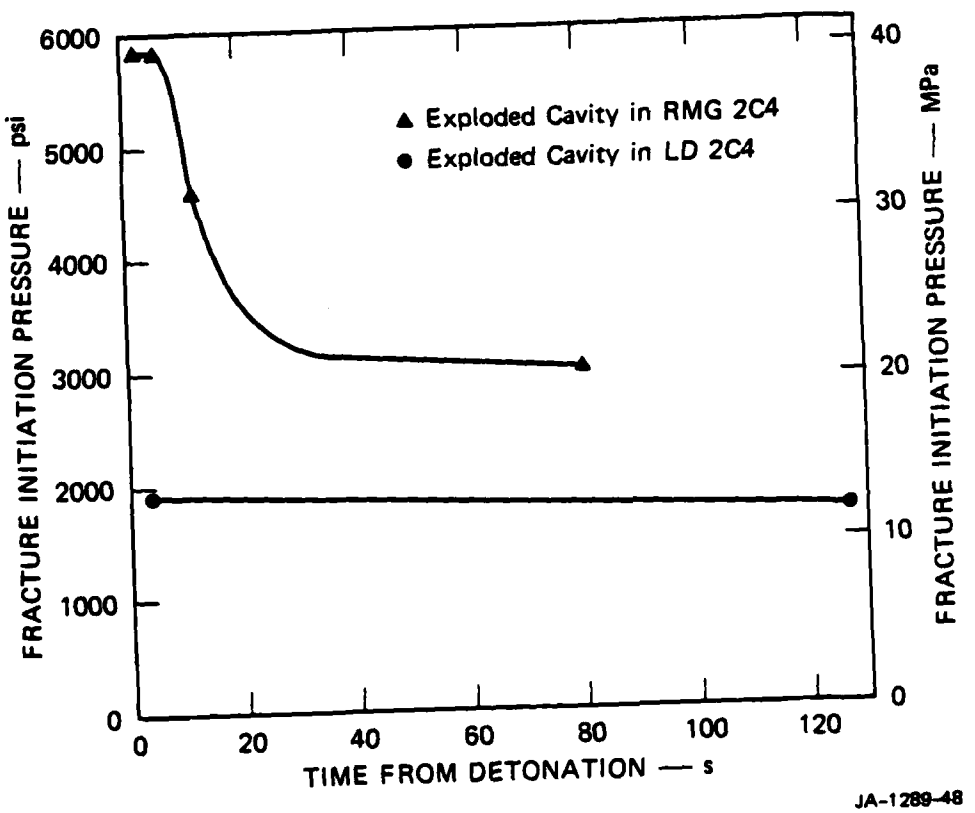

FIGURE 3.5 FRACTURE INITIATION PRESSURES FOR UNVENTED EXPLODED CAVITY TESTS-STRESS RELAXATION EFFECT IN RMG 2C4 AND LD 2C4

Series 5 - Flow Rate/Stress Relaxation (LD 2C4)

The pressure records for exploded cavity LD 2C4 spheres hydrofractured at two different flow rates (4.26 and 122.4 cm^3/min) are shown in Figure 3.6. The low flow rate tests (215 and 216) were performed previously[7] and are typical results included for comparison purposes. The high flow rate tests (262 and 266) provide hydrofracture results for the scaled times of relevance. As the flow rate was increased, the average fracture initiation pressure increased from 1720 psi (11.86 MPa) to 1940 psi (13.38 MPa), and as shown in Figure 3.5, the corresponding fracture initiation time decreased from 127 seconds to 3.4 seconds. Because these average pressures are comparable to the corresponding values of 1570 psi (10.82 MPa) and 1870 psi (12.89 MPa) for unexploded cavity LD 2C4 spheres, the residual stress field surrounding an exploded cavity in LD 2C4 is weak. In addition, because the 13% increase in fracture initiation pressure with flow rate for the exploded cavity tests is comparable to the 19% increase observed for the unexploded cavity tests (series 2), flow rate effects dominate any residual stress decay in the low-density material.

Series 6 - Material Property (LD 2C4 versus RMG 2C4)

Hydrofracture results for RMG 2C4 and LD 2C4 are compared in Figure 3.7 to show the effects on containment of a change in material properties. Exploded cavity tests in RMG 2C4 are characterized by an initially strong residual stress field which decays rapidly soon after charge detonation. Exploded cavity tests in LD 2C4 are characterized by a weak residual stress field. The significant distinction of the low-density material in comparison with RMG 2C4 is a 13% air void content, which represents a property shift from tuff to alluvium. This feature allows for the formation of an exploded cavity with a final-to-initial radius ratio of 2.3, compared with the ratio of 2.0 for RMG 2C4.

Dynamic pressure pulses measured at the bottom of the containment vessel during several tests are shown in Figure C.2. The average maximum reflected pressure and impulse for LD 2C4 are 238 psi (1.64 MPa) and 2.7 psi·ms (0.019 MPa·ms), respectively. The corresponding maximum values

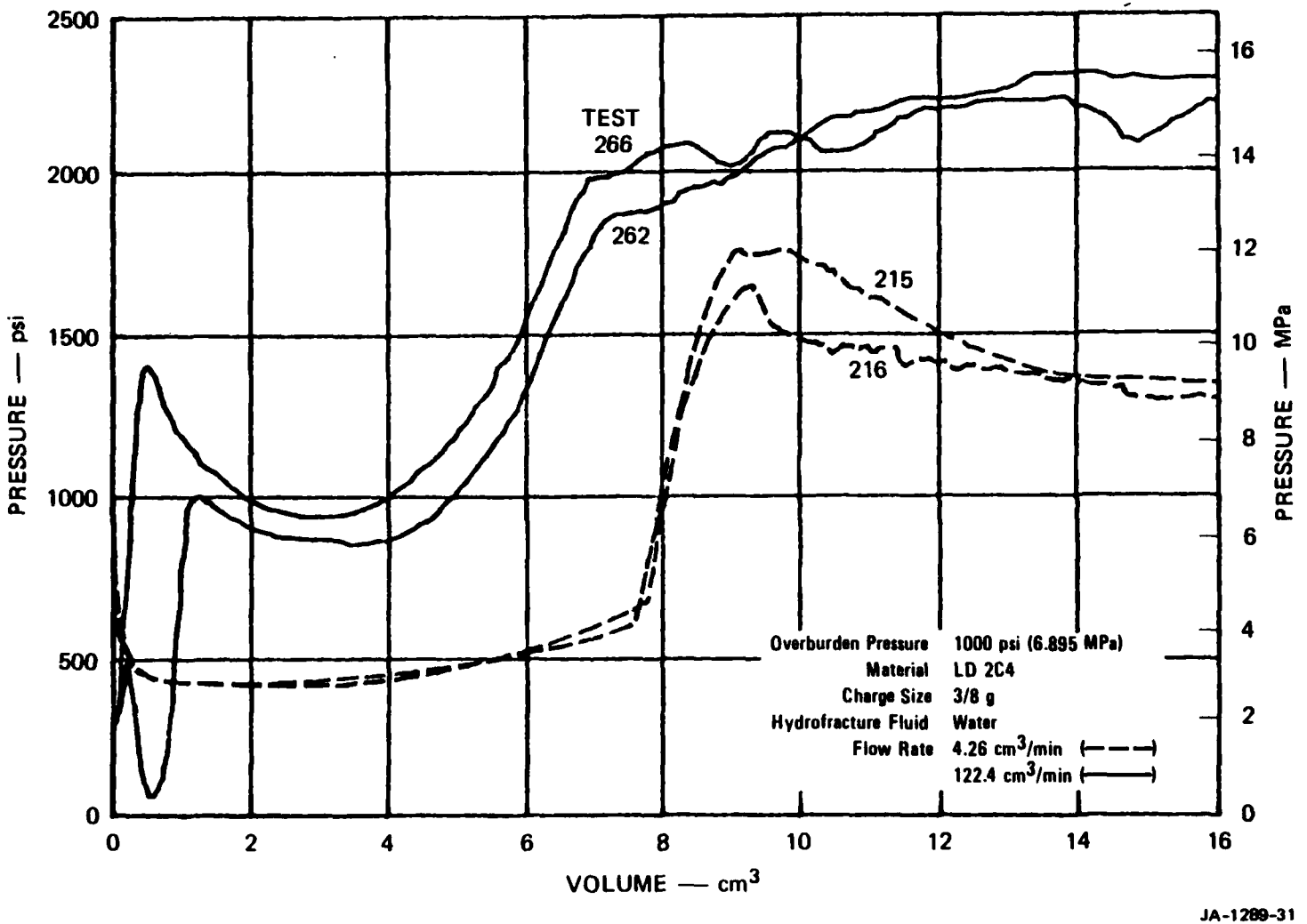

FIGURE 3.6 HYDROFRACTURE PRESSURES FOR UNVENTED EXPLODED CAVITY TESTS– FLOW RATE AND STRESS RELAXATION EFFECTS IN LD 2C4

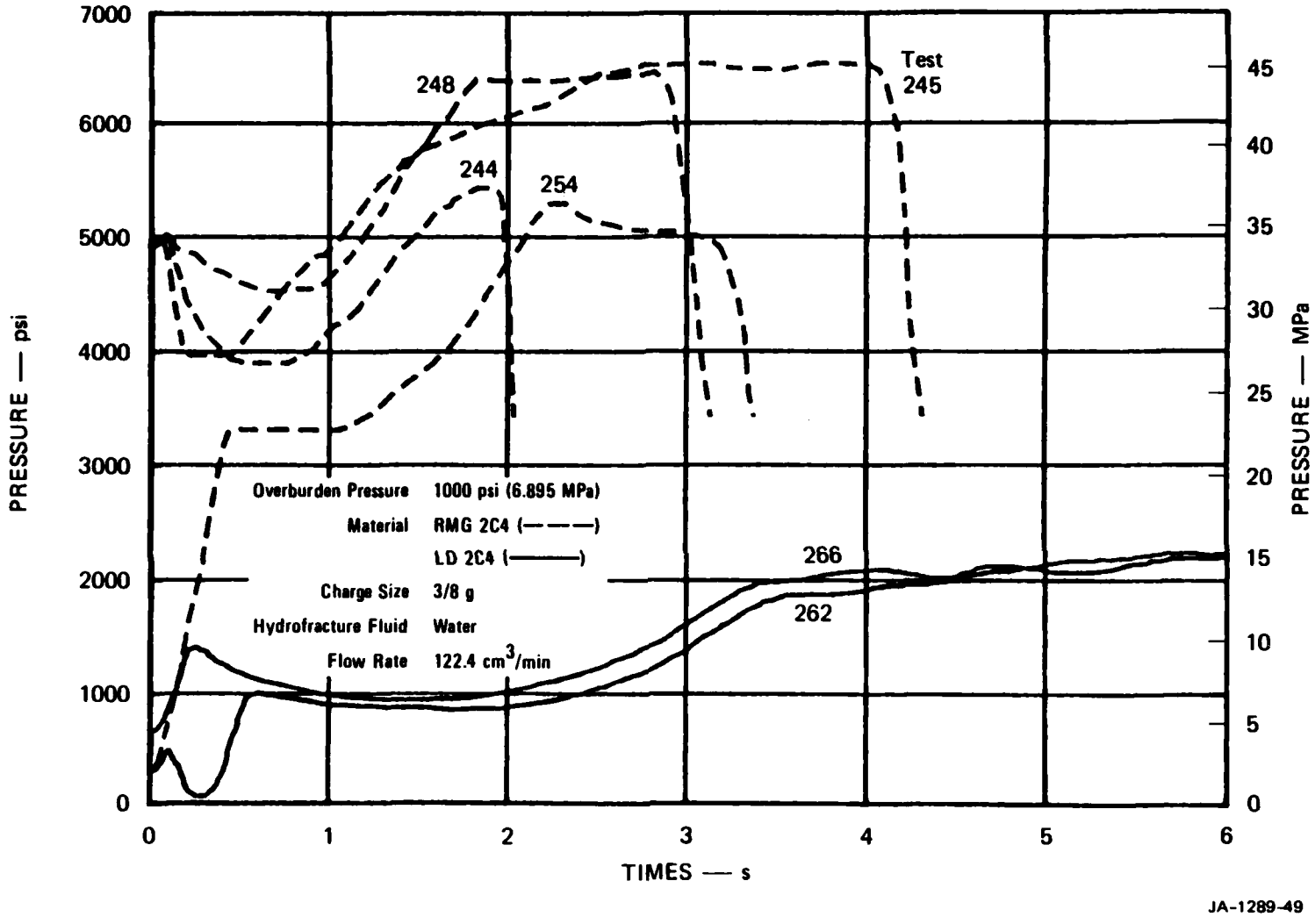

FIGURE 3.7 HYDROFRACTURE PRESSURES FOR UNVENTED EXPLODED CAVITY TESTS–MATERIAL PROPERTY EFFECT (LD 2C4 versus RMG 2C4)

for RMG 2C4 are 822 psi (5.67 MPa) and 12.1 psi·ms (0.083 MPa·ms). Hence, attenuation of the stress wave associated with charge detonation is more pronounced in the low-density material. Explosive crushing of air voids is the process by which energy is absorbed without the generation of significant residual stresses.

Series 7 - Uncoupled Cavity (3R and 1.5R)

A series of uncoupled cavity tests was performed for the relevant coupling parameters of 1.5 and 3 to assess the containment ability of these configurations. In addition, corresponding tests were performed in a rigid steel vessel to provide data for evaluating the results in RMG 2C4.

As shown in Figure 3.8, the hydrofracture record for the 3R test 261 is consistent with the record for the rigid cavity test A9. Hence, test 261 is considered to represent a valid uncoupled cavity test. The 2250-psi (15.51-MPa) fracture initiation pressure is considerably less than the 5610-psi (38.68-MPa) average for the corresponding fully coupled cavities, but is comparable to the 2140-psi (14.75-MPa) average for unexploded cavity tests in RMG at the same flow rate (122.4 cm^3/min). Hence, a negligible residual stress field is generated in the regior surrounding the uncoupled exploded cavity. The negligible cavity growth associated with charge detonation supports this conclusion.

Figure 3.9 shows the hydrofracture records for two additional 3R uncoupled cavity tests (267 and 268). The fracture initiation pressures in these tests are well below 2250 psi (15.51 MPa) value for test 267 because a drainline from the cavity acted as a stress concentrator that allowed local dynamic fracture. Although these experiments were for development of a system to prevent water from occupying the space around the charge, the hydrofracture results are included here to emphasize that perturbing features may have a large effect on containment pressures.

Figure 3.10 shows the hydrofracture records for a series of 3R tests in which various amounts of water were in the cavity at the time of charge detonation. Water entered the cavity inadvertently in tests 263 and 282,

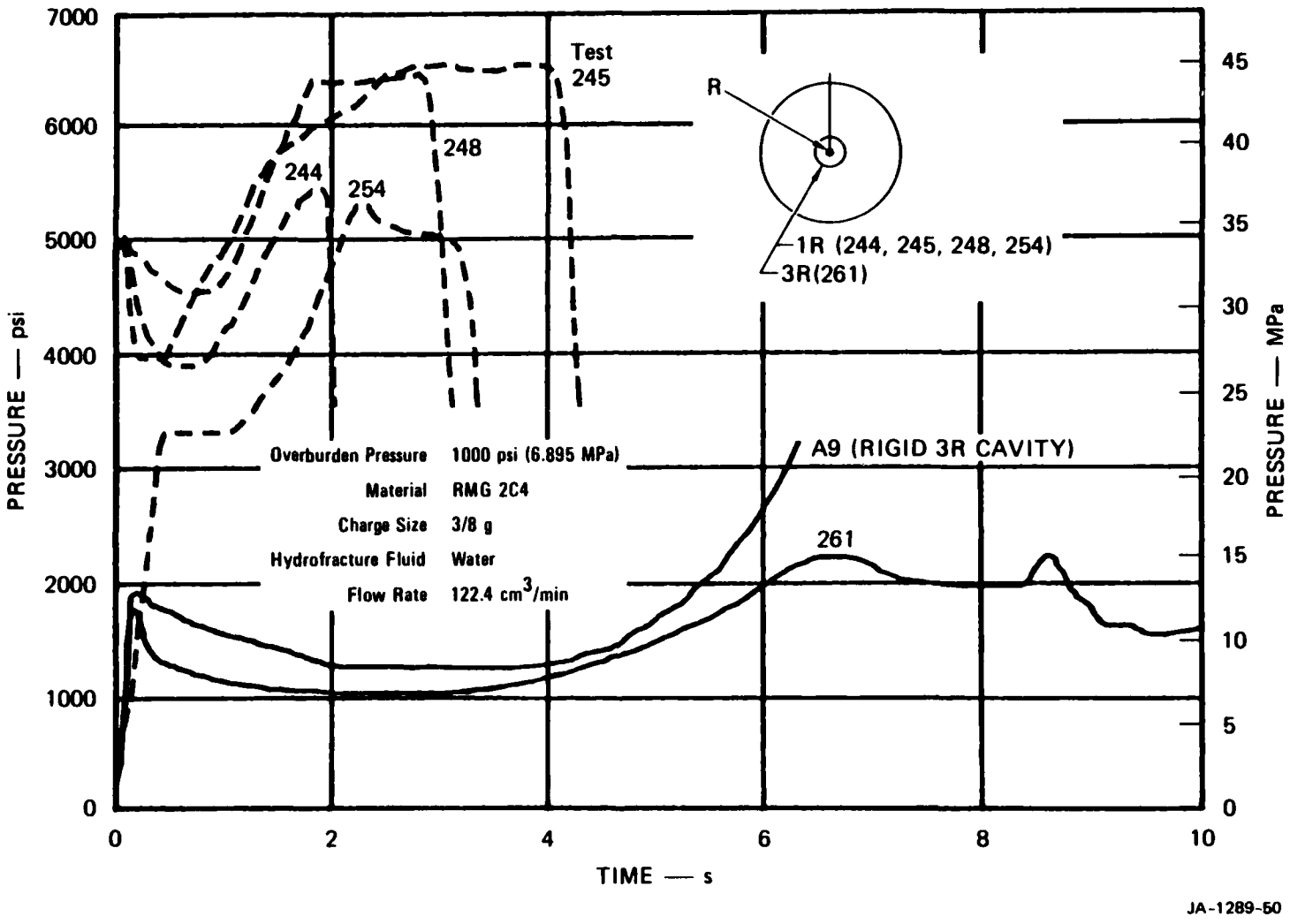

FIGURE 3.8 HYDROFRACTURE PRESSURES FOR UNVENTED EXPLODED CAVITY TESTS–3R UNCOUPLED CAVITY EFFECT

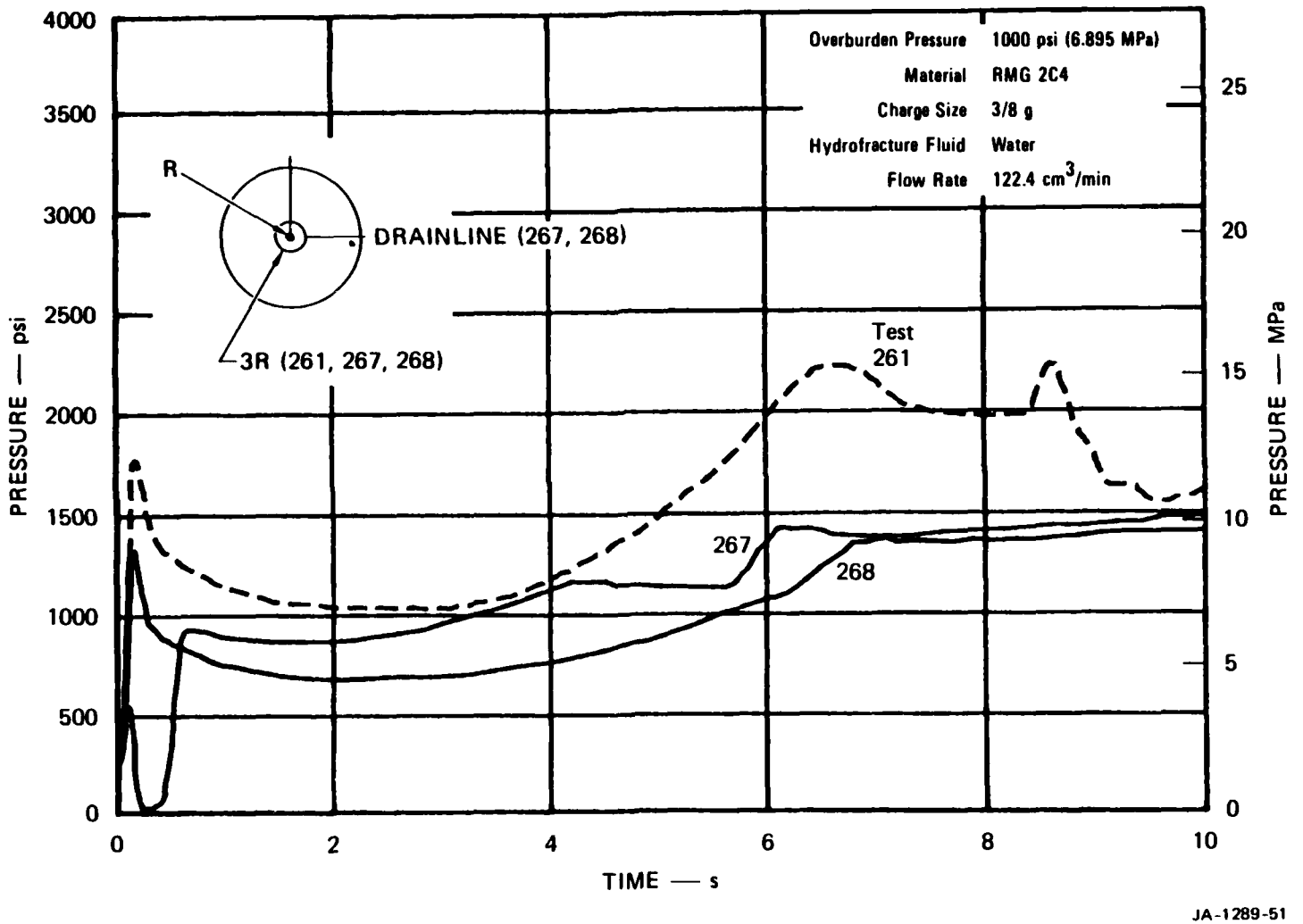

FIGURE 3.9 HYDROFRACTURE PRESSURES FOR 3R UNCOUPLED EXPLODED CAVITY TESTS–DRAINLINE EFFECT

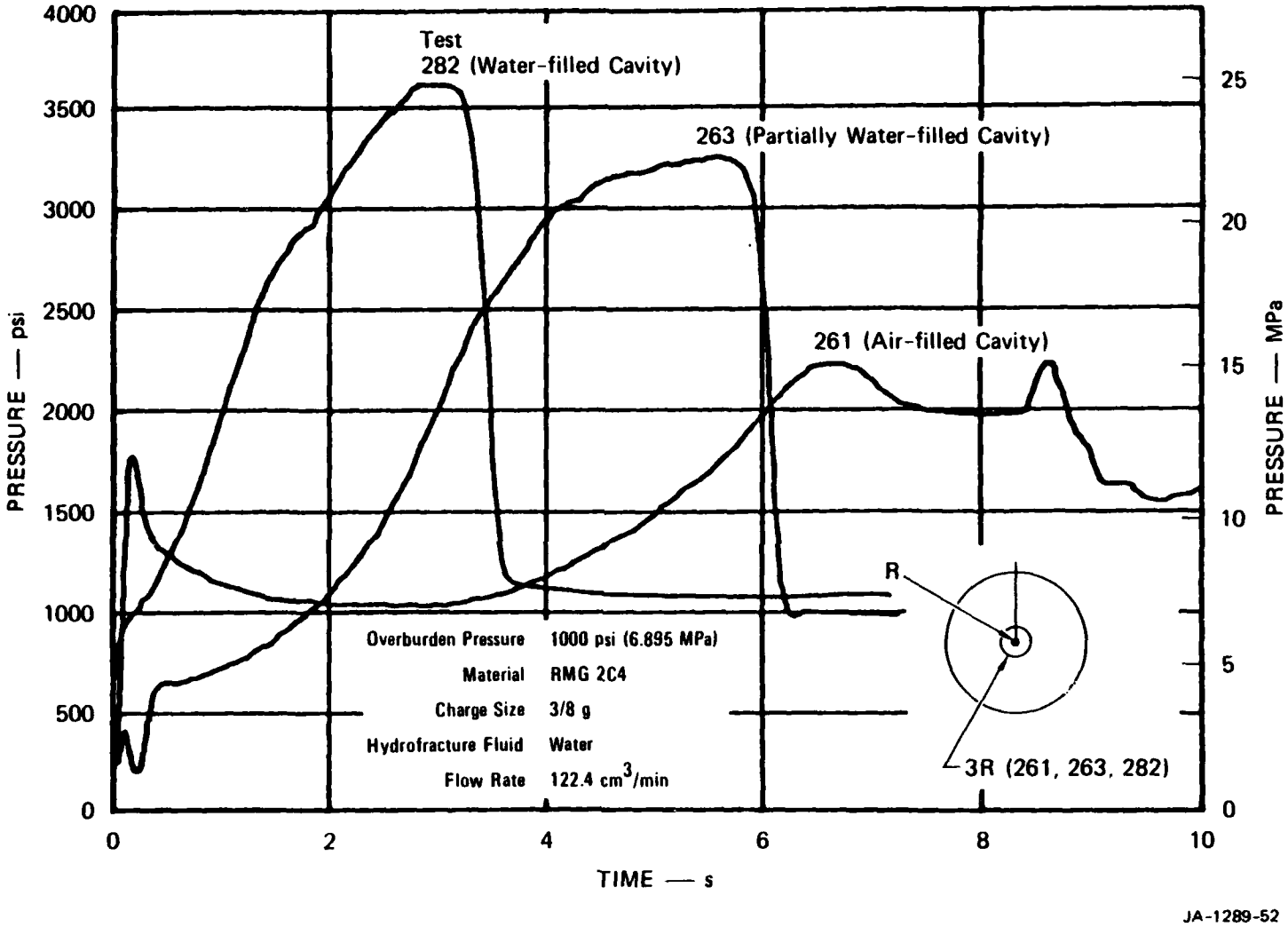

FIGURE 3.10 HYDROFRACTURE PRESSURES FOR 3R UNCOUPLED EXPLODED CAVITY TESTS–WATER IN CAVITY EFFECT

but the results are presented to show that the water serves as the effective coupling between the charge and surrounding material by increasing the fracture initiation pressure. Also, a rigid cavity test was performed with the cavity half-filled with water to simulate the conditions in a partially filled cavity in RMG 2C4. The initial pressure in the rigid cavity was 700 psi (4.83 MPa) and the subsequent decay was slow. These results are consistent with the results of test 263 and indicate that water in the cavity also provides an effective means of reducing the initial cavity gas pressure.

Dynamic pressure pulses measured at the bottom of the containment vessel during the 3R tests are shown in Figure C.4. The pulses for the cavities that remained dry (tests 261, 267, and 268) are similar, having an average peak pressure of 860 psi (5.93 MPa) and an average impulse of 3.2 psi•ms (0.022 MPa•ms). The pulses for the cavities with water (tests 263 and 285) are distinctly different, having a peak pressure of 1380 psi (9.51 MPa) and an impulse of 7.2 psi•ms (0.050 MPa•ms) for the partially filled cavity (test 263), and a peak pressure and impulse of 1270 psi (8.76 MPa) and 13.6 psi•ms (0.094 MPa•ms) for the completely filled cavity (test 282).

The hydrofracture records for two 1.5R uncoupled cavity tests (259 and 260) are shown in Figure 3.11. The exploded cavity diameter in these tests was found to equal that of the fully coupled configuration [0.808 inch (2.05 cm)]. Hence, cavity gas pressure should be comparable. Because the cavity gas pressure for the 1.5R tests [approximately 2500 psi (17.24 MPa) - 0.6 second] was significantly below the corresponding values for fully coupled RMG 2C4 cavities and a rigid 2R cavity (test A12), the indication is that the 1.5R configuration contained water at the time of charge detonation. The early breakdown of the sphere in test 259 is attributed to a dynamically induced fracture along the access tube.

Dynamic pressure pulses measured at the bottom of the containment vessel during the 1.5R tests are shown in Figure C.5.

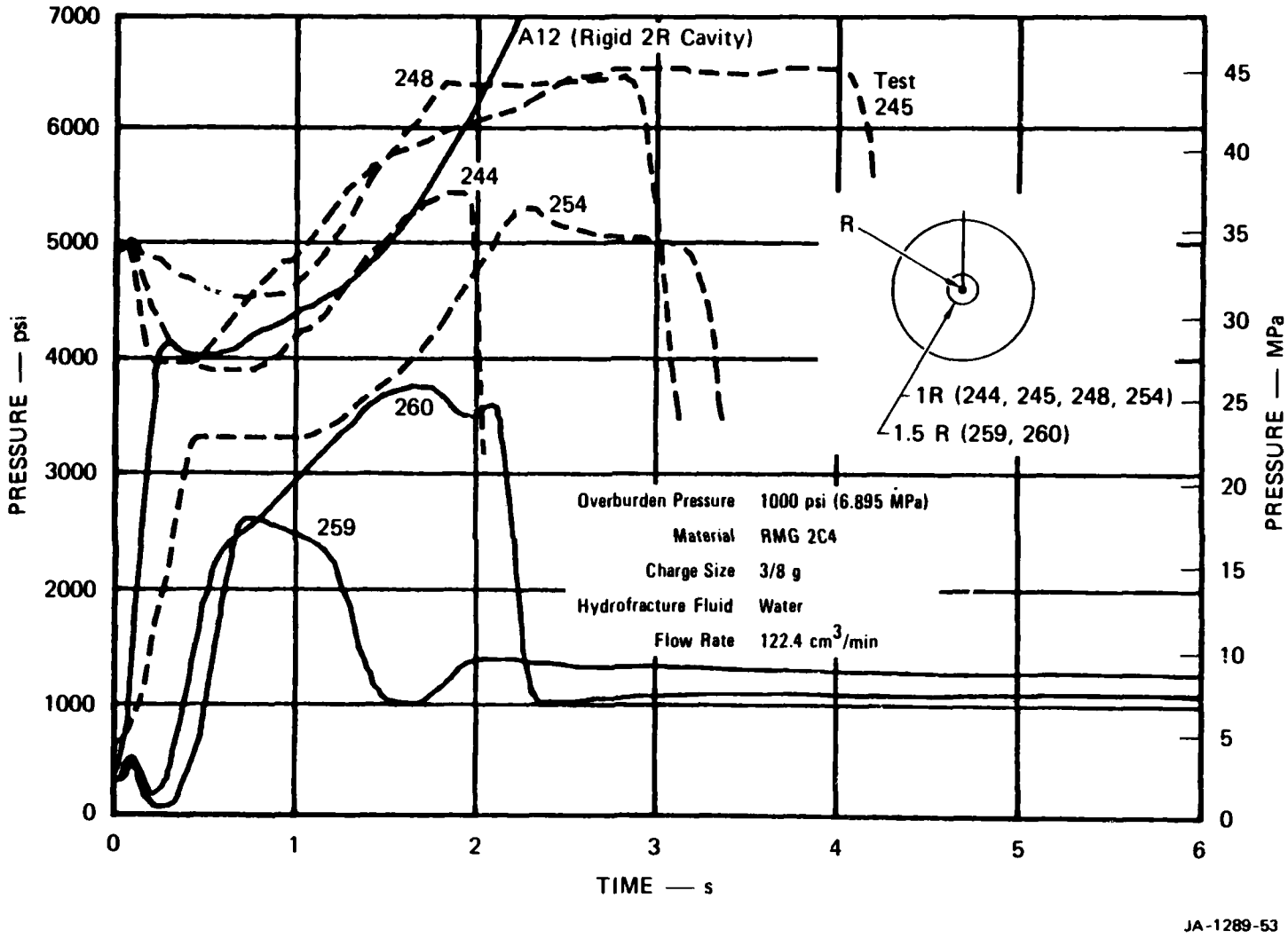

FIGURE 3.11 HYDROFRACTURE PRESSURES FOR UNVENTED EXPLODED CAVITY TESTS–1.5R UNCOUPLED CAVITY EFFECT

Series 8 - Reduced Overburden (Coupled and 3R Uncoupled Cavity)

The hydrofracture records for exploded cavity RMG 2C4 spheres subjected to confining pressures of 1000 psi (6.895 MPa) and 500 psi (3.447 MPa) are shown in Figure 3.12. The higher overburden tests (244, 245, 248, and 254) were previously performed.[8] The lower overburden test (270) was performed to assess the effects on containment of a reduced depth-of-burial. Similarity of the pressure records implies that a residual stress field dominates the overburden stress and consequently that underground nuclear tests may not always need to be buried so deeply. Previous tests have shown, however, that if the overburden pressure is further reduced, dynamic cracking may occur before the residual stress field is established.

Dynamic pressure pulses measured at the bottom of the containment vessel are shown in Figure C.1. The pulse generated during the reduced overburden test is typical of results for all exploded cavity tests in RMG 2C4.

Figure 3.13 shows the hydrofracture records for 3R uncoupled cavity spheres subjected to confining pressures of 1000 psi (6.895 MPa) and 500 psi (3.447 MPa). The 1520 psi (10.48 MPa) fracture initiation pressure for the reduced overburden test (285) is 670 psi (4.76 MPa) lower than the value for the test at the standard overburden (261). This result is also observed in unexploded cavity tests, and thus represents further evidence that the residual stress field surrounding a 3R uncoupled cavity is negligible.

Although the initial cavity gas pressure in both 3R tests was similar, the decay was more rapid in test 285 and is attributed to a leak path along the charge wires. The reduced overburden and weak residual stress apparently did not provide a sufficient compressive stress field to adequately seal the cavity. The unloading at the cavity wall due to this loss of pressure probably had negligible effect on the fracture initiation pressure because the initial loading into the plastic range was small.

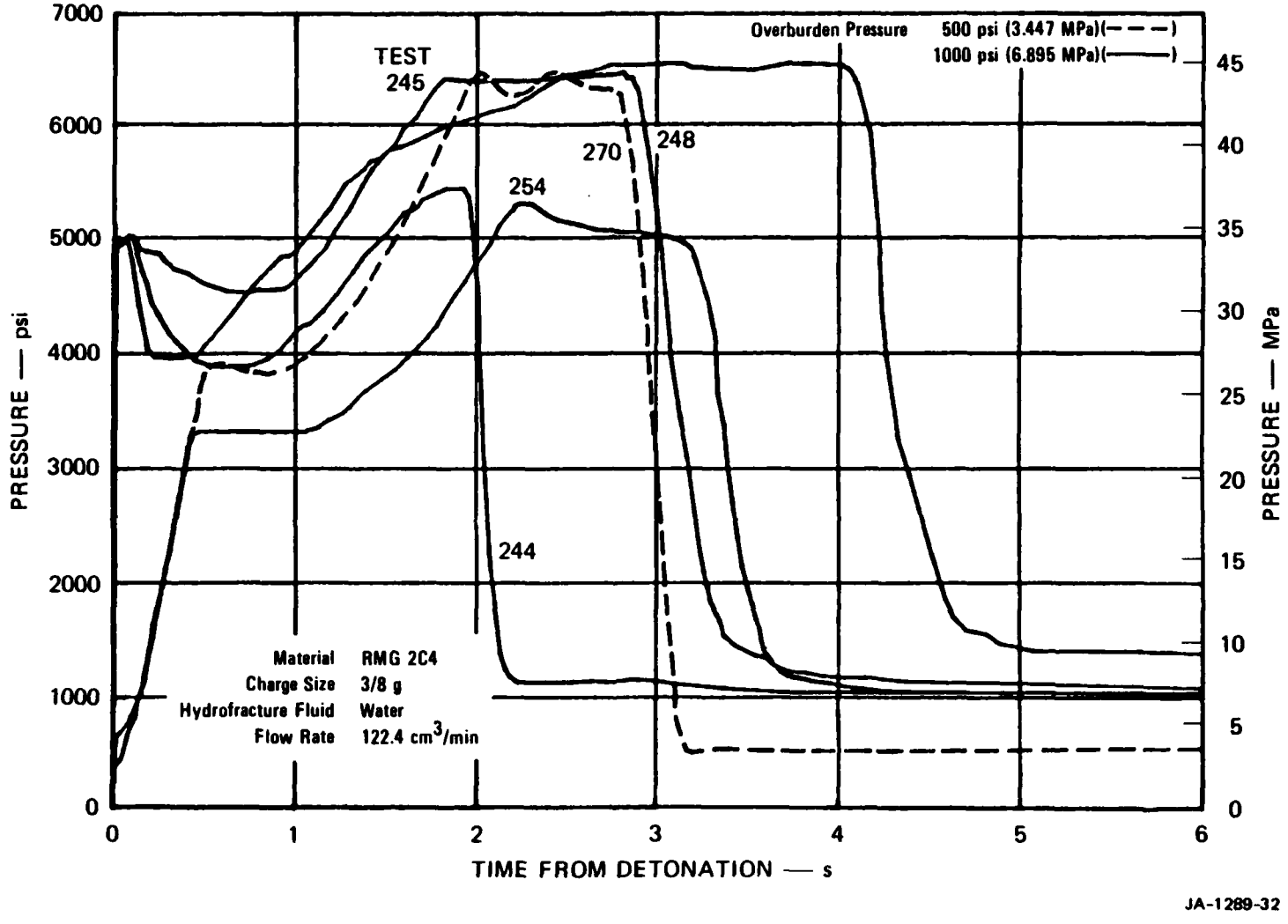

FIGURE 3.12 HYDROFRACTURE PRESSURES FOR UNVENTED EXPLODED CAVITY TESTS–OVERBURDEN EFFECT

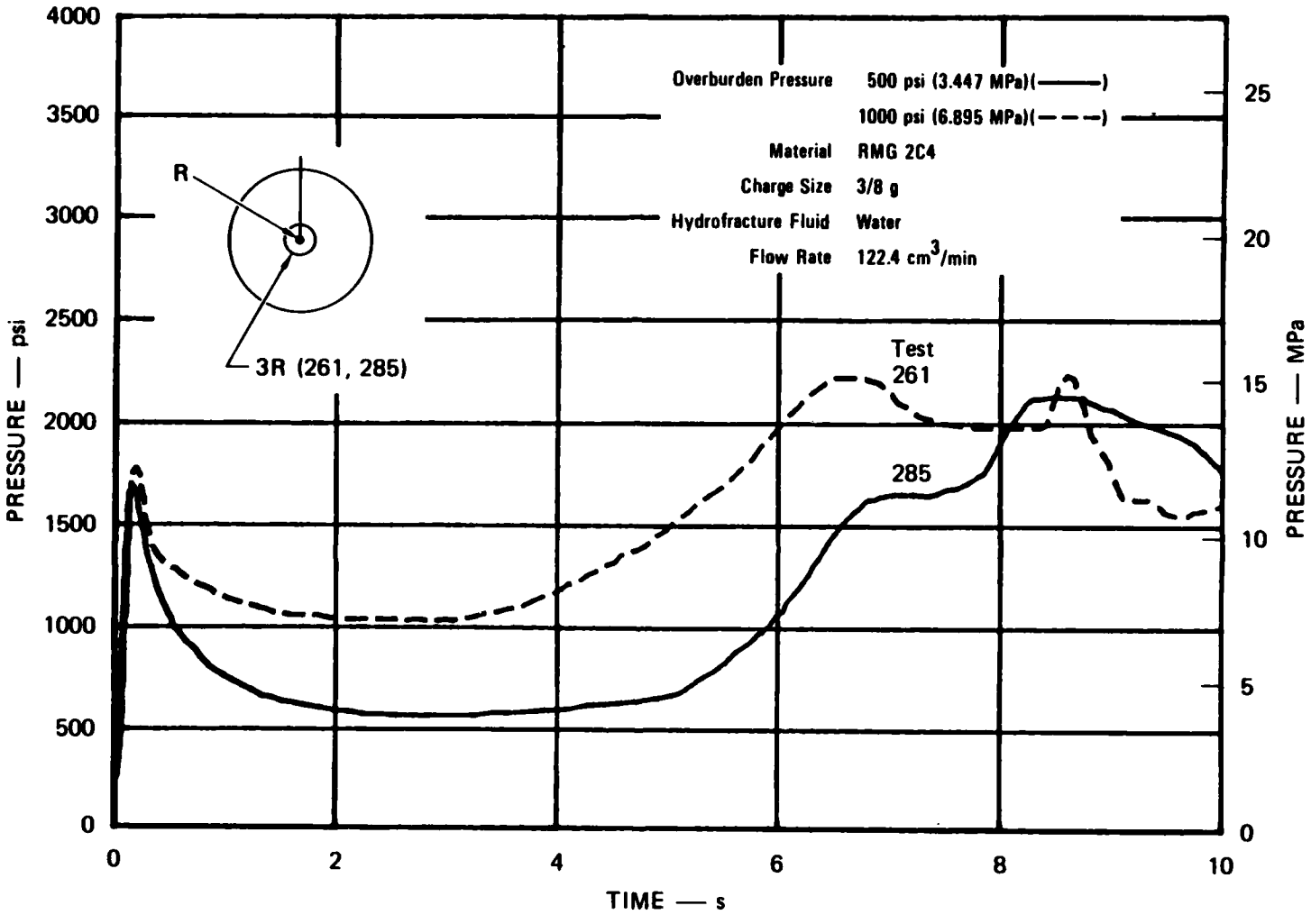

FIGURE 3.13 HYDROFRACTURE PRESSURES FOR 3R UNCOUPLED EXPLODED CAVITY TESTS–OVERBURDEN EFFECT

Series 9 - Nearby Explosive Charge

Tests were performed on RMG 2C4 spheres containing two explosive charges to assess the effects on containment of simultaneous nearby underground nuclear explosions. The insert in Figure 3.14 shows the basic configuration.

A preliminary test (279), performed with an overburden of 1000 psi (6.895 MPa), resulted in a dynamic fracture extending to the surface of the sphere. Hydrofracture was not performed. In this test, the dynamically expanding cavities overlapped and produced a nonspherical cavity with a volume less than that of two standard exploded cavities. The resulting gas pressure was higher than the pressure in a standard exploded cavity, and was sufficient to propagate a fracture to the surface of the sphere.

For tests 280 and 283, the overburden was increased to 1500 psi (10.34 MPa). In test 283, a nonspherical exploded cavity with a volume greater than that of two standard exploded cavities was produced. Cavity gases were contained and the resulting hydrofracture record is shown in Figure 3.14. The 4400 psi (30.34 MPa) fracture initiation pressure is 22% less than the 5610 psi (38.68 MPa) average for the standard exploded cavity tests. The reduction is attributed to a less effective asymmetric residual stress field surrounding the cavity.

In test 280, one charge detonated properly and one charge apparently burned. The resulting hydrofracture was typical of single charge explosions, as shown in Figure 3.14.

Pressure pulses measured at the bottom of the containment vessel for the nearby charge tests (279 and 283) are shown in Figure C.6. Although maximum pressures were comparable to those for single charge explosions, the maximum impulses were higher, especially for the contained nearby charge test (283).

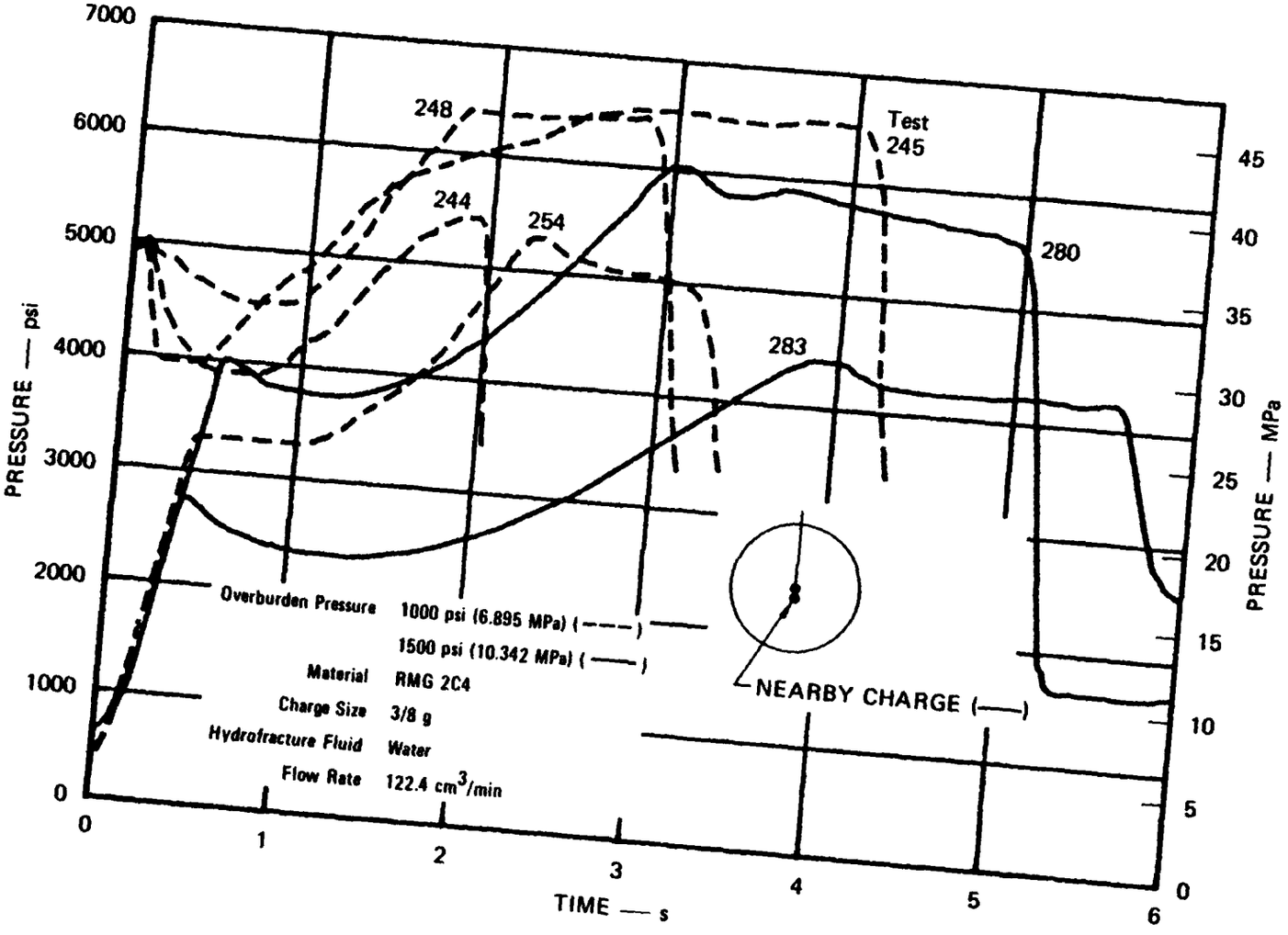

FIGURE 3.14 HYDROFRACTURE PRESSURES FOR UNVENTED EXPLODED CAVITY TESTS–NEARBY CHARGE EFFECT

JA-1289-56

Series 10 - Material Property and Geometry (Tuff Cylinder versus RMG 2C4 Sphere)

Hydrofracture test 278 was performed on an exploded cavity tuff cylinder to determine the response of NTS material. The configuration for the test is shown in Figure 2.11. Charge detonation resulted in an exploded cavity diameter of 0.562 inch (1.43 cm), compared to 0.808 inch (2.05 cm) for RMG 2C4. A TIGER code estimate for the pressure in a 0.500-inch-diameter (1.27-cm) cavity is 141,000 psi (972.16 MPa). As would be expected, the small cavity fractured dynamically. However, the crack was contained within the tuff cylinder. Figure 3.15 shows that a maximum hydrofracture pressure of 4780 psi (32.96 MPa) was generated before the existing fracture propagated to the surface.

A comparison of the uniaxial strain curves for tuff and RMG 2C4 shown in Figure E.4 suggests the reason for different exploded cavity diameters. Charge detonation produces an estimated initial cavity pressure of 37 kbars. At pressures above 4 kbars tuff apparently is stiffer than RMG 2C4. Further evidence of a stiffer material is provided by the pressure pulse measured in the bottom of the containment vessel. As shown in Figure C.7, the maximum pressure for tuff was 77% greater than the typical value for RMG 2C4.

3.4 PARTICLE VELOCITY TESTS

The basic configuration for particle velocity measurements has been described in a previous report.[12] The tests in this investigation were performed on 11-inch-diameter (27.94-cm) RMG 2C4 spheres.

Series 11 - Coupled Cavity

Figure 3.16 shows the particle velocity history at five radii (0.64, 1.27, 1.90, 2.54, and 4.00 cm) following charge detonation in a fully coupled exploded cavity sphere (test 273). The largest radius coincides with the extent of the plastic region surrounding an exploded cavity in RMG 2C4. The recording time shown in Figure 3.16 (80 μs) is the approximate time required for the generated wave to reflect from the surface of the sphere and return to the outermost gage. The results are thus representative of motion in an infinite medium. As expected, the inner

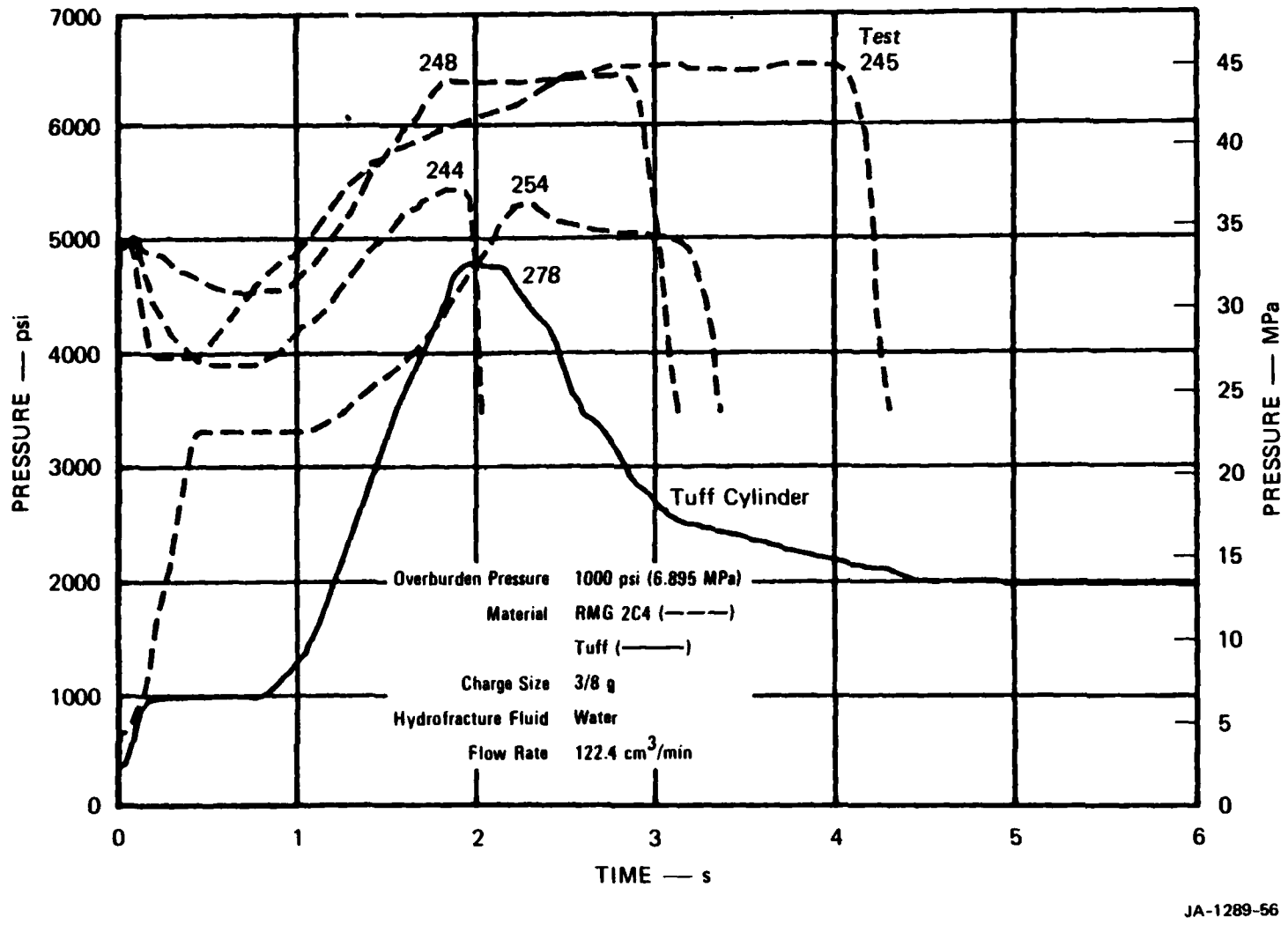

FIGURE 3.15 HYDROFRACTURE PRESSURES FOR UNVENTED EXPLODED CAVITY TESTS–MATERIAL PROPERTY AND GEOMETRY EFFECTS (Tuff Cylinder versus RMG 2C4 Sphere)

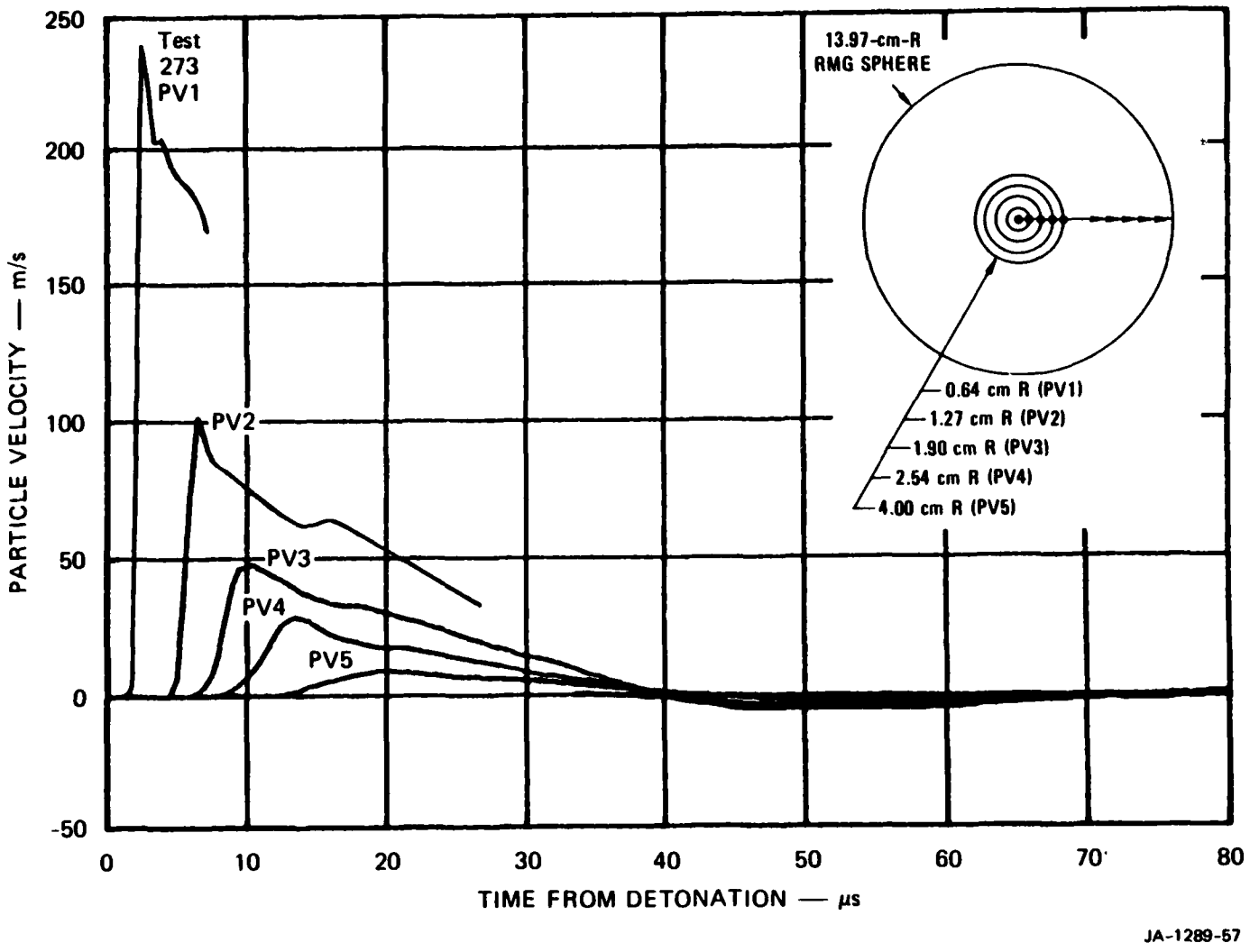

FIGURE 3.16 PARTICLE VELOCITIES AT FIVE LOCATIONS DURING COUPLED CAVITY EXPLOSION

two gage wires broke during outward motion because of excessive strain. Complete outward and rebound motion was measured by each of the outer three gages. As an indication of reproducibility, Figure 3.17 shows particle velocity records obtained at the outer three gage locations during two identical tests (272 and 273).

The above results indicate that rebound in the plastic region of the grout spheres is a cavity effect and not a surface effect. Because the residual stress field around an exploded cavity is believed to be established once rebound has occurred, RMG 2C4 spheres 11 inches (27.94 cm) in diameter or larger are adequate for investigating residual stress formation.

Figure B.1 shows the circumferential strain profiles obtained from the particle velocity records by integrating and dividing by the wire loop radius.

Series 12 - Uncoupled Cavity (3R)

Figures 3.18 and 3.19 show the particle velocity history at four radii (1.59, 1.90, 2.54, and 4.00 cm) following charge detonation in two uncoupled exploded cavity spheres (tests 274 and 277). The coupling parameter (ratio of initial cavity diameter to charge diameter) was three. The outer three gage locations correspond to gage locations in the fully coupled tests (Figure 3.17). A comparison of the results shows that the pulse produced by the uncoupled charge has only one-half the duration of the pulse produced by a fully coupled charge and that the maximum outward velocities are comparably reduced.

Figure B.2 shows the circumferential strain profiles obtained from the particle velocity records for the uncoupled tests. The maximum strains at the outer three gage locations are only one-fifth the corresponding values obtained in the fully coupled tests (Figure B.1). These low strains are consistent with the negligible residual stress observed in hydrofracture of 3R uncoupled cavity spheres.

The relatively large test-to-test variation in strain obtained in tests 274 and 277 from the gage nearest the cavity (PV1, Figure B.2) is attributed to the technique used for installing the gage. A simple modification is available for improving this technique.

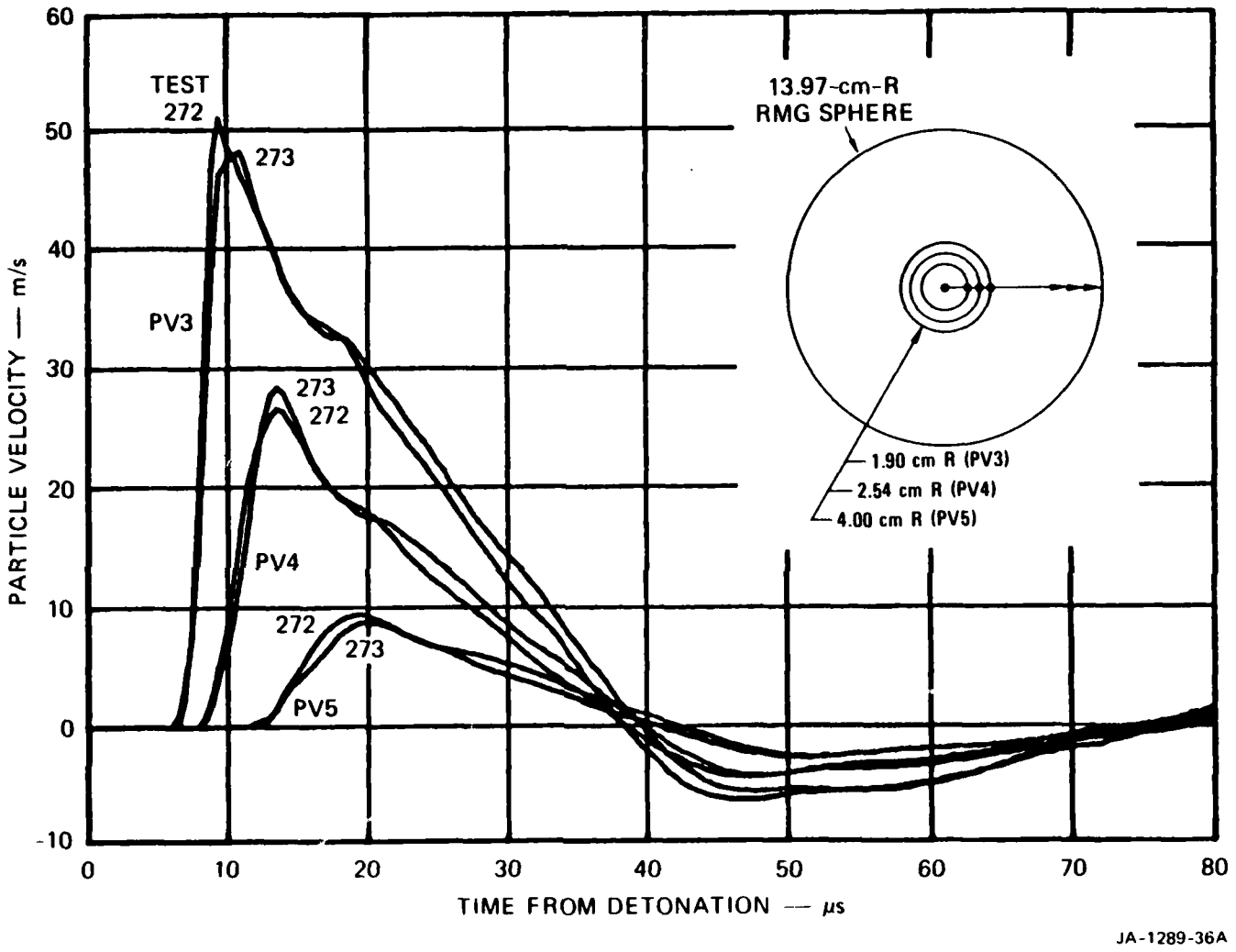

FIGURE 3.17 PARTICLE VELOCITIES AT THREE LOCATIONS DURING COUPLED CAVITY EXPLOSIONS

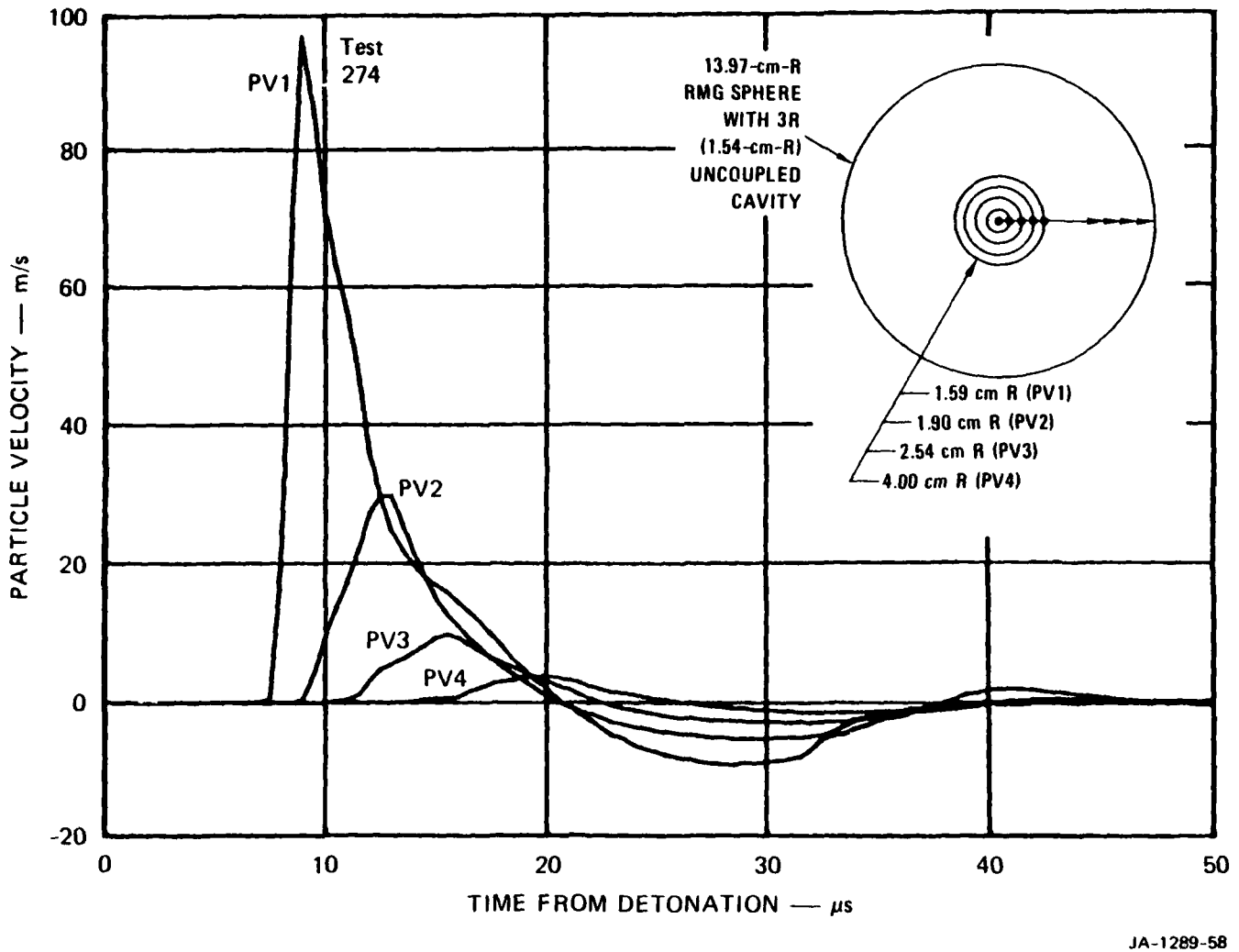

FIGURE 3.18 PARTICLE VELOCITIES AT THREE LOCATIONS DURING 3R UNCOUPLED CAVITY EXPLOSION–TEST 274

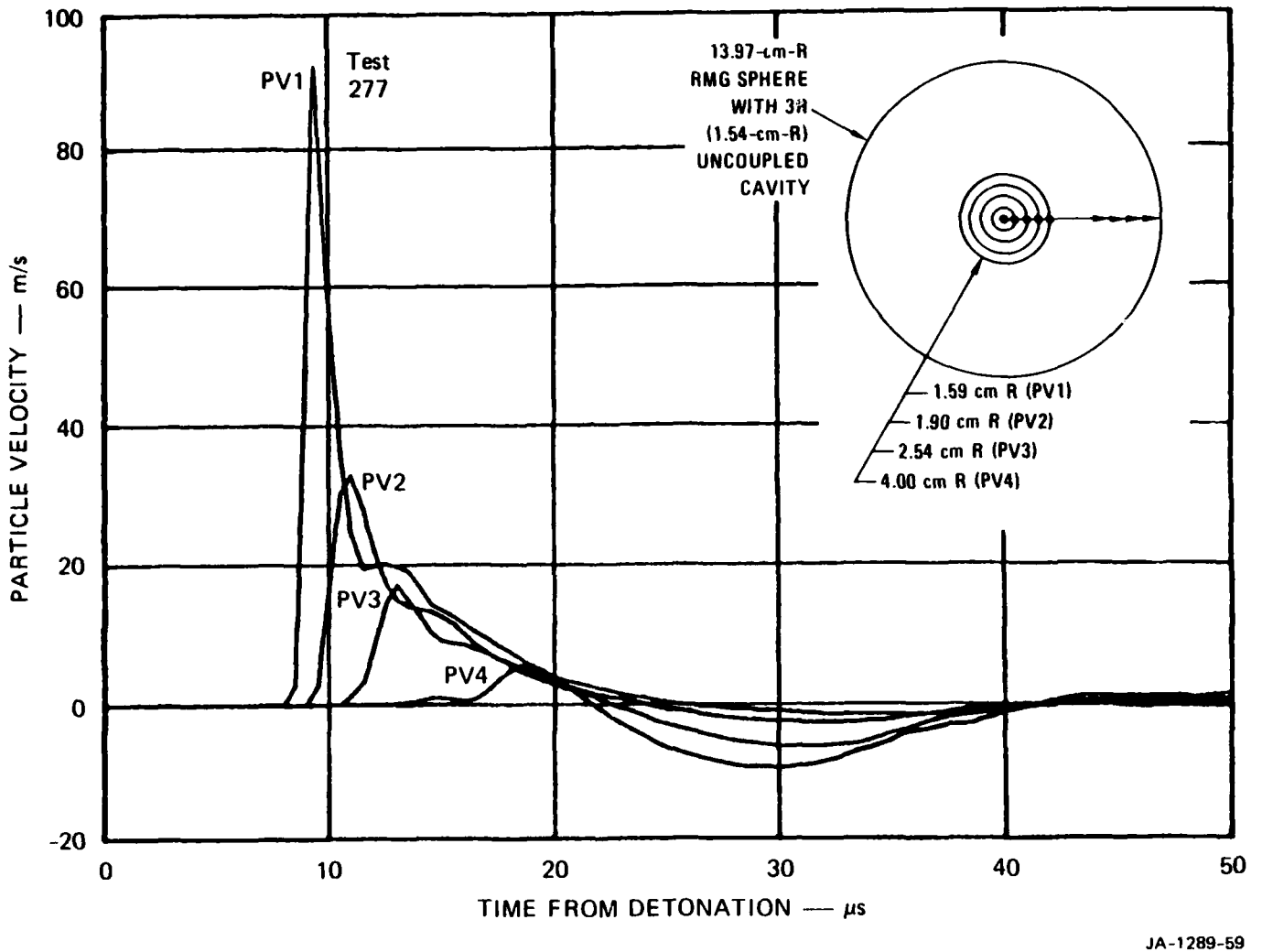

FIGURE 3.19 PARTICLE VELOCITIES AT THREE LOCATIONS DURING 3R UNCOUPLED CAVITY EXPLOSION–TEST 277

APPENDIX A

UNCOUPLED RIGID CAVITY TESTS (2R and 3R)

Gas pressure decay curves associated with charge detonation in rigid spherical cavities are presented in this appendix. Results for 2R and 3R uncoupled cavities are shown in Figure A.1. Also included are the initial portion of the hydrofracture record associated with each of the coupling parameters.

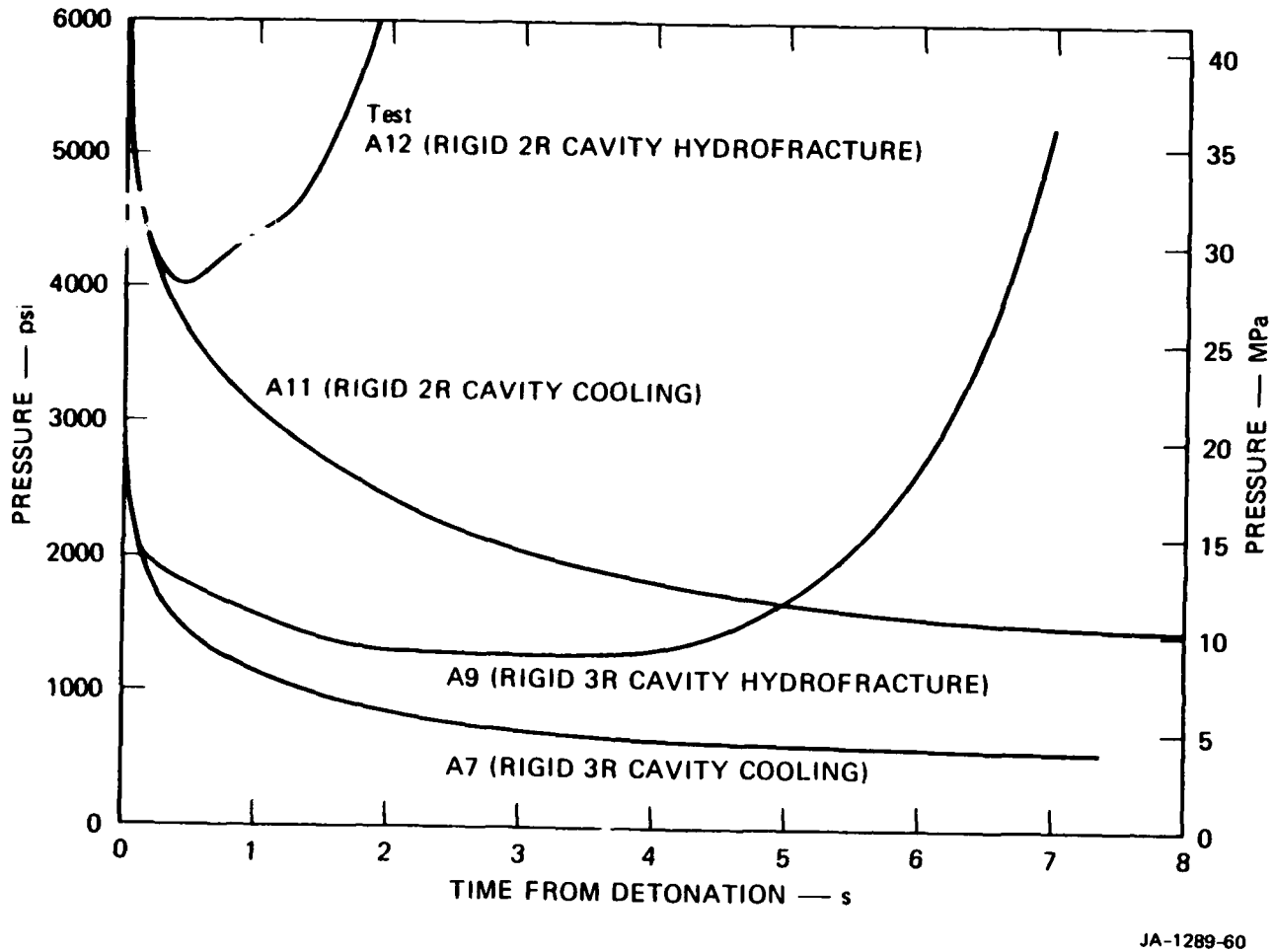

FIGURE A.1 HYDROFRACTURE PRESSURES AND DECAY PRESSURES FOR RIGID 2R AND 3R UNCOUPLED CAVITY TESTS

APPENDIX B

CIRCUMFERENTIAL STRAIN FROM PARTICLE VELOCITY RECORDS

The circumferential strain profiles in Figures B.1 and B.2 were generated by first integrating the corresponding particle velocity records of Section 3.4 to obtain particle displacement profiles, and then employing the following definition for small circumferential strain in cylindrical coordinates:

$$\varepsilon_\theta = u/r$$

where u is the radial displacement at a radius r. For simplicity, this definition was applied even to those cases in which the strains are relatively large.

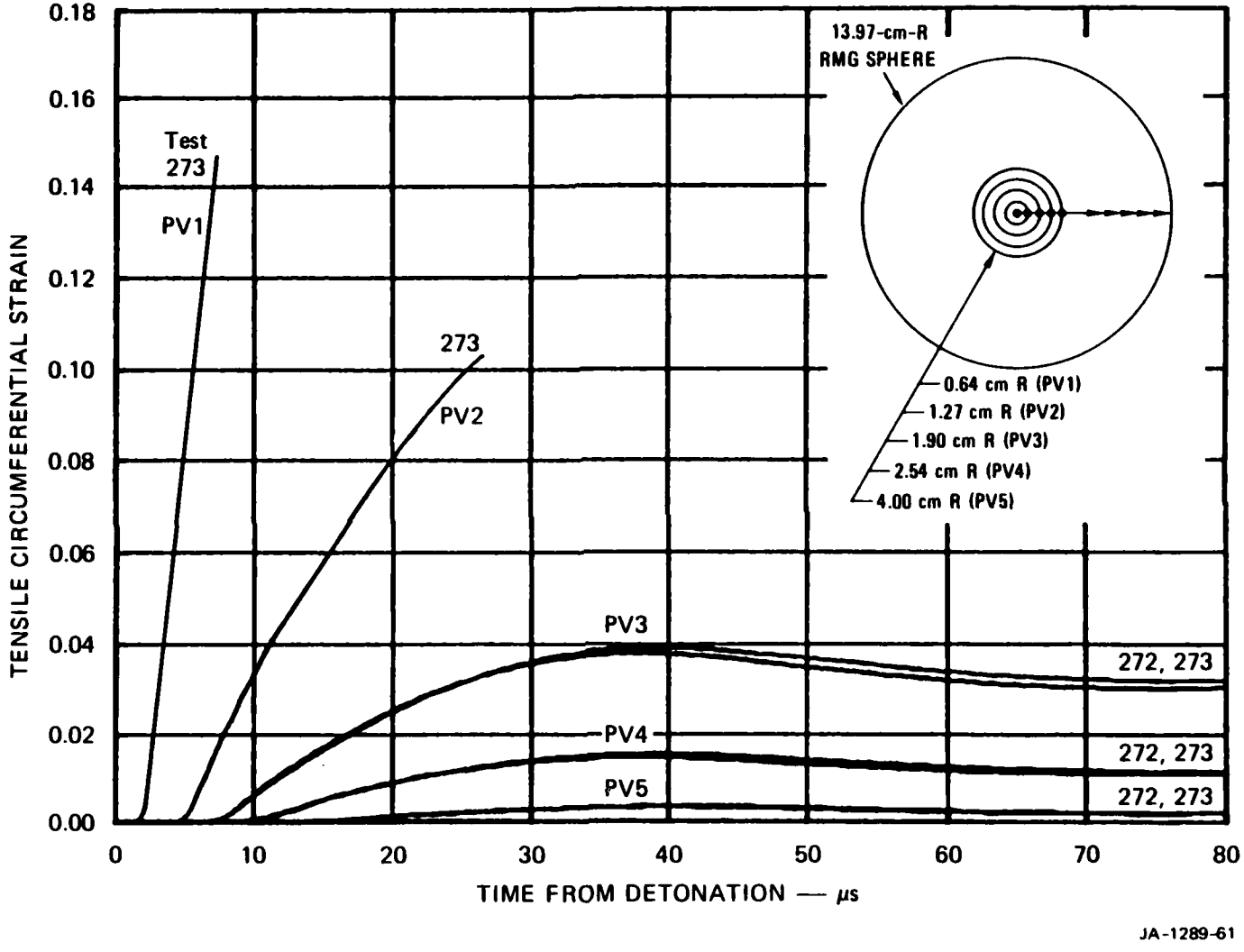

FIGURE B.1 CIRCUMFERENTIAL STRAINS AT FIVE LOCATIONS DURING COUPLED CAVITY EXPLOSIONS

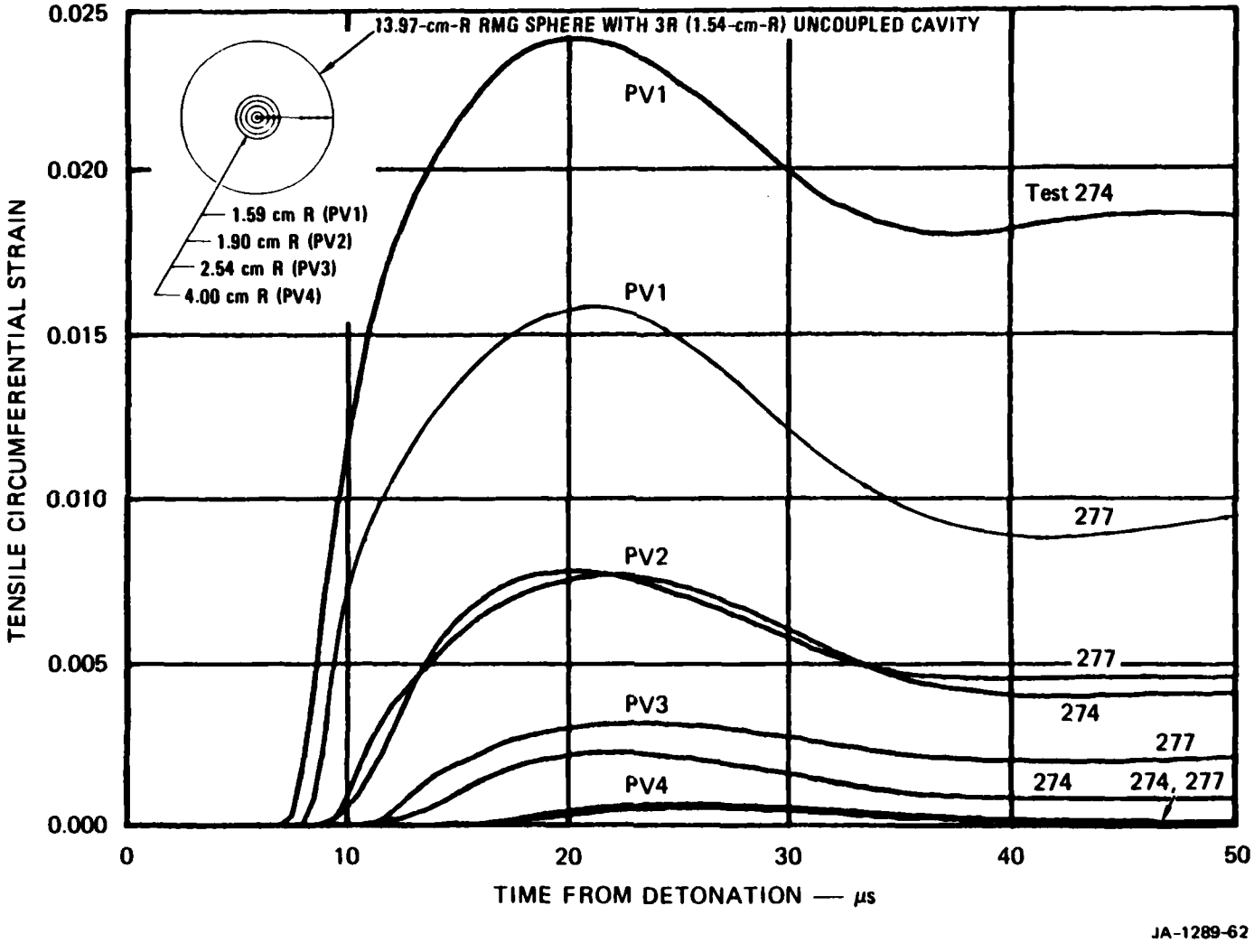

FIGURE B.2 CIRCUMFERENTIAL STRAINS AT THREE LOCATIONS DURING 3R UNCOUPLED CAVITY EXPLOSIONS

APPENDIX C

PRESSURE PULSE MEASUREMENTS IN CONTAINMENT VESSEL

The pressure pulses generated during exploded cavity tests and measured by a quartz gage in the bottom of the containment vessel are presented in this appendix in Figures C.1 through C.7.

A summary of results is given in Table C.1, where tests are categorized according to the relevant parameters. Maximum reflected pressure and impulse as well as pulse duration are listed for each test. For calculation of pulse duration and impulse, the pressure pulse was assumed to end when the pressure dropped to the initial value.

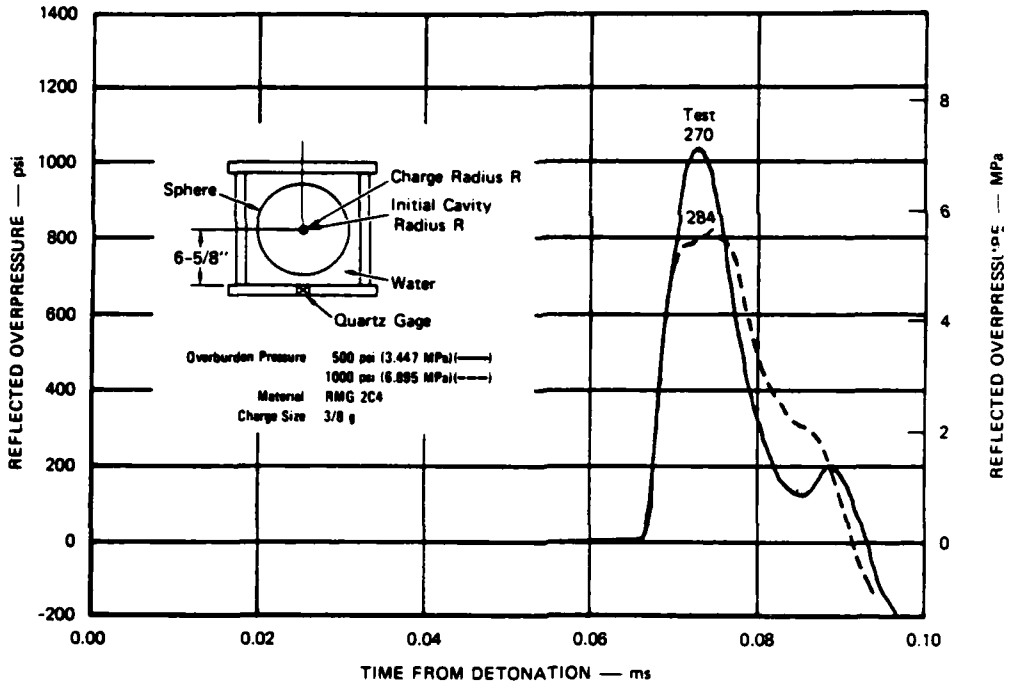

(a) REFLECTED PRESSURE

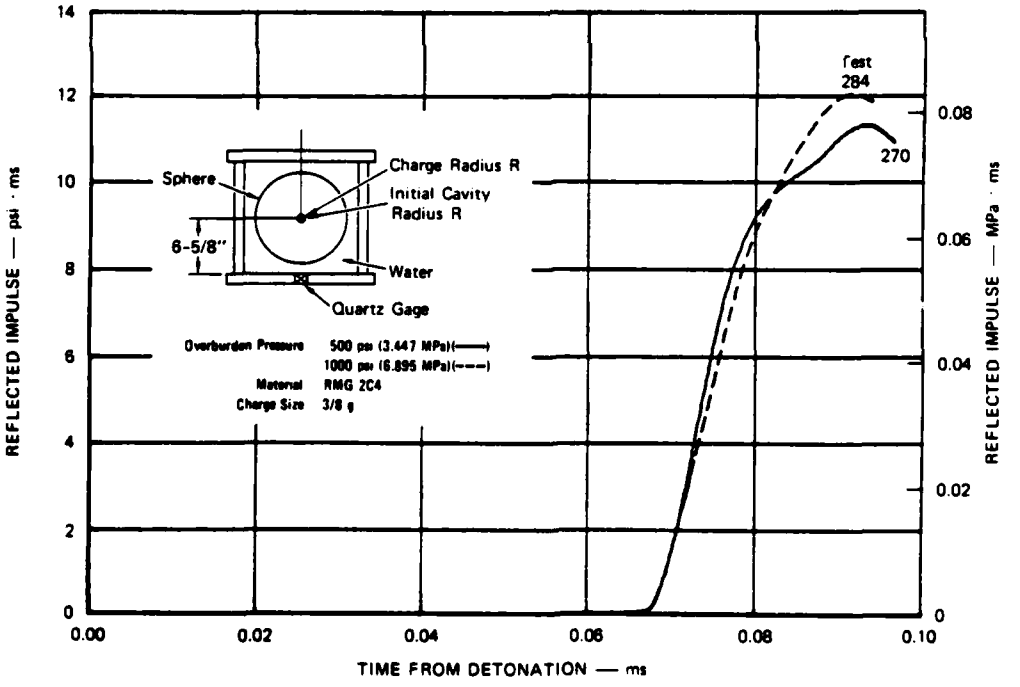

(b) REFLECTED IMPULSE

JA-1288-83

FIGURE C.1 REFLECTED PRESSURE AND IMPULSE FROM COUPLED CAVITY EXPLOSIONS–OVERBURDEN EFFECT

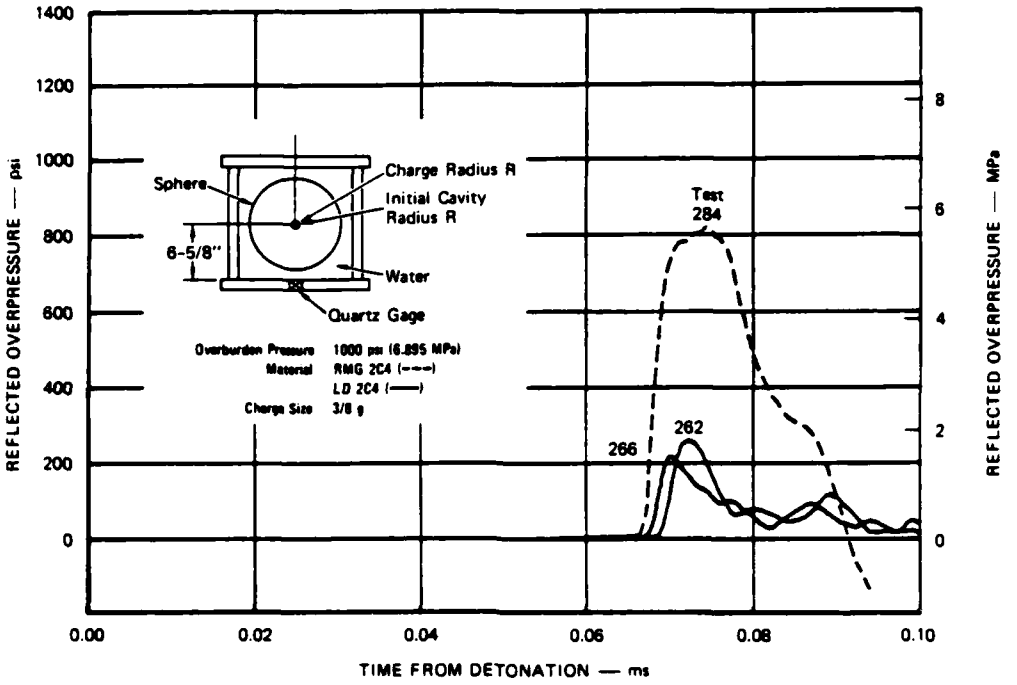

(a) REFLECTED PRESSURE

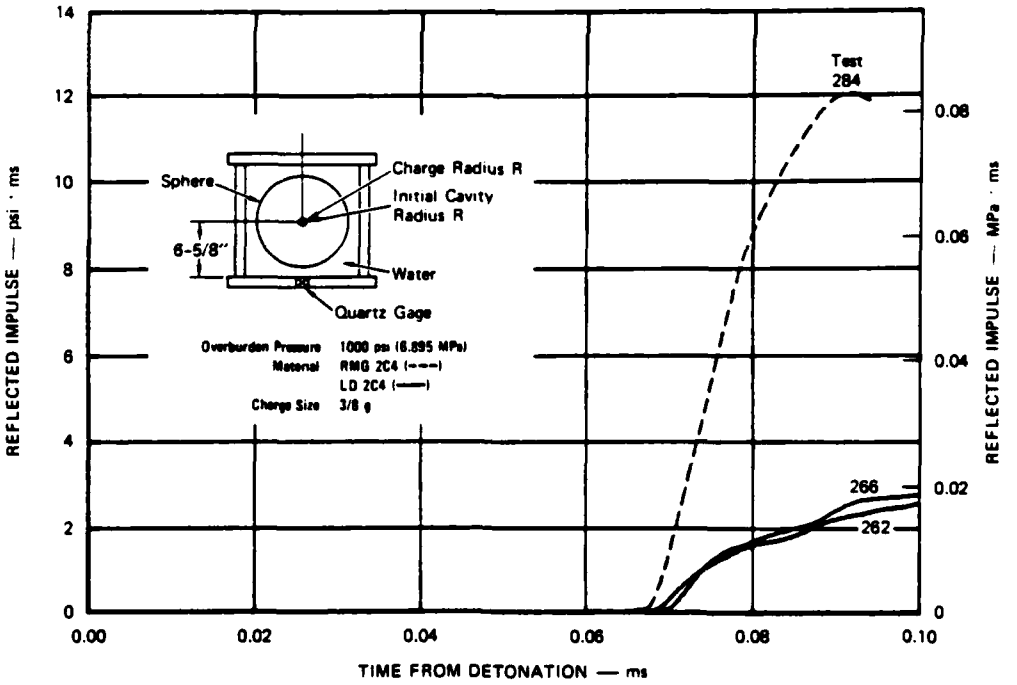

(b) REFLECTED IMPULSE

JA-1288-84

FIGURE C.2 REFLECTED PRESSURE AND IMPULSE FROM COUPLED CAVITY EXPLOSIONS–MATERIAL PROPERTY EFFECT (LD 2C4 versus RMG 2C4)

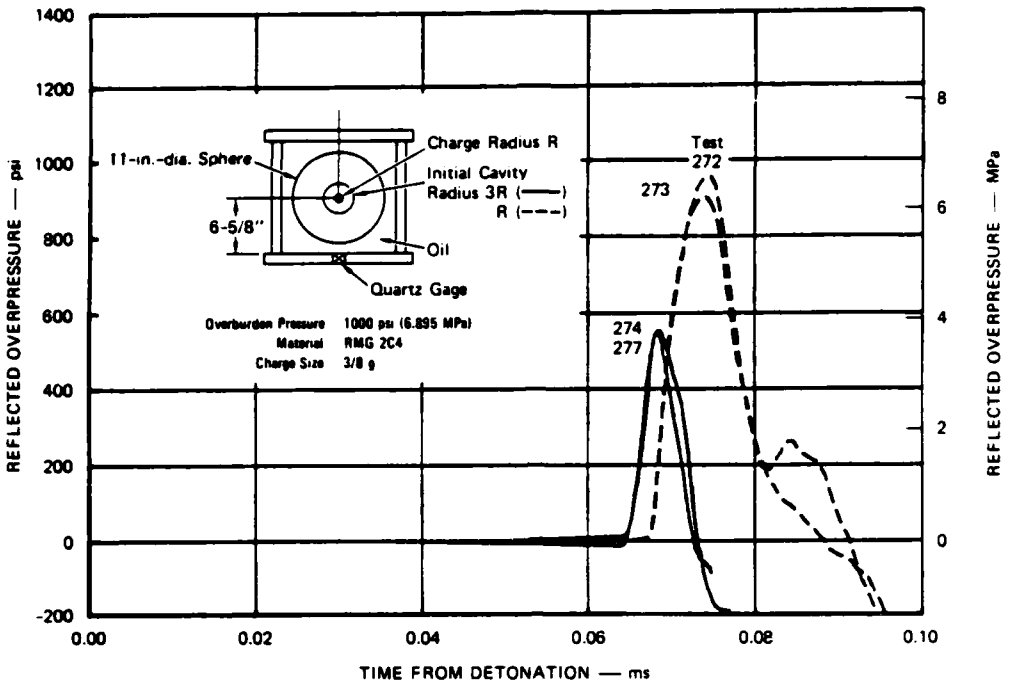

(a) REFLECTED PRESSURE

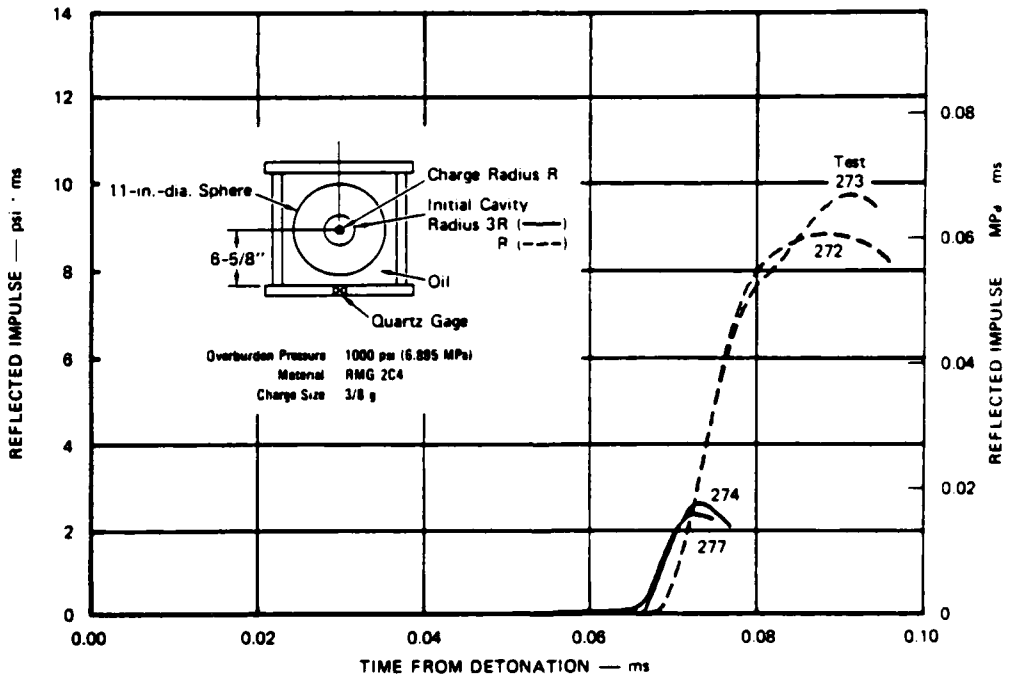

(b) REFLECTED IMPULSE

JA-1289-65

FIGURE C.3 REFLECTED PRESSURE AND IMPULSE FROM COUPLED AND 3R UNCOUPLED CAVITY EXPLOSIONS

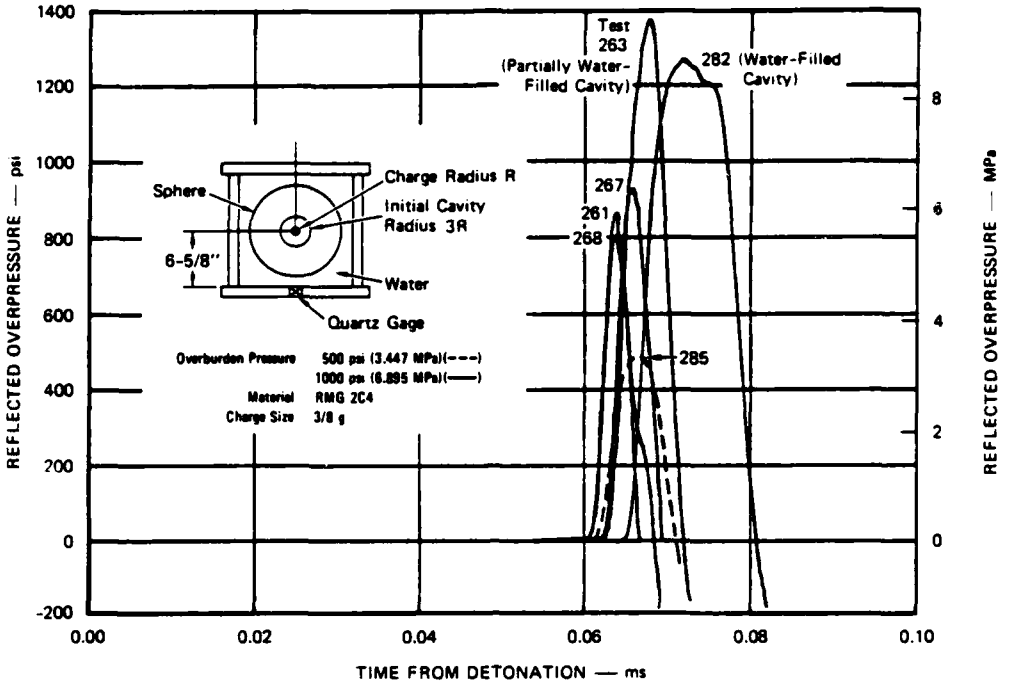

(a) REFLECTED PRESSURE

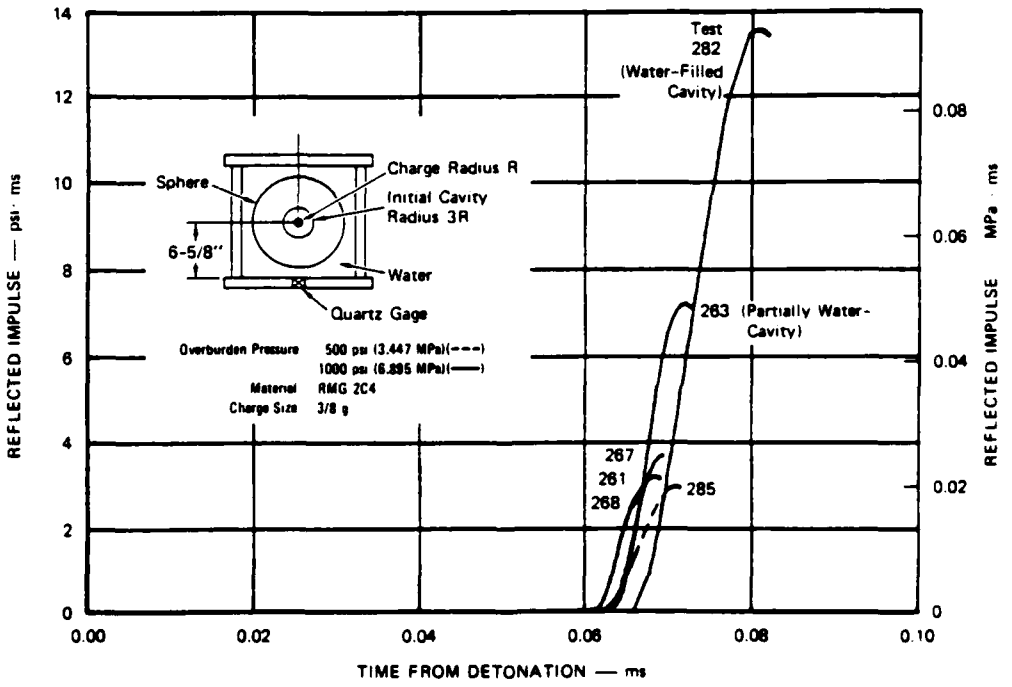

(b) REFLECTED IMPULSE

JA-1269-88

FIGURE C.4 REFLECTED PRESSURE AND IMPULSE FROM 3R UNCOUPLED CAVITY EXPLOSIONS–WATER IN CAVITY AND OVERBURDEN EFFECTS

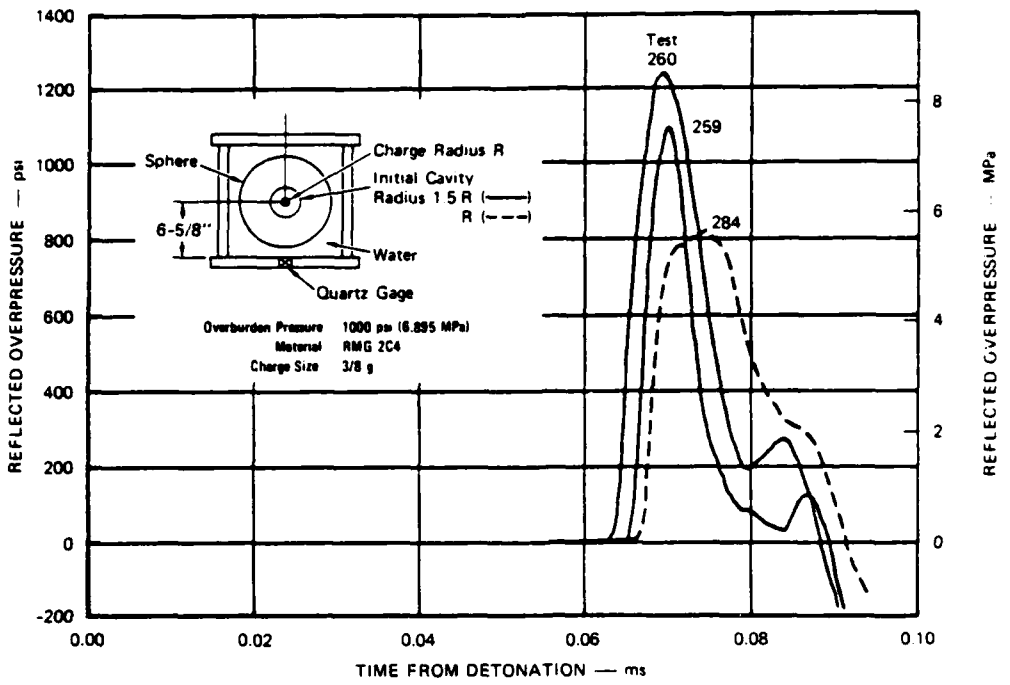

(a) REFLECTED PRESSURE

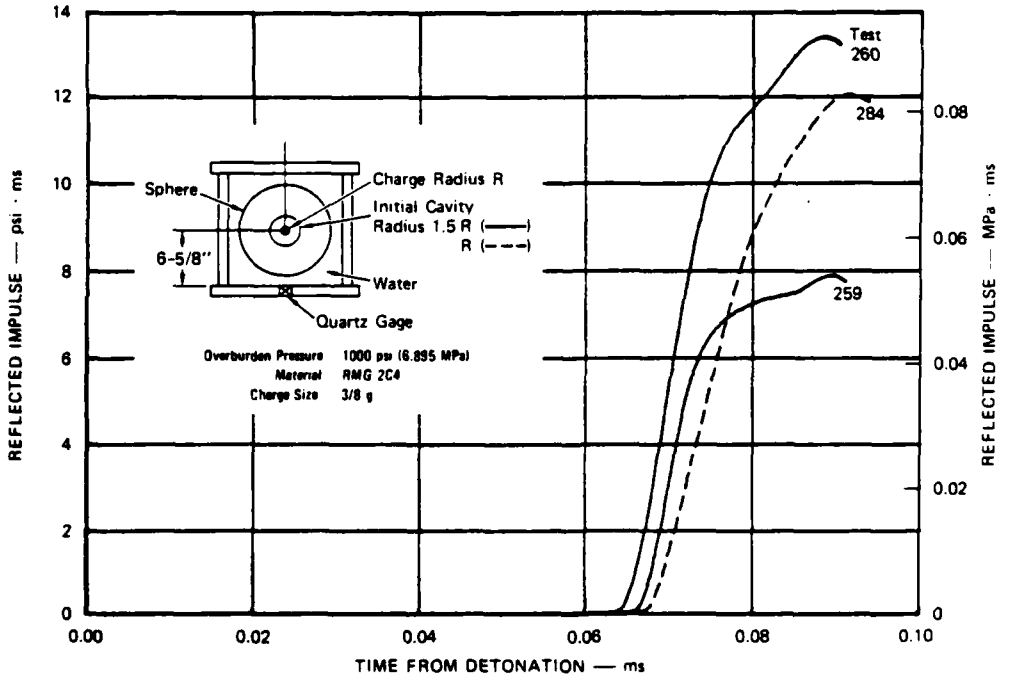

(b) REFLECTED IMPULSE

JA-1289-87

FIGURE C.5 REFLECTED PRESSURE AND IMPULSE FROM COUPLED AND 1.5R UNCOUPLED CAVITY EXPLOSIONS

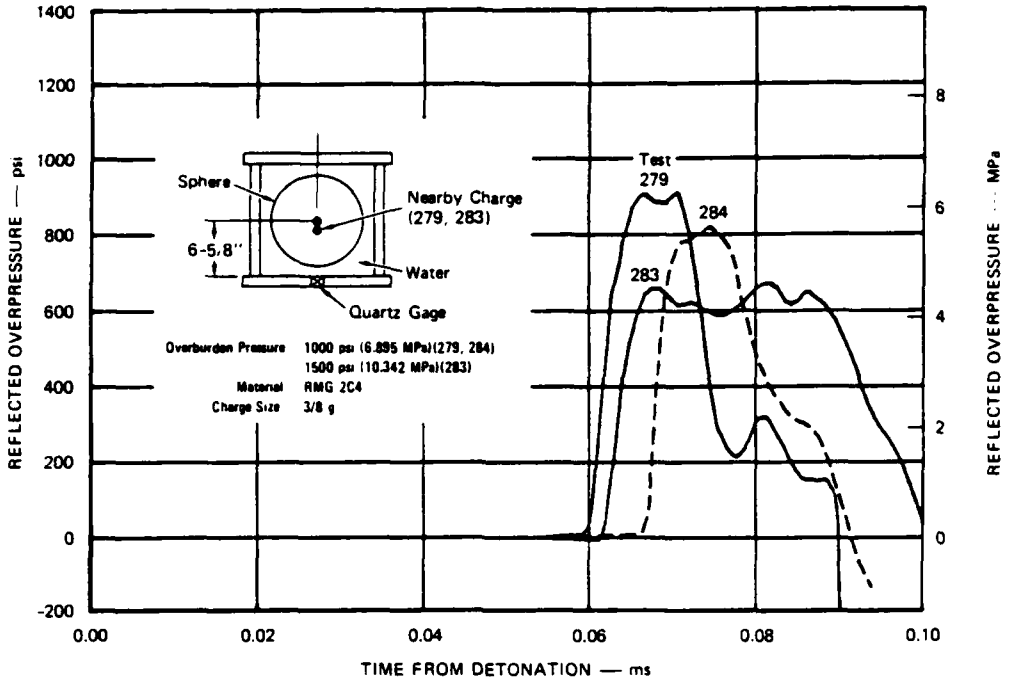

(a) REFLECTED PRESSURE

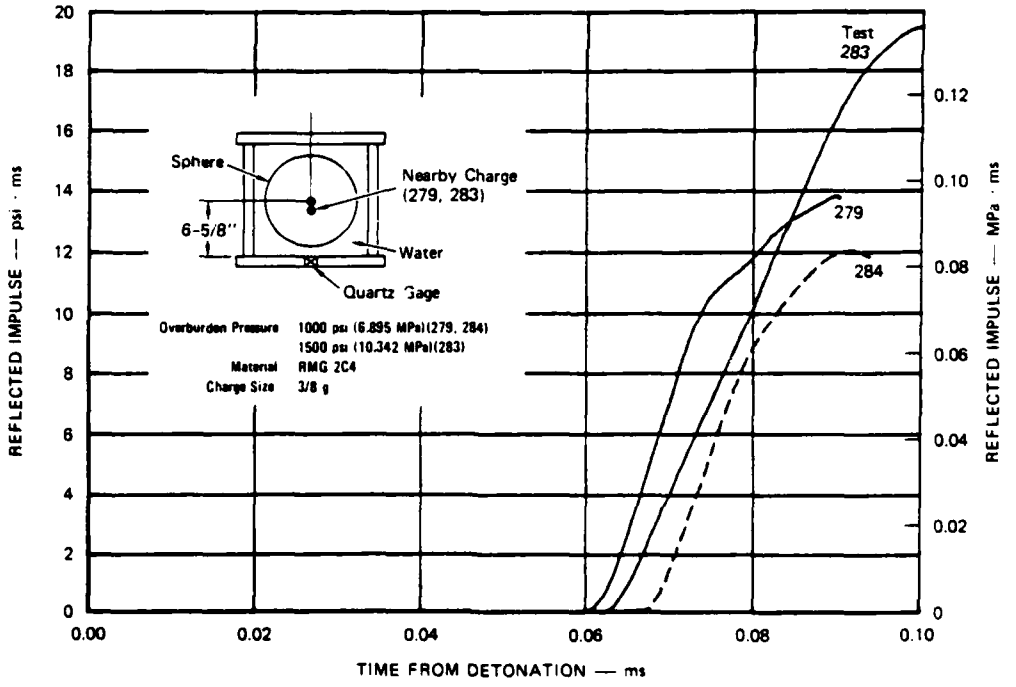

(b) REFLECTED IMPULSE

JA-1289-68

FIGURE C.6 REFLECTED PRESSURE AND IMPULSE FROM COUPLED CAVITY EXPLOSIONS–NEARBY CHARGE EFFECT

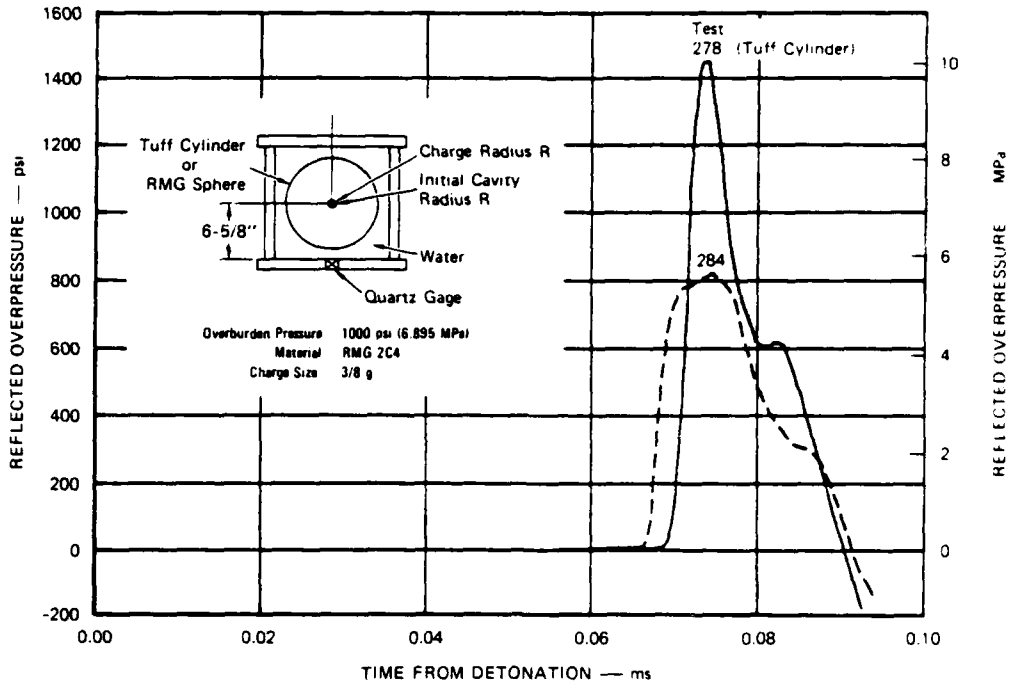

(a) REFLECTED PRESSURE

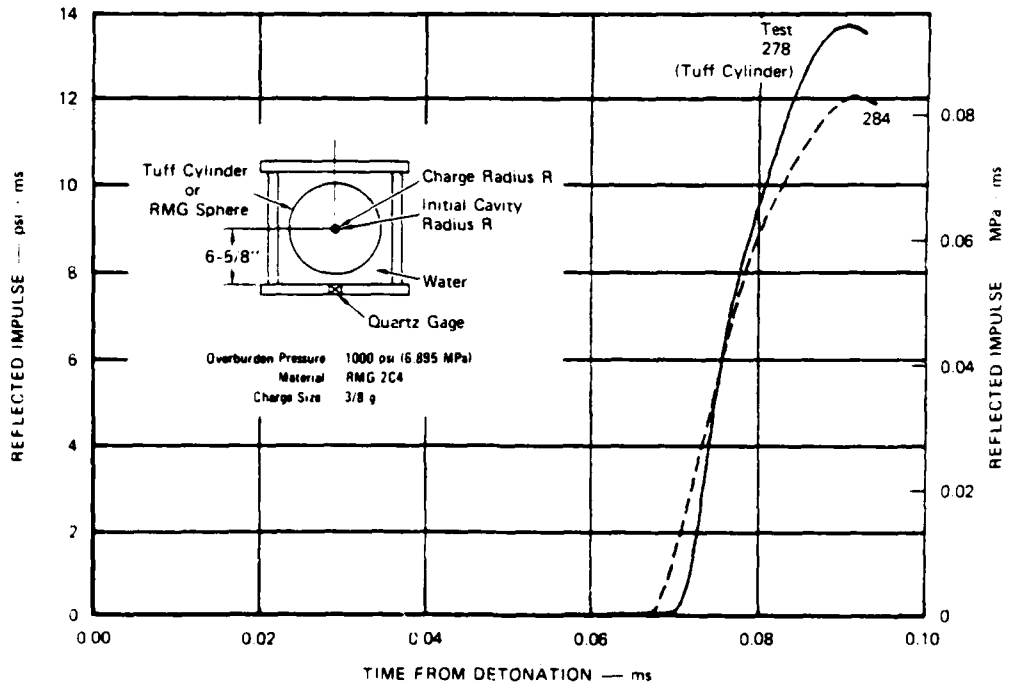

(b) REFLECTED IMPULSE

JA-1289-69

FIGURE C.7 REFLECTED PRESSURE AND IMPULSE FROM COUPLED CAVITY EXPLOSIONS-MATERIAL PROPERTY AND GEOMETRY EFFECTS
(Tuff Cylinder versus RMG 2C4 Sphere)

Table C.1

SUMMARY OF PRESSURE PULSES FOR EXPLODED CAVITY TESTS

Test No.	Material and Geometry	Coupling Parameter	Overburden Pressure (psi)	Maximum Reflected Pressure (psi)	Pulse Duration (μs)	Maximum Reflected Impulse (psi·ms)
270	RMG Sphere	1	500	1035	26.6	11.3
272	RMG Sphere[a]	1	1000	953	21.2	8.8
273	RMG Sphere[a]	1	1000	902	24.5	9.7
284	RMG Sphere	1	1000	822	25.0	12.1
262	LD Sphere	1	1000	257	32.0	2.6
266	LD Sphere	1	1000	220	34.7	2.8
278	Tuff Cylinder	1	1000	1453	21.4	13.8
279	RMG Sphere	1[b]	1000	912	30.5	13.8
283	RMG Sphere	1[b]	1500	669	39.5	19.5
259	RMG Sphere	1.5[c]	1000	1094	24.4	7.9
260	RMG Sphere	1.5[c]	1000	1240	25.4	13.4
285	RMG Sphere	3	500	488	9.5	3.0
261	RMG Sphere	3	1000	858	7.6	3.2
267	RMG Sphere	3	1000	926	7.7	3.9
268	RMG Sphere	3	1000	800	6.2	2.6
274	RMG Sphere[a]	3	1000	537	8.1	2.6
277	RMG Sphere[a]	3	1000	565	8.7	2.4
263	RMG Sphere	3[c]	1000	1376	9.3	7.2
282	RMG Sphere	3[c]	1000	1269	15.8	13.6

[a] 11-inch-diameter (27.94-cm)

[b] Nearby explosive charge

[c] Water in cavity

APPENDIX D
SPHERICAL ELASTIC WAVES

Introduction

The simple elastodynamic analysis presented here was performed to allow a comparison of the records from particle velocity gages embedded in the region of the 2C4 grout that remains elastic during spherical wave propagation. The idea is to choose the gage closest to the explosive where the grout remains elastic and imagine that a spherical cavity exists having a radius equal to the radial coordinate of the gage (radius of the loop gage). The wall of this cavity is given the velocity history of the gage record and elastodynamic analysis is used to predict the particle velocities at the gages farther out for comparison with the gages' records.

The analysis is also used to determine the stress histories at points in the elastic region and in particular to determine the radius of the plastic region.

Formulation

The equation of spherically symmetric motion is

$$\frac{\partial \sigma_r}{\partial r} + \frac{2}{r}(\sigma_r - \sigma_\theta) = -\rho \frac{\partial^2 u}{\partial t^2} \qquad (1)$$

where $u = u(r,t)$ is the radial displacement and ρ is the constant material density. Because we are describing a diverging compressive wave we adopt the convention that the stress components σ_r and σ_θ ($\sigma_\phi = \sigma_\theta$) are positive when compressive. Similarly, contracting strains ε_r and ε_θ ($\varepsilon_\phi = \varepsilon_\theta$) are chosen to be positive. The strains are related to the stresses by Hooke's law

$$\sigma_r = \frac{2G}{1 - 2\nu} [(1 - \nu)\varepsilon_r + 2\nu\varepsilon_\theta] \tag{2}$$

$$\sigma_\theta = \frac{2G}{1 - 2\nu} [\nu\varepsilon_r + \varepsilon_\theta] \tag{3}$$

and to the radial displacement by the kinematic relations

$$\varepsilon_r = - \frac{\partial u}{\partial r} \qquad \varepsilon_\theta = - \frac{u}{r} \tag{4}$$

In (2) and (3), ν is Poisson's ratio and G is the modulus of rigidity. Relations (2), (3), and (4) allow the equation of motion (1) to be expressed as

$$\frac{\partial^2 u}{\partial r^2} + \frac{2}{r} \frac{\partial u}{\partial r} - \frac{2}{r^2} u = \frac{1}{c^2} \frac{\partial^2 u}{\partial t^2} \tag{5}$$

where the elastic dilatational velocity, c, is given by

$$c^2 = \frac{2G}{\rho} \cdot \frac{1 - \nu}{1 - 2\nu} \tag{6}$$

If we introduce the displacement potential ϕ by

$$u = \frac{\partial \phi}{\partial r} \tag{7}$$

the governing equation (5) becomes

$$\frac{\partial^2 (r\phi)}{\partial r^2} = \frac{1}{c^2} \frac{\partial^2 (r\phi)}{\partial t^2} \tag{8}$$

which has an outgoing wave solution of the form

$$\phi = \frac{1}{r} f(t - \frac{r - a}{c}) \tag{9}$$

where a is the cavity radius. The specific functional form of f depends on the cavity wall conditions. We let

$$s = t - \frac{r - a}{c} \tag{10}$$

which is the time that has elapsed after the wave has arrived at radius r.

In terms of r and f(s) the displacement potential, displacement, strains, and stresses are

$$\phi = \frac{1}{r} f(s) \tag{11}$$

$$u = - \frac{f'}{cr} - \frac{f}{r^2} \tag{12}$$

$$\varepsilon_r = - \frac{f''}{c^2 r} - \frac{2f'}{cr^2} - \frac{2f}{r^3} \tag{13}$$

$$\varepsilon_\theta = \frac{f'}{cr^2} + \frac{f}{r^3} \tag{14}$$

$$\sigma_r = - \rho \left[\frac{f''}{r} + \frac{2(1 - 2\nu)c^2}{1 - \nu} \left(\frac{f'}{cr^2} + \frac{f}{r^3} \right) \right] \tag{15}$$

$$\sigma_\theta = - \rho \left[\frac{\nu}{1 - \nu} \frac{f''}{r} - \frac{(1 - 2\nu)c^2}{1 - \nu} \left(\frac{f'}{cr^2} + \frac{f}{r^3} \right) \right] \tag{16}$$

where

$$f' = \frac{df}{ds}.$$

From (12), the particle velocity is

$$\frac{\partial u}{\partial t} = - \frac{f''}{cr} - \frac{f'}{r^2} \tag{17}$$

and if we specify the cavity wall velocity by

$$\frac{\partial u}{\partial t}(a,t) = v(t) \tag{18}$$

we see that f(s) is governed by the equation

$$f'' + \frac{c}{a} f' = - ca \cdot v(s) \tag{19}$$

Displacement continuity at the front (s = 0) of a wave moving into a material at rest requires that $f(0) = f'(0) = 0$.

The solution of (19) satisfying $f'(0) = 0$ is

$$f'(s) = - cae^{-\frac{c}{a}s} \int_0^s e^{\frac{c}{a}\tau} v(\tau)\, d\tau \tag{20}$$

which, according to (17), gives the particle velocity

$$\frac{\partial u}{\partial t}(r,s) = \frac{a}{r} v(s) - \left(1 - \frac{a}{r}\right) \frac{a}{r} \frac{c}{a} e^{-\frac{c}{a}s} \int_0^s e^{\frac{c}{a}\tau} v(\tau)\, d\tau \tag{21}$$

and, with f(0) = 0, allows us to determine the quantities in (11)-(16).

Linear Cavity-Wall Velocity

For a specified constant acceleration of the cavity wall we want to determine the nature of the velocity increase in the material and the corresponding stress state. On the cavity wall, r = a, let

$$v(t) = \begin{cases} 0 & t < 0 \\ \alpha t & t > 0 \end{cases} \tag{22}$$

Then the particle velocity, by (21), is given by

$$\frac{1}{\alpha} \cdot \frac{\partial u}{\partial t} = \frac{a^2}{r^2} s + (1 - \frac{a}{r}) \frac{a}{r} \frac{a}{c} \left(1 - e^{-\frac{c}{a} s}\right) \tag{23}$$

and the acceleration is given by

$$\frac{1}{\alpha} \cdot \frac{\partial^2 u}{\partial t^2} = \frac{a^2}{r^2} + (1 - \frac{a}{r}) \frac{a}{r} e^{-\frac{c}{a} s} \tag{24}$$

If we recall from (10) that s is the time measured from the wave arrival we see from (23) and (24) that the velocity is not linear and the acceleration decreases in time from its initial value of $(a/r)\alpha$. This conclusion fits the observation that the particle velocity records become more rounded the farther the gages are from the cavity. Also, the initial slopes of the records vary spatially as a/r.

The stress state is found by substituting (20) in the stress formulas (15) and (16). If we evaluate the resulting expressions at the cavity wall we obtain

$$\frac{\sigma_r}{\rho a \alpha} = 1 - e^{-\frac{c}{a} s} + \frac{1 - 2\nu}{1 - \nu} (\frac{c}{a} s)^2 \tag{25}$$

$$\frac{\sigma_\theta}{\rho a \alpha} = \frac{\nu}{1 - \nu} \left(1 - e^{-\frac{c}{a} s}\right) - \frac{1 - 2\nu}{2(1 - \nu)} (\frac{c}{a} s)^2 \tag{26}$$

From (25) and (26) the mean stress and stress difference are given by

$$\frac{\sigma_m}{\rho a \alpha} = \frac{\sigma_r + 2\sigma_\theta}{3\rho a \alpha} = \frac{1}{3} \frac{1 + \nu}{1 - \nu} \left(1 - e^{-\frac{c}{a} s}\right) \tag{27}$$

$$\frac{\sigma_r - \sigma_\theta}{\rho a \alpha} = \frac{1 - 2\nu}{1 - \nu} \left(1 - e^{-\frac{c}{a} s}\right) + \frac{3(1 - 2\nu}{2(1 - \nu)} (\frac{c}{a} s)^2 \tag{28}$$

Formulas (27) and (28) are useful for determining the onset of plasticity by plotting the values to see where the trajectory crosses the failure envelope.

In the next section we examine particle velocity records from an experiment assuming a piecewise linear approximation to the cavity-wall velocity. Thus, for a velocity at r = a of

$$v(t) = m_i t + b_i \qquad t_{i-1} < t < t_i$$

$$\text{where } m_i = \frac{v_i - v_{i-1}}{s_i - s_{i-1}}, \qquad b_i = \frac{v_{i-1} s_i - v_i s_{i-1}}{s_i - s_{i-1}},$$

$$i = 1, 2, \ldots, n \tag{29}$$

and where n = number of piecewise linear segments, the particle velocity at radius r is

$$\frac{\partial u}{\partial t} = \frac{a}{r}(m_i s + b_i) - \left(1 - \frac{a}{r}\right)\frac{a}{r} \cdot \frac{c}{a} e^{-\frac{c}{a}s} \sum_{j=1}^{i} \int_{s_{j-1}}^{s_j} e^{\frac{c}{a}\tau}(m_j\tau + b_j)d\tau \tag{30}$$

where $s_{i-1} < s < s_i$

and

$$\int_{s_{j-1}}^{s_j} e^{\frac{c}{a}\tau}(m_j\tau + b_j)d\tau = \frac{m_j a^2}{c^2}\left[\left(\frac{c}{a}s_j - 1\right)e^{\frac{c}{a}s_j} - \left(\frac{c}{a}s_{j-1} - 1\right)e^{\frac{c}{a}s_{j-1}}\right] + \frac{b_j a}{c}\left(e^{\frac{c}{a}s_j} - e^{\frac{c}{a}s_{j-1}}\right)$$

Experimental and Theoretical Particle Velocities

Figure D.1 shows particle velocity records obtained at radii of 4, 5.08, and 10.16 cm; the gages are labeled PV2, PV3, and PV4 respectively. The low-amplitude apparent precursors are attributable to the small pulse generated by the mild detonating fuse used to detonate the spherical charge of PETN. Consequently we have extrapolated the main velocity rise signal back to the zero velocity base line. We now imagine that the particle velocities monitored by PV3 and PV4 are generated by a cavity of 4-cm radius having the wall velocity of PV2. Gage PV2 was selected because it was in the neighborhood of the final elastic-plastic interface and as a result most of the wave propagation beyond PV2 was elastic.

For the theoretical treatment, the cavity wall velocity is approximated by 12 linear segments. These lines provide the values of m_i, b_i, and t_i in (29). The particle velocity predictions for PV3 and PV4 according to (30) are shown dashed in Figure D.1 for comparison with the experimental records.

The initial rise is reproduced very well for PV3 and approximately for PV4. Later portions of the decay are also reproduced. However, because the experimental peaks are lower than the analytical values, some inelastic response apparently occurs at PV3 and PV4. Finally, according to the stress difference formula (28), the static failure envelope of the grout at the cavity wall is reached after about 4 μs, which means that some plastic deformation occurs at PV2 before the wave reaches PV3.

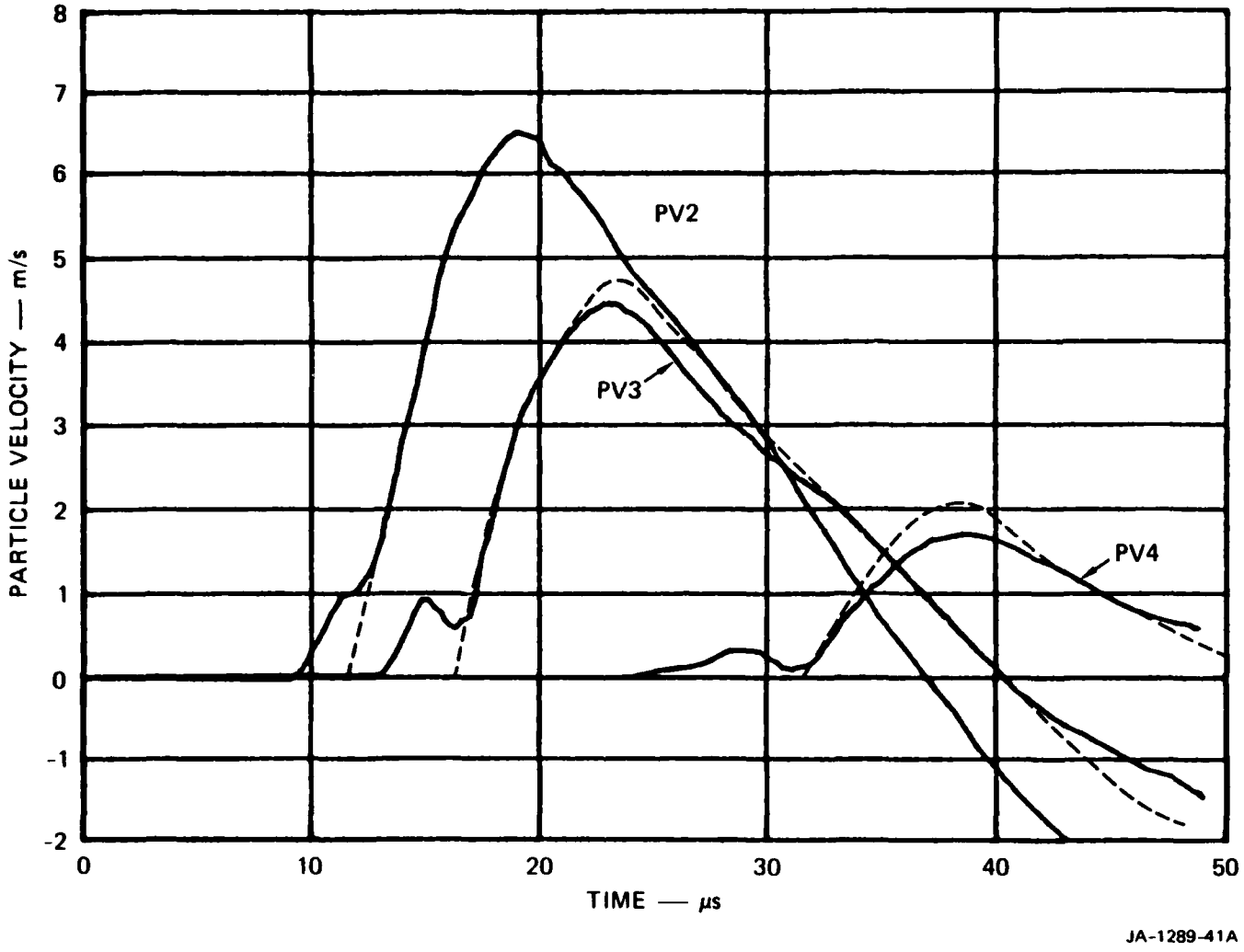

FIGURE D.1 THEORETICAL AND EXPERIMENTAL PARTICLE VELOCITY PROFILES IN THE ELASTIC REGION SURROUNDING AN EXPLODED CAVITY

APPENDIX E
MATERIAL PROPERTIES

Presented here are material properties of rock-matching grout RMG 2C4, low density rock-matching grout LD 2C4, and Nevada Test Site tuff. The RMG and tuff properties include representative data selected from the results of recent Terra Tek test programs.[13,14]

Table E.1 provides the mixture and heat curing cycle for rock-matching grout and low density rock-matching grout. Table E.2 summarizes commonly used physical and mechanical properties of RMG 2C4, LD 2C4, and tuff.

The scatter in unconfined crush strength and tensile strength associated with the testing of a large number of standard 2-inch-diameter (5.08-cm) cylinders of RMG 2C4 is shown in Figures E.1 and E.2. These figures show that, in general, reasonable tolerance is maintained on material strength. Additional strength properties of RMG 2C4 and tuff are shown in Figures E.3 and E.4.

Table E.1

MIXTURES[a] FOR ROCK-MATCHING GROUT RMG 2C4 AND LOW DENSITY ROCK-MATCHING GROUT LD 2C4

Component	RMG 2C4	LD 2C4
Type I-II Portland cement	32.691%	32.063%
Sand (20-40 Monterey)	21.896%	21.476%
Barite (barium sulfate)	20.848%	20.447%
Bentonite (gel)	2.837%	2.783%
CFR 2 (concrete friction-reducing compound)	0.078%	0.077%
Water	21.650%	21.234%
Microballoons (Q-CEL 300)	-	1.920%

[a]28-day Aging procedure: sealed in plastic and submerged in water with the following temperature sequence: raise to 54°C over 48-hour period, hold at 54°C for 48 hours, lower to 25°C over 36-hour period.

Table E.2

PROPERTIES OF ROCK-MATCHING GROUT RMG 2C4,
LOW DENSITY ROCK-MATCHING GROUT LD 2C4,
AND NEVADA TEST SITE TUFF

(a) PHYSICAL PROPERTIES

Physical Property	RMG 2C4	LD 2C4	Tuff
Density (g/cm^3)			
Aged	2.15	1.90	1.87
Dry	1.75	1.57	1.54
Grain	2.87	2.68	2.34
Water by wet weight (%)	18.6	17.4	17.9
Porosity (%)	39	43	34
Saturation (%)	100	86	97.6
Air voids (%)	0-3	13.4	1.8
Longitudinal velocity (km/sec)	3.29	3.13	2.95
Shear velocity (km/sec)	1.82	1.78	1.53
Modulus in compression (psi)	2.64×10^6	2.20×10^6	1.67×10^6
Shear modulus (psi)	1.03×10^6	8.74×10^5	0.63×10^6
Bulk modulus (psi)	2.00×10^6	1.53×10^6	1.55×10^6
Poisson's ratio	0.28	0.26	0.32
Permeability (μd)	3.0	-	-

(b) MECHANICAL PROPERTIES

Material	Average Strain Rate (sec^{-1})	Compressive Strength (psi)	Tensile Strength (psi)
RMG 2C4	Static	3970	530
RMG 2C4	0.15	5330	900
LD 2C4	Static	3200	460
LD 2C4	0.15	5000	780
Tuff	Static	3530	364

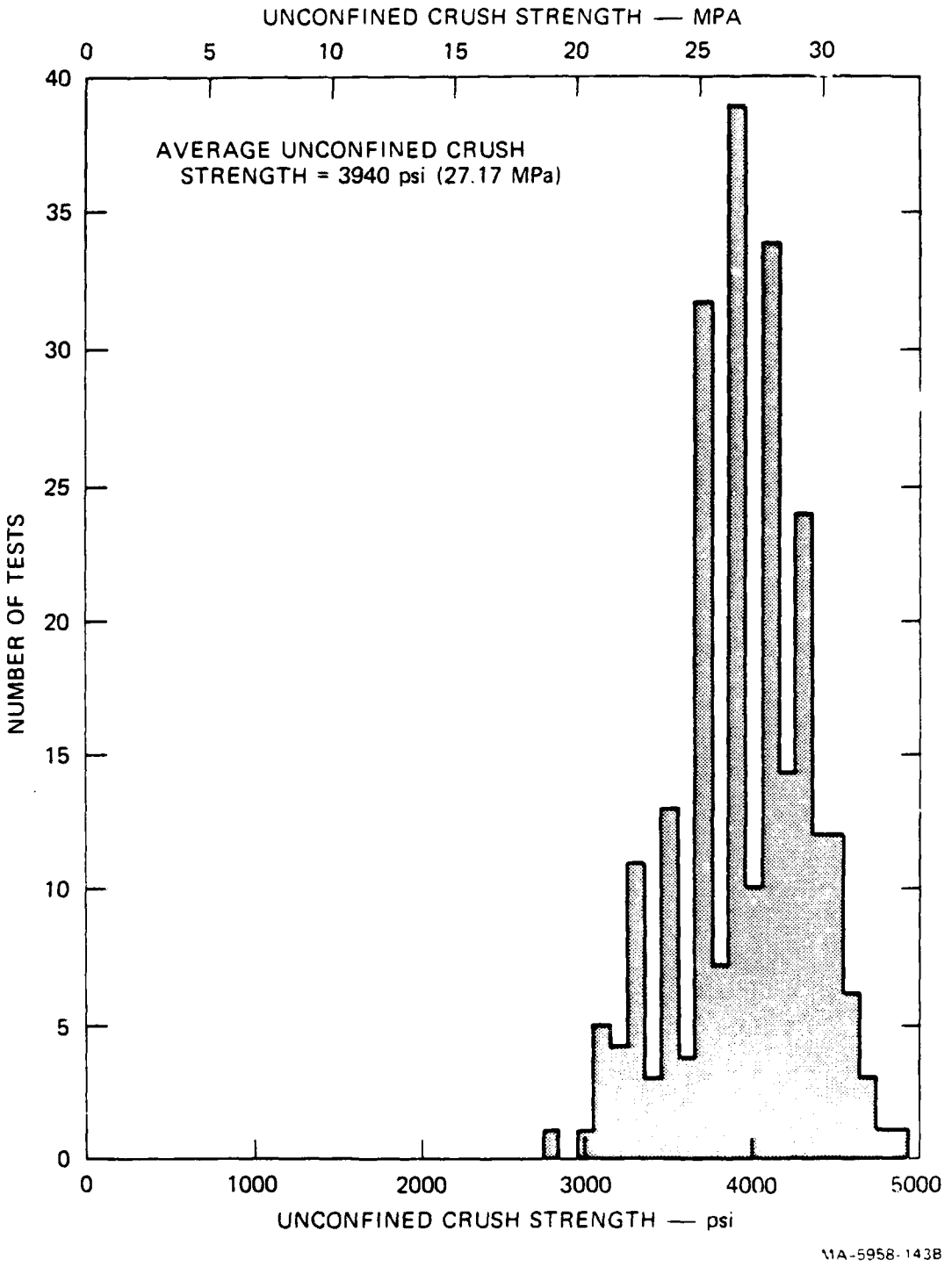

FIGURE E.1 UNCONFINED CRUSH STRENGTH OF ROCK-MATCHING GROUT RMG 2C4

AD-A130 292 LABORATORY INVESTIGATION OF CONTAINMENT IN UNDERGROUND NUCLEAR TESTS(U) SRI INTERNATIONAL MENLO PARK CA J C CIZEK ET AL. 15 FEB 82 DNA-6121F DNA001-80-C-0040 2/2

UNCLASSIFIED F/G 18/3 NL

END
DATE FILMED
8-83
DTIC

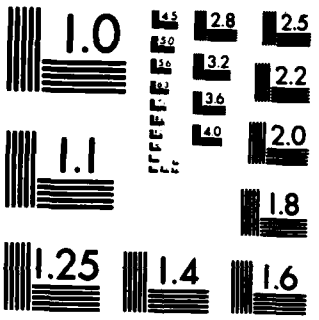

MICROCOPY RESOLUTION TEST CHART
NATIONAL BUREAU OF STANDARDS-1963-A

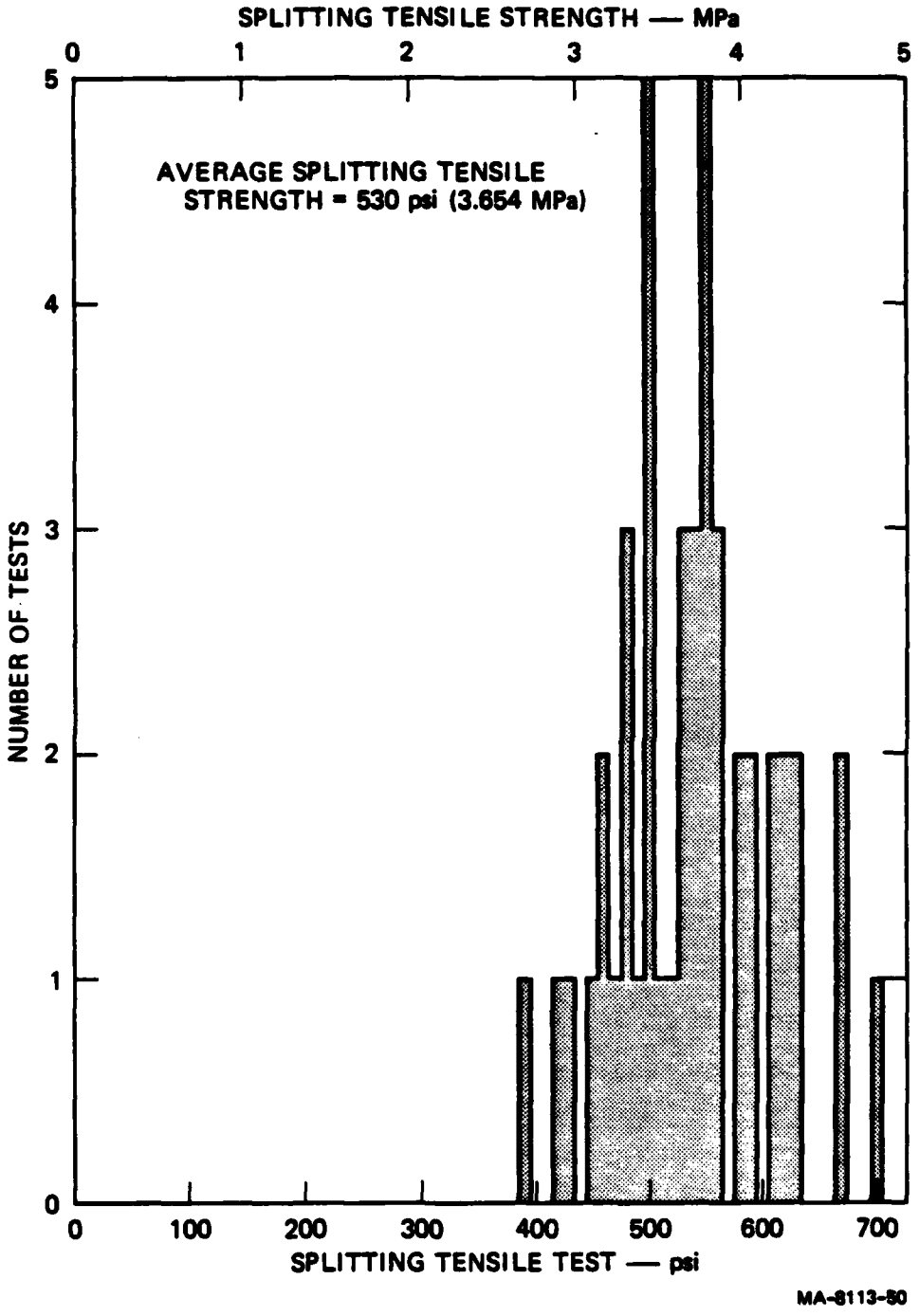

FIGURE E.2 SPLITTING TENSILE STRENGTH OF ROCK-MATCHING GROUT RMG 2C4

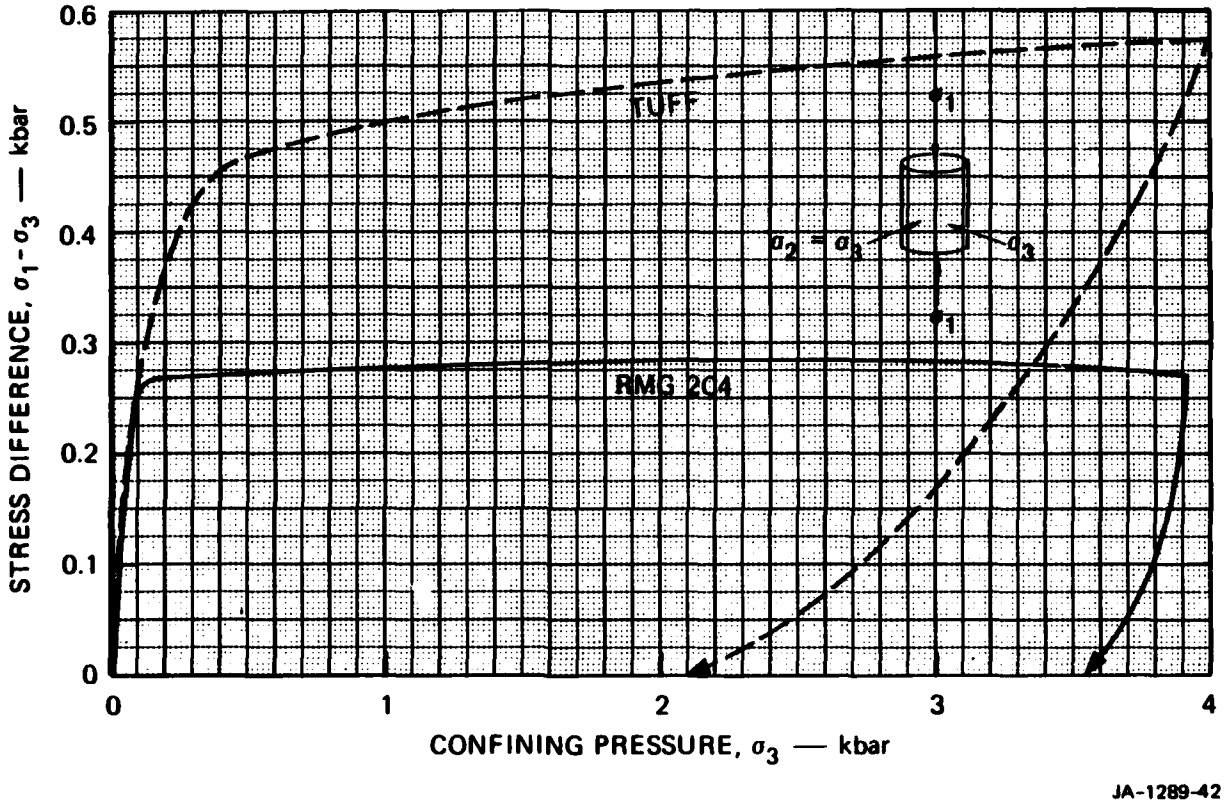

FIGURE E.3 UNIAXIAL STRAIN RESPONSE OF ROCK-MATCHING GROUT RMG 2C4 AND NEVADA TEST SITE TUFF: STRESS DIFFERENCE VERSUS CONFINING PRESSURE

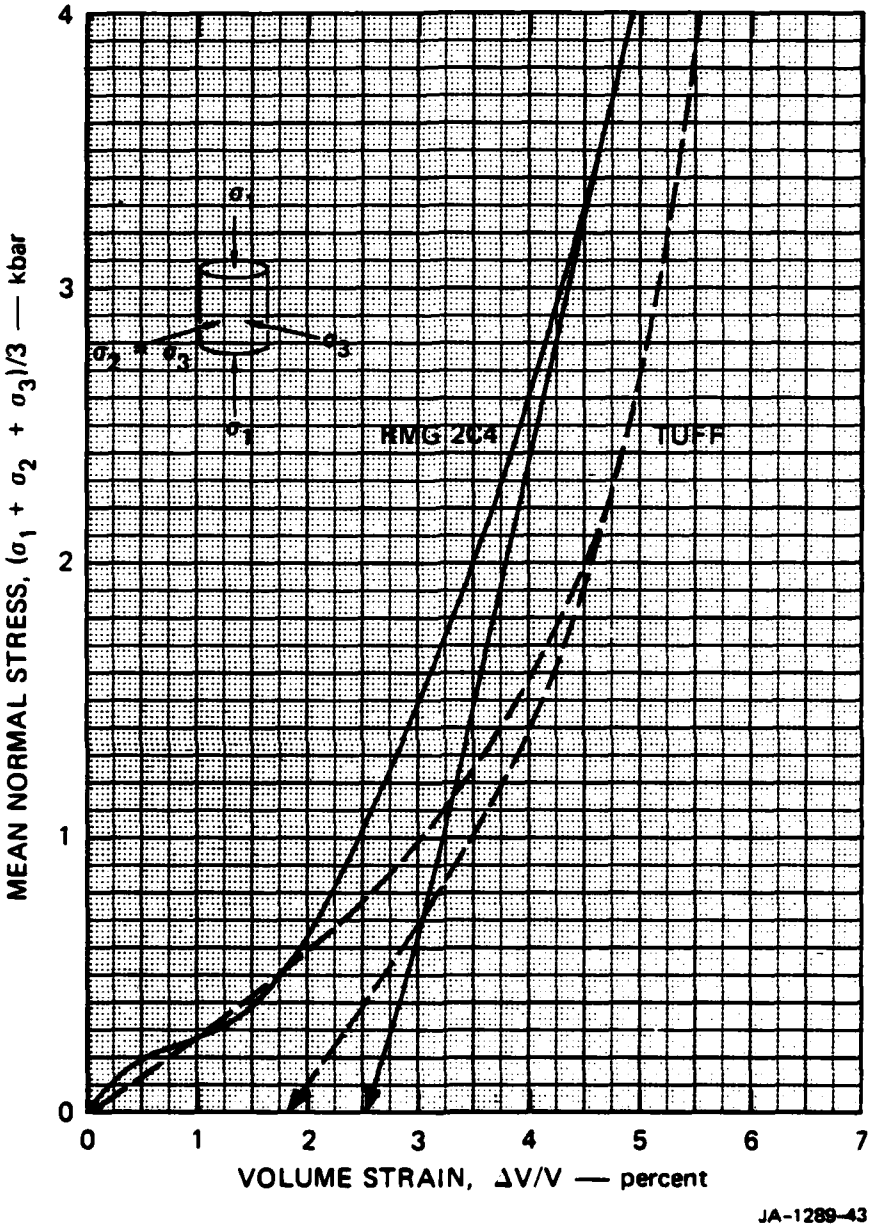

FIGURE E.4 UNIAXIAL STRAIN RESPONSE OF ROCK-MATCHING GROUT RMG 2C4 AND NEVADA TEST SITE TUFF: MEAN NORMAL STRESS VERSUS VOLUME STRAIN

REFERENCES

1. R. W. Gates and C. F. Petersen, "A Laboratory Method for Studying Stemming of Line-of-Sight Tunnels in Underground Nuclear Tests," Final Report, DNA 3058Z, Contract DNA001-72-C-0047, Stanford Research Institute (November 1972).

2. R. W. Gates, C. F. Petersen, and A. L. Florence, "Laboratory Method for Studying Stemming of Line-of-Sight Tunnels in Underground Nuclear Tests," Final Report, DNA 3592F, Contract DNA001-73-C-0122, Stanford Research Institute (December 1973).

3. A. L. Florence, "Laboratory Investigation of Stemming of Horizontal Line-of-Sight (HLOS) Underground Nuclear Tests," Final Report, DNA 3684F, Contract DNA001-74-C-0101, Stanford Research Institute (February 1975).

4. A. L. Florence, "Laboratory Investigation of Stemming and Containment In Underground Nuclear Tests," Final Report, DNA 4149F, Contract DNA001-75-C-0083, Stanford Research Institute (October 1976).

5. J. C. Cizek and A. L. Flornece, "Laboratory Studies of Containment in Underground Nuclear Tests," Final Report, DNA 4846F, Contract DNA001-77-C-0025, SRI International (January 1978).

6. J. C. Cizek and A. L. Florence, "Laboratory Studies of Containment in Underground Nuclear Tests," Final Report, DNA 4847F, Contract DNA001-77-C-0025, SRI International (January 1979).

7. J. C. Cizek and A. L. Florence, "Laboratory Studies of Containment in Underground Nuclear Tests," Final Report, DNA 5601F, Contract DNA001-79-C-0094, SRI International (January 1980).

8. J. C. Cizek and A. L. Florence, "Laboratory Investigation of Containment in Underground Nuclear Tests," Final Report, DNA 5731F, Contract DNA001-80-C-0040, SRI International (February 1981).

9. A. L. Florence and T. C. Kennedy, "A Simple Analysis for Containment Studies," Topical Report 76-3702-2, Contract DNA001-75-C-0083, Stanford Research Institute (August 1976).

10. L. Seaman, "SRI PUFF 3 Computer Code for Stress Wave Propagation," prepared for Air Force Weapons Laboratory, Air Force Systems Command, Kirtland AFB, New Mexico, Technical Report No. AFWL-TR-70-51, Stanford Research Institute (September 1970).

11. N. Rimer and K. Lie, "Spherically Symmetric Numerical Simulation of the SRI Grout Spheres Containment Experiments," Topical Report SSS-R-79-3831, Contract DNA001-77-C-0099, Systems, Science, and Software (October 1978).

12. J. C. Cizek, A. L. Florence, and D. D. Keough, "Experimental Study of the Effects of Faults on Spherical Wave Propagation," Final Report, DARPA Order No. 3749-A1, Contract DNA001-80-C-0287, SRI International (January 1981).

13. S. W. Butters, J. M. Gronseth, and J. F. Patterson, "Material Properties of Nevada Test Site Tuff and Grout," Final Report TR 80-35, Contract DNA001-78-C-0395, Terra Tek (May 1980).

14. C. H. Cooley, et al., "Material Properties of 2C-4 Grout in Support of the Nevada Test Site Nuclear Test Program," Draft Report TR 81-56, Contract DNA001-81-C-0037, Terra Tek (May 1981).

DISTRIBUTION LIST

DEPARTMENT OF DEFENSE

Defense Nuclear Agency
ATTN: SPTD, T. Kennedy
4 cy ATTN: TITL

Defense Technical Information Ctr
12 cy ATTN: DD

Field Command
Defense Nuclear Agency
ATTN: FCTT, G. Ganong
ATTN: FCTT, W. Summa
ATTN: FCT, COL C. Ballantine
3 cy ATTN: FCTK, B. Ristvet
3 cy ATTN: FCTK, C. Keller

DEPARTMENT OF ENERGY

Department of Energy
ATTN: R. Newman

OTHER GOVERNMENT AGENCY

Department of the Interior
ATTN: R. Carroll
ATTN: A. Fernald

DEPARTMENT OF ENERGY CONTRACTORS

Desert Research Institute
ATTN: D. Schulke Sec Off for P. Fenske
ATTN: D. Schulke Sec Off for C. Case

University of California
Lawrence Livermore National Lab
ATTN: B. Hudson
ATTN: F. Morrison
ATTN: L-209, G. Higgins
ATTN: R. Terhune
ATTN: L. Makague

DEPARTMENT OF ENERGY CONTRACTORS (Continued)

Los Alamos National Lab
ATTN: T. Kunkle, ESS-5
ATTN: R. Brownlee
ATTN: C. Keller
ATTN: F. App
ATTN: B. Travis

Sandia National Lab
ATTN: C. Smith
ATTN: ORG 7112, C. Mehl

DEPARTMENT OF DEFENSE CONTRACTORS

California Research & Technology, Inc
ATTN: M. Rosenblatt

Kaman Tempo
ATTN: DASIAC

Pacific-Sierra Research Corp
ATTN: H. Brode, Chairman SAGE

Pacifica Technology
ATTN: D. Patch

Physics International Co
ATTN: E. Moore
ATTN: D. Mumma

R&D Associates
ATTN: P. Haas

S-CUBED
ATTN: R. Duff
ATTN: C. Dismukes

SRI International
4 cy ATTN: A. Florence
4 cy ATTN: J. Cizek

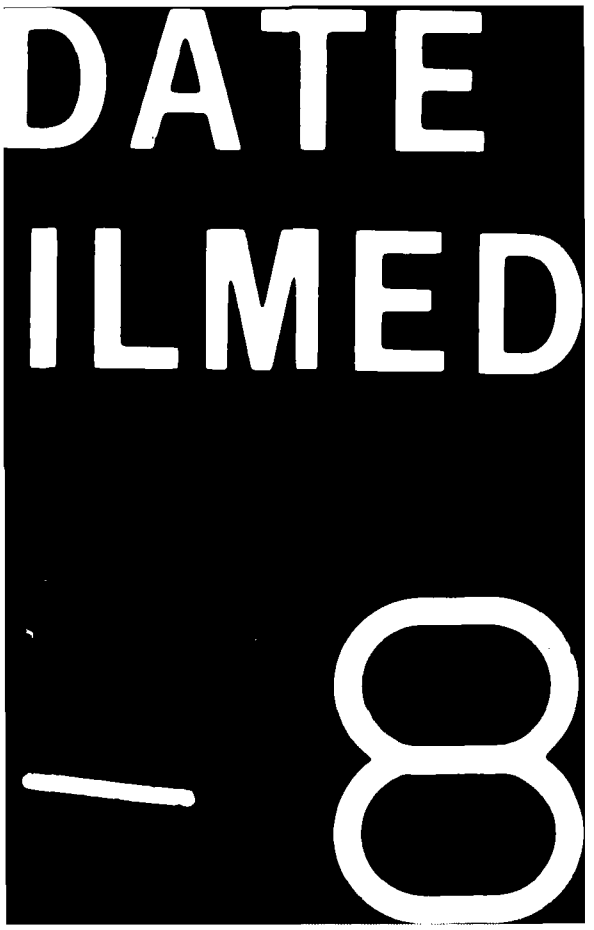
DATE
ILMED
8